Etude électrique et spectroscopique de l'influence de l'électrode sur les capteurs de gaz à base de SnO2

Johan Bertrand

Ecole Nationale Supérieure des Mines
SAINT-ETIENNE

N° d'ordre : **487 GP**.

THESE

présentée par

Johan BERTRAND

Pour obtenir le grade de Docteur
de l'Ecole Nationale Supérieure des Mines de Saint-Etienne

Spécialité : **Génie des procédés**

Etude électrique et spectroscopique de l'influence de l'électrode sur les capteurs de gaz à base de SnO_2

Soutenue à **Saint Etienne** le **27 juin 2008**

Membres du jury

Président :	Pr Michel Labeau	LMGP/ INP Grenoble Minatec
Rapporteurs :	Pr. Thomas Chassé	Condensed matter/university of Tuebinguen
	Dr Odile Merdrignac Conanec	Verres et céramiques/université de Rennes1
Examinateurs :	Dr. Udo Weimar	IPC/university of Tuebinguen
	Dr Jean-Paul Viricelle	MICC/ école des mines de St Étienne
	Dr. Thierry Pagnier	LEPMI / ENSEEG, Grenoble
Directeur(s) de thèse :	Dr.Nicolae Barsan	IPC/university of Tuebinguen
	Pr. Christophe Pijolat	MICC/ école des mines de St Étienne

◘ **Spécialités doctorales :**	**Responsables :**
SCIENCES ET GENIE DES MATERIAUX	**J. DRIVER** Directeur de recherche – Centre SMS
MECANIQUE ET INGENIERIE	**A. VAUTRIN** Professeur – Centre SMS
GENIE DES PROCEDES	**G. THOMAS** Professeur – Centre SPIN
SCIENCES DE LA TERRE	**B. GUY** Maitre de recherche – Centre SPIN
SCIENCES ET GENIE DE L'ENVIRONNEMENT	**J. BOURGOIS** Professeur – Centre SITE
MATHEMATIQUES APPLIQUEES	**E. TOUBOUL** Ingénieur – Centre G2I
INFORMATIQUE	**O. BOISSIER** Professeur – Centre G2I
IMAGE, VISION, SIGNAL	**JC. PINOLI** Professeur – Centre CIS
GENIE INDUSTRIEL	**P. BURLAT** Professeur – Centre G2I
MICROELECTRONIQUE	**Ph. COLLOT** Professeur – Centre CMP

◘ **Enseignants-chercheurs et chercheurs autorisés à diriger des thèses de doctorat** (titulaires d'un doctorat d'Etat ou d'une HDR)

AVRIL	Stéphane	MA	Mécanique & Ingénierie	CIS
BATTON-HUBERT	Mireille	MA	Sciences & Génie de l'Environnement	SITE
BENABEN	Patrick	PR 2	Sciences & Génie des Matériaux	SMS
BERNACHE-ASSOLANT	Didier	PR 1	Génie des Procédés	CIS
BIGOT	Jean-Pierre	MR	Génie des Procédés	SPIN
BILAL	Essaïd	DR	Sciences de la Terre	SPIN
BOISSIER	Olivier	PR 2	Informatique	G2I
BOUCHER	Xavier	MA	Génie Industriel	G2I
BOUDAREL	Marie-Reine	MA	Sciences de l'inform. & com.	DF
BOURGOIS	Jacques	PR 1	Sciences & Génie de l'Environnement	SITE
BRODHAG	Christian	MR	Sciences & Génie de l'Environnement	SITE
BURLAT	Patrick	PR 2	Génie industriel	G2I
CARRARO	Laurent	PR 1	Mathématiques Appliquées	G2I
COLLOT	Philippe	PR 1	Microélectronique	CMP
COURNIL	Michel	PR 1	Génie des Procédés	SPIN
DAUZERE-PERES	Stéphane	PR 1	Génie industriel	CMP
DARRIEULAT	Michel	ICM	Sciences & Génie des Matériaux	SMS
DECHOMETS	Roland	PR 1	Sciences & Génie de l'Environnement	SITE
DESRAYAUD	Christophe	MA	Mécanique & Ingénierie	SMS
DELAFOSSE	David	PR 2	Sciences & Génie des Matériaux	SMS
DOLGUI	Alexandre	PR 1	Génie Industriel	G2I
DRAPIER	Sylvain	PR 2	Mécanique & Ingénierie	CIS
DRIVER	Julian	DR	Sciences & Génie des Matériaux	SMS
FOREST	Bernard	PR 1	Sciences & Génie des Matériaux	CIS
FORMISYN	Pascal	PR 1	Sciences & Génie de l'Environnement	SITE
FORTUNIER	Roland	PR 1	Sciences & Génie des Matériaux	CMP
FRACZKIEWICZ	Anna	MR	Sciences & Génie des Matériaux	SMS
GARCIA	Daniel	CR	Génie des Procédés	SPIN
GIRARDOT	Jean-Jacques	MR	Informatique	G2I
GOEURIOT	Dominique	MR	Sciences & Génie des Matériaux	SMS
GOEURIOT	Patrice	MR	Sciences & Génie des Matériaux	SMS
GRAILLOT	Didier	DR	Sciences & Génie de l'Environnement	SITE
GROSSEAU	Philippe	MR	Génie des Procédés	SPIN
GRUY	Frédéric	MR	Génie des Procédés	SPIN
GUILHOT	Bernard	DR	Génie des Procédés	CIS
GUY	Bernard	MR	Sciences de la Terre	SPIN
GUYONNET	René	DR	Génie des Procédés	SPIN
HERRI	Jean-Michel	PR 2	Génie des Procédés	SPIN
KLÖCKER	Helmut	MR	Sciences & Génie des Matériaux	SMS
LAFOREST	Valérie	CR	Sciences & Génie de l'Environnement	SITE
LI	Jean-Michel	EC (CCI MP)	Microélectronique	CMP
LONDICHE	Henry	MR	Sciences & Génie de l'Environnement	SITE
MOLIMARD	Jérôme	MA	Sciences & Génie des Matériaux	SMS
MONTHEILLET	Frank	DR 1 CNRS	Sciences & Génie des Matériaux	SMS
PERIER-CAMBY	Laurent	PR1	Génie des Procédés	SPIN
PIJOLAT	Christophe	PR 1	Génie des Procédés	SPIN
PIJOLAT	Michèle	PR 1	Génie des Procédés	SPIN
PINOLI	Jean-Charles	PR 1	Image, Vision, Signal	CIS
STOLARZ	Jacques	CR	Sciences & Génie des Matériaux	SMS
SZAFNICKI	Konrad	CR	Sciences de la Terre	SITE
THOMAS	Gérard	PR 1	Génie des Procédés	SPIN
VALDIVIESO	François	MA	Sciences & Génie des Matériaux	SMS
VAUTRIN	Alain	PR 1	Mécanique & Ingénierie	SMS
VIRICELLE	Jean-Paul	MR	Génie des procédés	SPIN
WOLSKI	Krzysztof	CR	Sciences & Génie des Matériaux	SMS
XIE	Xiaolan	PR 1	Génie industriel	CIS

Glossaire :

PR 1 Professeur 1ère catégorie
PR 2 Professeur 2ème catégorie
MA(MDC) Maître assistant
DR (DR1) Directeur de recherche
Ing. Ingénieur
MR(DR2) Maître de recherche
CR Chargé de recherche
EC Enseignant-chercheur
ICM Ingénieur en chef des mines

Centres :

SMS Sciences des Matériaux et des Structures
SPIN Sciences des Processus Industriels et Naturels
SITE Sciences Information et Technologies pour l'Environnement
G2I Génie Industriel et Informatique
CMP Centre de Microélectronique de Provence
CIS Centre Ingénierie et Santé

Introduction

Human beings need a regular supply of food and water and essentially continuous supply of air. The requirements for air and water are relatively constant (10–20 m^3 and 1–2 litres per day, respectively). That all people should have free access to air and water of acceptable quality should be a fundamental human right. The atmosphere we live in contains numerous chemicals, natural and artificial, some of which are vital to life while many others are more or less harmful. Recognizing our need for clean air, in 1987 the WHO Regional Office [1] for Europe published *Air quality guidelines for Europe (1),* containing health risk assessments for 28 chemical air contaminants.

Various chemicals are emitted into the air from both natural and man-made (anthropogenic) sources. The quantities may range from hundreds to millions of tonnes annually. Natural air pollution stems from various biotic and abiotic sources such as plants, radiological decomposition, forest fires, volcanoes and other sources such as geothermal, as well as emissions from land and water. These result in a natural background concentration that varies according to local sources or specific weather conditions. Anthropogenic air pollution has existed since people learned to use fire, at least. However, it has increased rapidly since the beginning of industrialization. The augmentation of air pollution resulting from the ever expanding use of fossil fuels, growth in the manufacture sector and widespread use of chemicals has been accompanied by mounting public awareness of its detrimental effects on health and the environment. Moreover, basic research on the nature, quantity, physicochemical behaviour and effects of air pollutants has greatly increased our knowledge in recent years. Nevertheless, there is a great deal more that needs to be understood. Several aspects concerning air pollutants effects on public health require further assessment; these include newer scientific areas such as reproductive or developmental toxicity. The proposed guidelines will undoubtedly be changed as future studies lead to new information.

The task of reducing levels of exposure to air pollutants is complex . It begins with an analysis to determine which chemicals are present in the air, where, at what levels, and whether the likely levels of exposure are hazardous to humans and the environment. Then, it must be decided whether an unacceptable risk is present. When a hazard is identified, mitigation strategies should be developed and implemented so as to prevent excessive risk to public health in the most efficient and cost-effective way.

Analyses of air pollution problems are exceedingly complicated but are an important issue for the 21st century.

There is a great variety of techniques to monitor the atmosphere pollutants: absorption spectrometry either in infrared or ultraviolet range, or chemical methods (flame spectroscopy, chemiluminescence and gas chromatography). Table 1-1 illustrates the variety of target compounds as well as the large number of analytical methods used for their measurement. All these techniques, often very precise, require a sampling. Besides the problems of homogeneity and accurate representation of samples, there are long, often costly techniques of analysis to be implemented, and which can be difficult or even impossible to use for continuous applications. One example that comes to mind is as part of detector of ambient pollution or for industrial site.

Table 1-1 :***Main pollutant gas , Concentration range And common analysis method*** **[2]**

Gas	Concentration (ppm) range		Common analysis method
	Air	Rejections	
SO_2	10^{-3} - 10	10 - 2000	Flame spectroscopy UV Fluorescence IR Absorption UV Absorption potentiostatic electrolysis
NOx	10^{-3} - 10	1 - 2000	Chemical Luminescence IR Absorption potentiostatic electrolysis
CO_2	300 - 1000	10^4 - $2*10^5$	IR Absorption Ion selective electrode (ISE) Thermal conductivity
O_3	10^{-3} - 1	_	Chemical Luminescence UV Absorption
NH_3	_	100 - 10^4 (local)	iso-phénolique method ISE (NH_3) Gas Chromatography
H_2S	_	1 - 1000 (local)	ISE (S^{2-}) methylene Blue Dosage

Therefore new gas sensors, able of discriminating, but also to measure these different pollutants in real-time are required.

Several gas sensors have been developed so far. Some, such as electrolyte solution based electrochemical or catalytic combustion sensors, were developed a long time ago for professionals. There are many different sensors based, in general, on a simple law of physics. Figure 1-1 summarizes a selection of gas sensors commonly used at present.

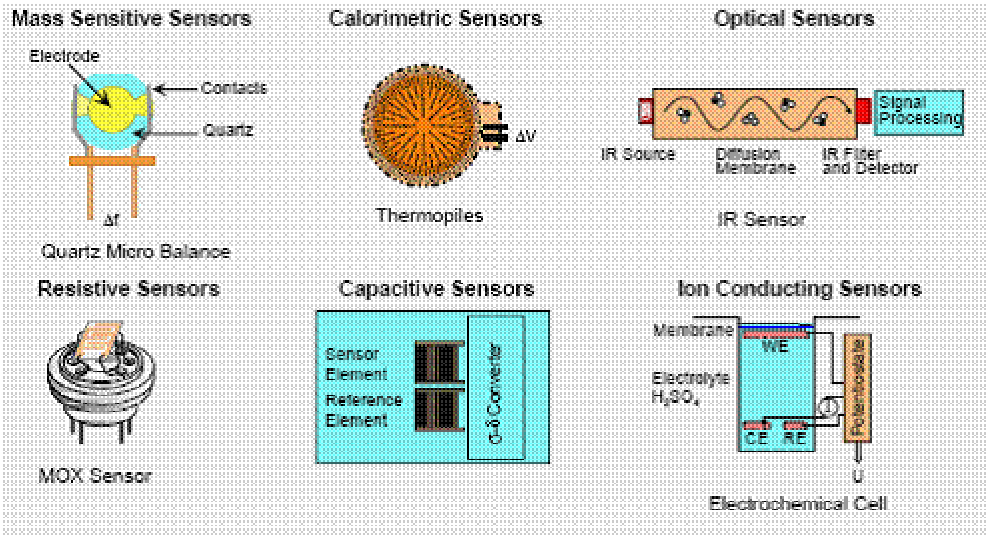

Figure 1-1 : An illustrated selection of gas sensor types

The era of sensors started in the 1970s during which semiconductor combustible gas, solid electrolyte oxygen and humidity sensors were commercialized for non-professional uses.

Metal oxides sensors (MOX sensors) in general and SnO_2, in particular, have attracted the attention of many users and scientists interested in gas sensing in changeable atmospheric conditions. This interest has been generated due to their low cost fabrication, simplicity of use and finally the large number of detectable gases possible.

With the advent of pollution and performance concerns in the automotive industries, intelligent homes & appliances market (Figure 1-2) and in general any industry working with gas these devices have come into demand.

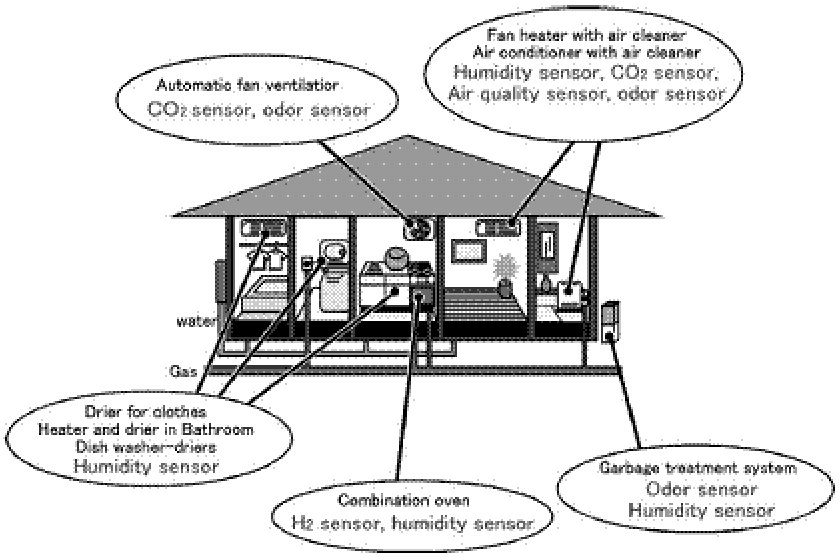

Figure 1-2 : application of sensor in the home automation (domotics) field

The principle of how the SnO_2 based-sensor works is quite simple and based on the change of electrical resistance when exposed to a certain gas or gasses. SnO_2 is the best understood oxide-based gas sensors. Nevertheless, there are highly specific and sensitive SnO_2 sensors not yet available or feasible. In real working conditions, SnO_2 sensors are confronted with the problem of high cross-sensitivity for other gasses, which strongly limits their application.

In order to be used in practice, a gas sensor should fulfil many requirements which depend on the purposes, locations and conditions of their operation. Among the sensor's prerequisites, first would be their effectiveness: sensitivity, selectivity and response time. Second level criterions would be: reliability: drift, stability.

Efficiency [3] and reliability are interconnected with each element [4-5] of the sensor - sensitive layers, substrates, heaters and electrodes. These function together in device so the sensor should be studied as a whole. The verification and optimization of each parameter have key roles to play in the research and development of gas sensors

The Laboratory M.I.C.C. (Microsystemes Intrusmentation et Capteurs Chimiques) managed by C. Pijolat located in St Etienne is interested in the development of gas sensor for industrial applications. Few years ago, they considered the fact that the electrodes which collect the output signal can have an influence on the overall performance of gas sensors. In fact, changing the nature of the electrode metal can greatly modify the results. They tried to explain this behaviour inside a physical-chemical model [6] (cf., chapter 1) which takes into account the role of the electrodes. The model stresses the main role of the three boundary points (interface of gas-electrode-Sensitive layer).

At the same time, at the University of Tübingen in Germany, the IPC (Institute for physical chemistry) group of Udo Weimar also tried to understand more about the electrodes influence. They developed new techniques to observe and understand gas sensors under actual working conditions: DRIFT (Diffuse Reflectance Infrared Fourier Transform), Kelvin probe, impedance spectroscopy [7].

Focus of the work

The focus of this work is primarily devoted to clarify the role of the electrode material on the properties of detection for gas sensor. Some earlier hypothesis have been suggested and summarized in the model of MICC but there is a lack of experimental proof. The objective of this is complete their promising work and hopefully improve our understanding of this crucial parameter by collaborating with both MICC in France and IPC in Germany.

This collaboration between the research centres takes place under the auspices of GOSPEL "General Olfaction and Sensing Projects on a European Level". This organization is a Network of Excellence funded by the European Community under the Sixth Framework Programme (IST-2002-507610) from 2002 to 2006. It is coordinated by the University of Tübingen and integrates the expertise of 25 research groups across Europe (the GOSPEL 'Members'). It also works with over 100 Associate Members from industry and academia worldwide.

The chosen approach is the combination of physico-chemical phenomena and spectroscopic techniques. For simplicity sake the target gas for detection is carbon monoxide CO.

This report is structured as following:

Chapter 1 is dedicated to the bibliography on SnO_2 based sensor, theoretical understanding of the tin dioxide gas sensor, as well a brief state of the art on the work of other authors concerned with the electrode's influence is summarized

Chapter 2 of this thesis deals with the preparation of the sensor, its electrical performance, and different powders used

Chapter 3 is related to the investigation of carbon monoxide interaction with tin oxide sensors, with metal, in air by means simultaneous DRIFT and DC resistance studies. Thermodesorption experiments complete the spectroscopy investigations on the oxygen chemisorption and the influence of the metal.

Chapter 4 reviews the principal outcomes of the thesis, focusing on the link between the results and on their originality. In addition, some major perspectives are proposed.

Contents

CHAPTER 1

1 Theoretical Basis and survey

De part son utilisation dans un grand nombre de domaines, le dioxyde d'étain fait l'objet de nombreuses publications. Ce chapitre est dédié à l'état de l'art sur SnO_2 en tant que matériau pour capteur de gaz. L'étude bibliographique du dioxyde d'étain se divise en quatre parties. Nous évoquerons dans un premier temps les caractéristiques du matériau SnO_2, et dans une seconde partie, comment il peut être utilisé comme capteur de gaz. Le troisième point concernera l'interaction de SnO_2 avec les principaux gaz. La modélisation de la conduction dans les couches de SnO_2 sera quant à elle traitée dans la dernière partie. L'accent sera mis sur le rôle des électrodes, objet de cette étude.

1.1 Introduction bibliographies

Conductometric chemical gas sensors based on semiconductor metal oxides are actually the most investigated. Although semiconductor gas sensors have been so far developed mostly by empirical research , further development and innovation seem to be impossible without a fundamental understanding of the gas-sensing mechanism and sensor design principles involved. This first chapter tries to sum up the particularity of the SnO_2 as material for gas sensor. Moreover, due to the fact that a large part of this study consists in spectroscopic investigations it is important to introduce the interaction of the gas and SnO_2. As you will see in this chapter many parameters affect the performance of the semiconductor which is complex and difficult to completely take all the factors into consideration. Each parameter has been almost totally investigated beginning with the history of metal oxide gas sensors with Tagushi in 1962 [8]. Despite these aforementioned numerous studies, the actual detection mechanisms of tin oxide sensors and especially the role of the electrodes are not fully understood. The motivation of our work is to explore the influence of the electrodes in the system of SnO_2 based gas sensors. A survey of pertinent publications on the influence of the metal is included. Special attention has been paid to the previous thesis of P Montmeat [6]. A model taking into account the role of the metal (gold electrodes) which enhances the creation of a space charge area at the three boundary points “gas–metal–oxide” was proposed and that is the starting point of our work.

1.2 Material Properties of Tin Dioxide

SnO_2 has various specific and unique properties, which makes this material very useful for many applications. Polycrystalline thin films and ceramics of SnO_2 have been extensively used in the production of resistors. Conducting SnO_2 films are well known as transparent electrode. When deposited on glass it is known as Nesa glass [9] [1]. SnO_2 films are also used as transparent heating elements, for the production of transistors, for transparent antistatic coatings and other parts in electric equipment where transparency is required.

1.2.1 Crystalline structure of SnO_2

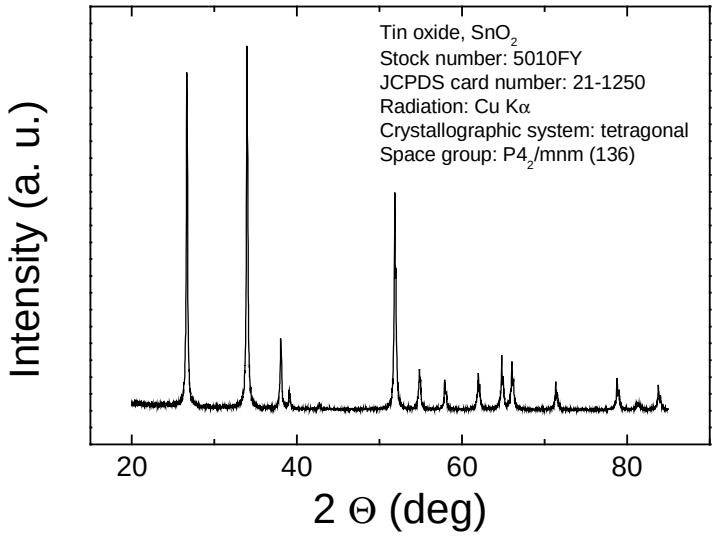

Figure 1-1 : SnO_2 X ray diffraction pattern diagram

SnO_2 is an anisotropic polar crystal, which crystallises in tetragonal rutile structure with space group D_{4h} [$P_{42/mm}$][10] [2]. The unit cell contains 6 atoms, 2 tins and 4 oxygen. Each tin atom is at the centre of six oxygen atoms placed approximately at the corners of a regular slightly deformed octahedron, and three tin atoms approximately at the corners of an equilateral triangle surround every oxygen atom (see Figure 1-2).

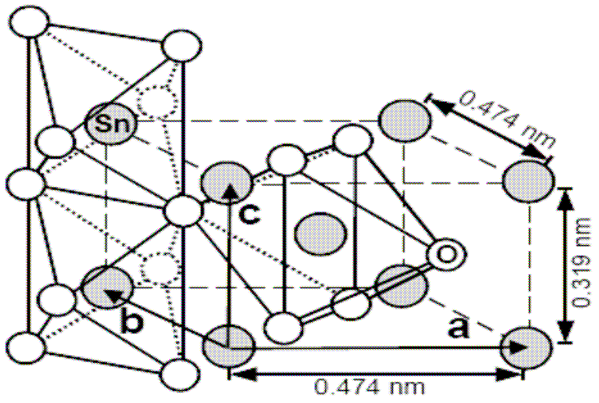

Figure 1-2 : Unit cell of SnO_2 with four O_2- anions and two Sn^{4+} cations. The crystalline structure of SnO_2 is rutile: Each tin atom is at the centre of six oxygen atoms placed approximately at the corners of a regular slightly deformed octahedron and three tin atoms approximately at the corners of an equilateral triangle surround every oxygen atom.

Thus, crystalline structure of tin dioxide is 6:3 coordination. The lattice parameters are a = b =4.737Å and c = 3.185Å. The $\frac{c}{a}$ ratio is 0.673. The ionic radii for O_2^- and Sn^{4+} are 1.40 and 0.71Å, respectively. The metal atoms (cations) are located at positions (0,0,0) and (½,½,½) in the unit cell, and the oxygen atoms (anions) at ± (*u*,*u*,0) and ± (½+*u*,½-*u*,½), where the internal parameter, *u*, takes the value 0.307. Each cation has two anions at a distance of 2*ua* (2.053Å) and four anions. Each cation has two anions at a distance of 2 *u·a* (*2.053Å*) and four anions at $[2(½-u)^2+(c/2a)2]½a$ (*2.597Å*).

1.2.2 Electronic properties

SnO_2 is a n-type, wide-band gap semiconductor. The origin of the n-type behaviour is the native non-stoichiometry caused by oxygen vacancies. The conduction band has its minimum at the Γ point in the Brillouin zone and is a 90% tin s-like state. The valence band consists of a set of three bands (2^+, 3^+ and 5^+). The valence band maximum is a Γ_3^+ state. In this way, SnO_2 has a direct band gap, with energy $Edir(\Gamma_{3v}^+-\Gamma_{1c}^+) = 3.596eV$ for $E\perp$ and $3.99eV$ for $E_{//}$,measured at 4K. Figure 1-3 shows the band diagram for SnO_2 and the projection of the density of states (DOS) for the 1-states of Sn and O. According to results of Barbarat et al. a large contribution of Sn(s)-states is found at the bottom of the valence band between –7 and –5eV [11]. From –5eV to the top of the valence band, the Sn (p)-states contribution is decreasing, as the Sn(d)-states are occupying the top of the valence band. A large and extended contribution of the O (p)-states is found in the valence band. Clearly, bonding between Sn and O is dominated by the p-states of the latter. Each anion in the unit cell is found to be bonded to the cations in a planar-trigonal configuration in such a way that the oxygen p orbitals contained in the four-atom plane, i.e., p_x and p_y orbitals, define the bonding plane. Consequently, the oxygen *p* orbitals perpendicular to the bonding plane, i.e., p_z orbitals, have a non-bonding character and are expected to form the upper valence levels [10] [4]. The conduction band shows a predominant contribution of Sn(s) states up to 9eV. For energies larger than 9eV an equal contribution of Sn- and O-states is found in the conduction band. More information, mainly about the valence band, can be found in [12,13,14] and references therein.

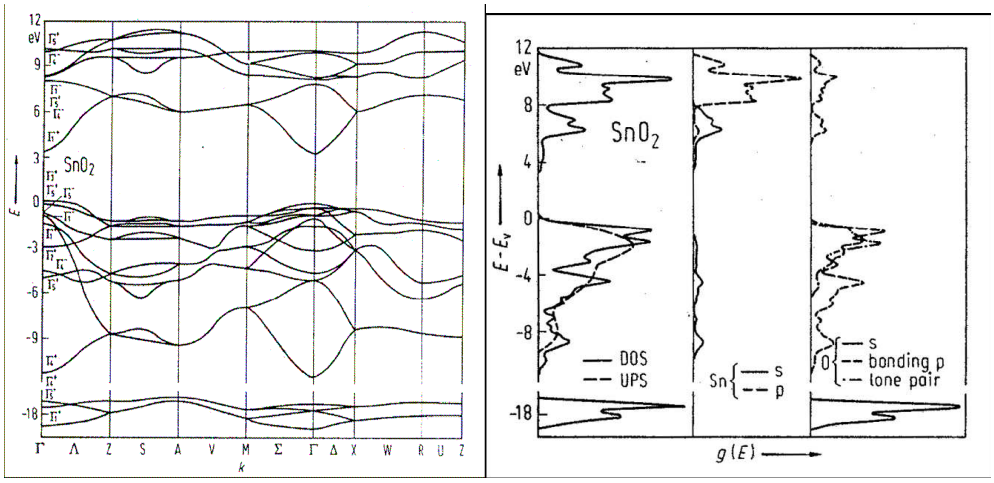

Figure 1-3: Band diagram of SnO_2 (left) and projection of the density of states (DOS) for the 1s states of SnO_2, Sn and O (right) [15]

When discussing the atomistic and electronic behaviour of a surface there are two dominant models in literature: the atomistic model [16], [17] or surface molecule model, generally preferred by chemists, and the band model [18], [19], generally preferred by physicists. The atomistic model is more appropriate for chemical processes at a solid surface. It describes the solid surface in terms of surface sites or atoms, ignoring the band structure of the solid. The band model is preferable for electron exchanges between (semiconductors) solids and surface groups that include a conductivity change for the solid. It describes the surface in terms of surface states, i.e. localised electronic energy levels available at the surface, ignoring the microscopic details of atom-atom interaction between surface species and its neighbouring atoms.

Both models have their merits, but to understand the surface reactions of semiconductors with gases both chemical and physical perspectives have to be considered [20].

From a chemical standpoint, a surface can be divided into surface sites of varying reactivity. Usually, more reactive sites can be associated with heterogeneous surface regions or surface imperfections. Examples of reactive sites are surface atoms with unoccupied or unsaturated orbitals (“dangling bonds”), surface atoms with unsaturated coordination sphere, crystallographic steps, intersections, interstitial defects or superstructures.

From a physical point of view the interruption of the crystal periodicity at the surface results in localised energy levels. These can function as acceptor or donor states, exchanging or sharing electrons with the non-localised energy bands in the bulk of the solid. Those energy levels in the band gap have an effect on the electronic properties of the solid, especially for

semiconductors. Surface states can result from non-ideal stoichiometry or bulk defects (intrinsic) or arise from (intentional) impurities, as for doping (extrinsic).

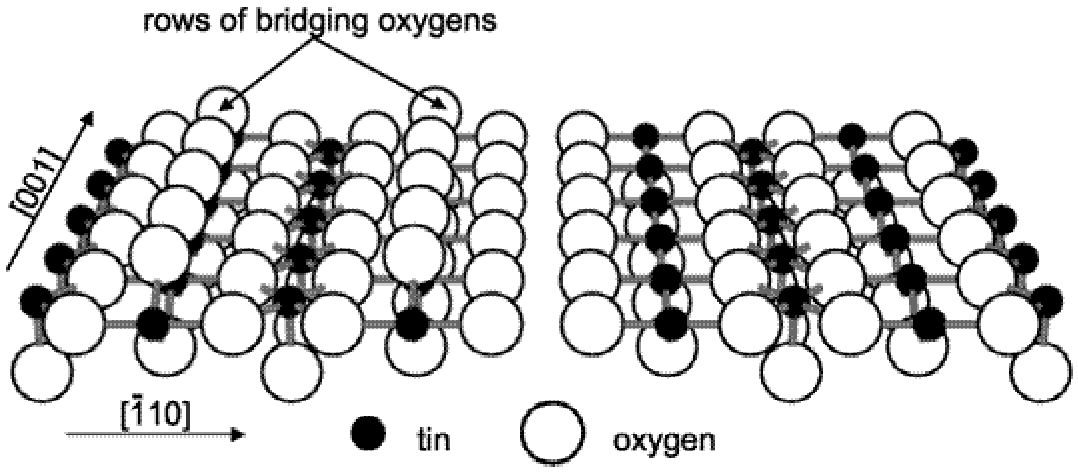

Figure 1-4: Ideal and reduced (compact) SnO_2 (110) surfaces; the schema on the right is obtained by removing the bridging oxygen layers

1.3 Sensor resistance /conductivity of tin oxide based gas sensors

The final objective of the R&D activities is the design and fabrication of quality gas sensors id est. suited for solving a certain application. It is important to keep in mind that the quality of a sensor is almost impossible to be defined without understanding the application needs, which besides the target gas/gases, possible cross-interferences and environmental conditions also relate to the cost/price restrictions of the instrument using the sensors.

A significant factor is–suitability – that is increasingly considered in addition to the 3 standard means of judging sensors (Sensitivity, Selectivity, Stability).

In order to understand the challenges in this field, we should have a look at the way in which the sensor signal is generated.

A sensor element (Figure 1-5) normally is comprised of the following parts:

- *Sensitive layer* deposited over the
- *Substrate* provided with
- *Electrodes* for the measurement of the electrical characteristics. The device is generally heated by its own
- *Heater*; this one is separated from the *sensitive layer* and the *electrodes* by an electrical insulating layer.

Such a device is normally operated in air, with the presence of humidity and residual gases (e.g. carbon dioxide).

In Figure 1-5 a typical gas sensor is presented. Note that the SnO2 layer is printed on top of the interdigitated electrodes. The heater on the back keeps the sensor at the operation temperature

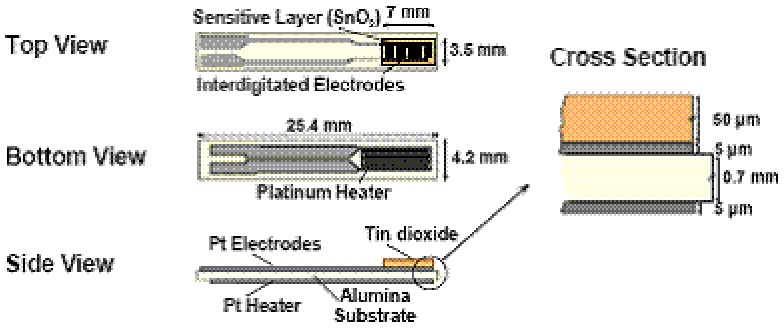

Figure 1-5 : Layout of the planar alumina substrate with Pt electrodes and Pt heater.

1.3.1 Receptor and transducer functions

An oxide semiconductor gas sensor detects a gas from the change in electric resistance of a polycrystalline element. It is commonly agreed that the resistance change from the exposure to a gas arises through a surface phenomenon of the semi conductor used [21] [22]. Generally, a chemical sensor has two functions:

- Receptor which recognizes or identifies a chemical substance
- Transducer which converts the chemical signal into an output signal.

Therefore, for the basic understanding of the semiconductor gas sensor, one needs to differentiate these two functions. Figure 1-6 shows schematically how a semiconductor sensor generates sensing signals upon contact with a gas.

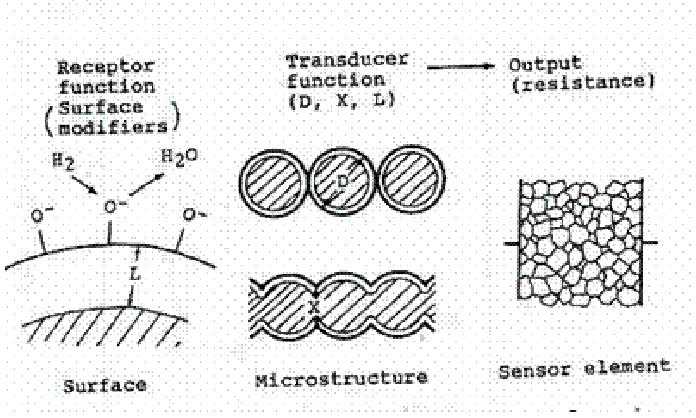

Figure 1-6: Receptor and transducer functions of semiconductor gas sensor [23].

Apparently, the receptor function is provided with the surface of each semiconductor particle. The obtained chemical signal is then converted through the microstructure of coagulating particles into the resistance of polycrystalline element.

1.3.2 Bulk properties

The conductivity σ_{tot} of a semiconductor crystal can be described as the sum of electronic (σ_e and σ_p) and ionic conductivity (σ_{ion}) if the conduction processes are considered independent. SnO_2 gas sensors are typically operated at temperatures between 200°C and 400°C. In this range the ionic contribution can be neglected and the conductivity of SnO_2 can be calculated according to:

$$\sigma_{Tot} = \sigma_e + \sigma_p + \sum \sigma_{ion,i\approx} \approx \sigma_e + \sigma_p \qquad \textbf{Eq 1-1}$$

The resistance of homogeneous bulk material with bulk conductivity σ_b, mobility μ, length l and cross section A=b (width) x d (high) can be calculated according to

$$R_b = \frac{l}{\sigma_b \cdot b \cdot d} = \frac{l}{\sigma_b \cdot A} \quad with \quad \sigma_b = \sigma_e + \sigma_p = n \cdot \mu_e \cdot e + p \cdot \mu_p \cdot e \qquad \textbf{Eq 1-2}$$

where the charge carrier concentrations **n(electron)** and **p(holes)** for an intrinsic semiconductor can be calculated according to:

$$n = \int_{E_C}^{\infty} D(E) f(E) dE \;\; ; \;\; p = \int_{-\infty}^{E_V} D(E)\left(1 - f(E)\right) dE \qquad \textbf{Eq 1-3}$$

With the Fermi-Dirac distribution f(E) and the density of states D(E), E_c: the energy level of the conduction and E_v energy level of the valence band:

$$D(E) = \frac{1}{2\pi^2}\left(\frac{2m_e}{\hbar^2}\right)^{\frac{3}{2}} (E - E_C)^{\frac{1}{2}} \;\; ; \;\; f(E) = \frac{1}{1 + \exp\left(\frac{E - E_F}{kT}\right)} \qquad \textbf{Eq 1-4}$$

For $E_C - E_F > 4$ kT, the charge carrier concentrations n and p can be approximated by

$$n = N_C \exp\left(\frac{E_F - E_C}{kT}\right) \;;\; N_C = 2\left(\frac{2\pi\, m_e kT}{h^2}\right)^{3/2}$$

$$p = N_V \exp\left(\frac{E_V - E_F}{kT}\right) \;;\; N_V = 2\left(\frac{2\pi\, m_p kT}{h^2}\right)^{3/2}$$

Eq 1-5

Where N_C and N_V are the effective density of states in the conduction and valence bands, respectively.

When the semiconductor is undoped, $n=p=n_i$ and $E_F = E_i$ which leads to the following equations for *n* and *p*:

$$n = n_i \exp\left(\frac{(E_F - E_d)}{KT}\right)$$

Eq 1-6

$$p = n_i \exp\left(\frac{(E_d - E_F)}{KT}\right)$$

Intrinsic carrier concentration n_i, Intrinsic Fermi energy level and the np product

If the semiconductor is not doped, then the concentration of electrons in the conduction band *n* is equal to the concentration of holes in the valence band *p*, hence $n=p=n_i$ where n_i is defined as the intrinsic carrier concentration. Using the equations above, it is easy to show that the product np is:

$$np = n_i^2 = N_C N_V e^{(E_V - E_C)/kT} = N_C N_V e^{-E_{gap}/kT}$$

Eq 1-7

Where $E_{gap}=E_C-E_V$. Thus we have an equation for the intrinsic carrier concentration:

$$n_i = \sqrt{N_C N_V e^{-E_{Gap}/kT}}$$ **Eq 1-8**

Besides the product *np*, we can equate *n* and *p* to obtain the intrinsic Fermi energy level:

$$n = p$$

$$N_C e^{(E_F - E_C)/kT} = N_V e^{(E_V - E_F)/kT}$$ **Eq 1-9**

$$E_i = \frac{E_C + E_V}{2} + \frac{kT}{2} \ln\left(\frac{N_C}{N_V}\right)$$ **Eq 1-10**

The n-type behaviour of SnO_2 is associated with oxygen deficiency in the bulk (see Figure 1-7).

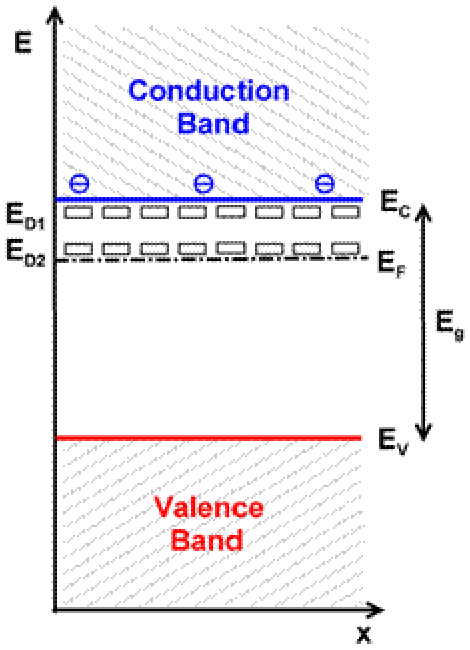

Figure 1-7 : Schematic band diagram of the SnO_2 bulk. Two vacancy donor levels ED1 and ED2 are located 0.03 and 0.15eV below the conduction band (EC = 0eV). The band gap (Eg) is 3.6eV.

The donors are singly and doubly ionised oxygen vacancies with donor levels ED1 and ED2 located around 0.03 and 0.15eV below the conduction band edge[24],[25]. In the case

of SnO_2 the extrinsic donors are multi-step donors. Therefore, donor and acceptor energy levels, concentrations, and the operation temperature determine the bulk conductivity of SnO_2. Experiments performed on various SnO_2 samples to determine the charge carrier density have resulted in values in the range of $2 \cdot 10^{15}$ to $6.8 \cdot 10^{20} cm^{-3}$ for operation at 300K. Hall measurement results indicate that the shallow donor levels (0.03eV) are completely ionised above 100K, the deep donor levels (0.15eV) are almost completely ionised around 400K. Hence, in the typical temperature range for sensor operation (200 - 400°C, i.e. 473 - 673K) the donors can be considered completely ionised.

1.4 Gas interactions

The surface, by definition, is the result of breaking the lattice periodicity. Its properties differ strongly from the bulk. The 'thickness' of the surface is determined by the depth of the space charge region, which is the distance, measured from the surface, at which the effects of the surface induced perturbation are no longer "felt" by the material.

1.4.1 Physisorption and Chemisorption

The fundamental phase for all surface processes is the adsorption of foreign atoms or molecules that causes essential rearrangements of surface chemical bonds and, consequently, the variation of the surface states density and surface potentials. When discussing the interaction of gaseous molecules with the surfaces of solids it is of interest to differentiate between physisorption and chemisorption[26] .

Table 1-1: Bond energies for different types of interaction [27].

Interaction type	**Energy [kJ/mol]**	**Comment**
covalent	120 - 800	chemical reaction
ion - ion	250	only between ions
coordination, complexion	8 - 200	weak chemical interaction
ion - dipole	15	between ions and polar molecules
hydrogen bond	20	hydrogen bond $A\text{-}H^{\delta+}\ldots B^{\delta-}$
dipole - dipole	0.3 - 30	between polar molecules

London (induced dipole to induced dipole)	0.1 - 2	physical interaction between all molecules

Physisorption takes place at a relatively large distance r from the surface (adsorbant). A gaseous molecule (adsorbate) approaching the surface is slightly polarised and induces an equivalent dipole in the adsorbant. This dipole - dipole bond between gas and surface results in an interaction energy ΔE = 0-30kJ/mol with $\Delta E \sim r^{-6}$ (see Table 1-1).

Physisorption is the first step in the interaction between a gas and the surface of a solid. Physisorbed molecules may thereafter become chemisorbed if they exchange electrons with the surface of the semiconductor. Physisorption is characterised by a high surface coverage with gaseous molecules at low temperatures and a low coverage at high temperatures. For the adsorption of up to one monolayer, this coverage θ is defined as follows:

$$\theta = \frac{N}{N_t}$$

With the number of molecules adsorbed per surface unit N and the total number of surface adsorption sites N_t.

Chemisorption introduces higher bonding energies and consequently stronger interactions between adsorbate and adsorbant. It results from a profound modification of the charge distribution of the adsorbed molecule: the bonding energies are of similar strength as for chemical bonds. One can distinguish between neutral chemisorption and ionosorption. Figure 1-8 details the potential energies in case of physisoption (E_{phys}) and chemisorption (E_{chem}) as a function of the distance r from the surface where; A is the curve for physisorption of a molecule; b is the curve for chemisorption of a molecule. Activation. energy E_a, dissociation energy E_{diss}, desorption energy E_{des}

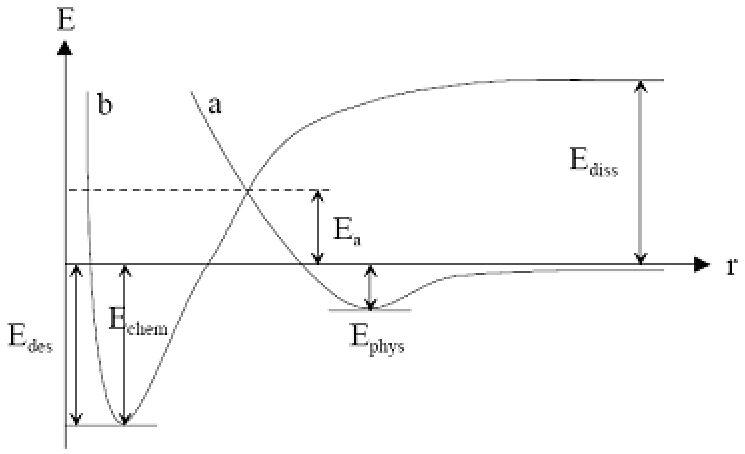

Figure 1-8 : Lennard-Jones model of physisorption and chemisorption:

If a gaseous molecule approaches the surface it will first be physisorbed, gaining ΔE equal to E_{phys}. Upon further movement towards the surface the molecule encounters a growing energy barrier, tending towards an infinite energy for a finite distance r. By spending the activation energy E_a the gaseous molecule can dissociate, thereby allowing a further advance to the surface. This stronger interaction with the surface (chemisorption) results in a higher energy gain ΔE equal to E_{chem} than during physisorption. This energy gain $\Delta E_{chem.}$ depends strongly on the individual surface sites available and their reactivity. The most reactive sites will therefore be occupied with gaseous molecules during thermodynamic equilibration. However, the chemisorption energy not only depends on the number of reactive sites (high potential gain in ΔE_{chem}) but also on the ambient gas concentration p_{gas} and temperature T (probability of molecules overcoming the energy barrier E_A).

As for chemisorption, desorption also requires the molecule to overcome an energy barrier $E_{des} = E_{chem} + E_a$. Therefore chemisorption and desorption are both activated processes requiring an activation energy supplied either thermally or by photoexcitation, contrary to physisorption which is a slightly exothermic process. The adsorption rate of gaseous molecules is proportional to the gas pressure and to the number of unoccupied adsorption sites according to

$$\frac{d\theta}{dt} = k_{ads}(1-\theta)p_{gas} \qquad \textbf{Eq 1-11}$$

With the adsorption constant $k_{ads} = A \cdot \exp(-E_A/kT)$.

The desorption rate is proportional to the number of occupied sites according to

$$\frac{d\theta}{dt} = k_{des}\theta \qquad \textbf{Eq 1-12}$$

With the desorption constant $k_{des} = B \cdot \exp(-E_{diss}/kT)$.

The net adsorption rate can therefore be described through Eq 1-11and Eq 1-12 by

$$\frac{d\theta}{dt} = k_{ads}(1-\theta)p_{gas} - k_{des}\theta \qquad \textbf{Eq 1-13}$$

With a resulting equilibrium coverage θ for dθ/dt=0 of

$$\theta = \frac{P_{gas}}{P_{gas} + \frac{K_{des}}{K_{ads}}} \qquad \textbf{θ = f (p}_{\textbf{gas}}\textbf{, T)} \qquad \textbf{Eq 1-14}$$

Equation (2.11) represents the Langmuir isotherm. It shows that all adsorption and desorption processes not only depend on the nature of the adsorbate and adsorbant but also on the availability of absorbates (partial pressure) and on the temperature. The above observations are correct only for adsorption and desorption of gaseous monolayers on surfaces of solids. Taking also multi-layer adsorption and desorption processes into consideration results in the Brunauer-Emmet-Teller (BET) isotherm with related rate constant equations .

1.4.2 Space Charge Effects

If we move from discussing the bulk properties of ideal crystals to surfaces in realistic environments, we have to accept a state of constant adsorption and desorption in thermodynamic equilibriums. It is of interest to analyse the effect the adsorption of oxygen has on the electrical properties of a semiconductor. Due to the high electronegativity of oxygen its adsorption leads to an oxidation of the semiconductor surface and a reduction of the gas, i.e. a transition of electrons from the conduction band E_C to surface acceptor states. A negative charge is created at the surface. This negative surface layer has to be compensated by a positive countercharge in the solid. If the adsorption took place on the surface of a metal, this would simply result in a planar countercharge: a double layer situation as for a capacitor. However, unlike a metal, a semiconductor does not have a large amount of mobile free charge carriers available at the surface. The countercharge will therefore be formed in the bulk (donor ions), resulting in a space charge region. According to the Schottky approximation,

this region is characterised by a total exhaustion of mobile charge carriers (all moved to the surface) and therefore called the depletion layer. Between these two space charge layers (the planar at the surface and a region in the bulk), an electric field develops. A measure characterizing this electrical field is the Debye-Length L_D:

$$L_D = \sqrt{\frac{\varepsilon_r \varepsilon_0 kT}{e^2 N_{(V)}}} \qquad \textbf{Eq 1-15}$$

Equation Eq 1-15 gives a relation between the Debye-Length L_D (the extension of the space charge region into the bulk) and the concentration of free charge carriers $N_{(V)}$: assuming a high enough temperature to allow mobility to all potentially free charge carriers, L_D is high for a low density of free charge carriers in the volume and vice-versa. Hereby, the concentration of free charge carriers $N_{(V)}$ can be set as equivalent to the concentration of free electrons $N_{e(V)}$, as the concentration of other charge carriers is negligible for standard operating temperatures (200-400°C) for SnO_2.

The space charge region corresponds to a band bending in the electronic band model of the semiconductor. The potential energy of an electron near the surface is increased by the electrostatic repulsion of the negative surface layer. This negative surface charge creates a surface barrier qV_S.

These considerations lead to an adaptation of the semiconductor band model for surface situations as detailed in Figure 1-9. In this illustration the flat band situation for an n-type semiconductor (SnO_2) in the bulk is on the left and the surface with oxygen adsorption is depicted on the right.. Note also the axis perpendicular to the surface z, the depletion region z_0, work function Φ, electron affinity χ and electrochemical potential μ.

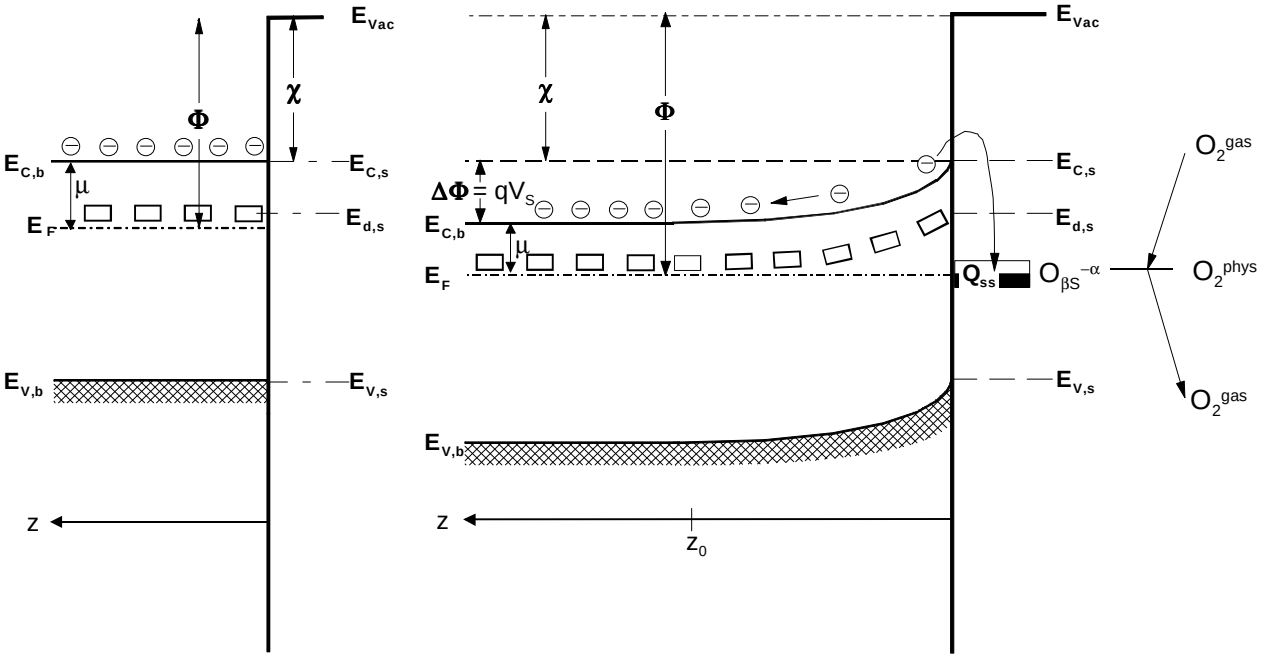

Figure 1-9: Typical schema for an n-type semiconductor (SnO_2)

The chemical and electrical characteristics of the semiconductor solid are strongly influenced by the development of double layers at the surface and can even be dominated.

From an electrical standpoint, the formation of a double layer represents injection or withdrawal of charge to or from the bands of the semiconductor. They represent a change in the density of current carriers. Additionally, through the relocation of the Fermi level E_F in relation to the vacuum energy E_{Vac}, the work function Φ of the solid changes.

The chemical properties of the solid surface are also governed in many cases by double layers. The newly introduced surface barrier translates to an activation energy increase $\Delta E_A = qV_S$ for an electron transfer between the semiconductor and a gaseous molecule (necessary for a chemical reaction). The availability of electrons and thereby the probability of a reaction is decreased. Or, differently put, the formation of the double layer will, by electrostatic repulsion, decrease the density of charge carriers near the surface, which, in turn, will decrease the rate and energy of further adsorptions.

1.4.3 From Charge Transfer to Sensor Signal

The band bending (i.e. surface energy barrier for electrons trying to travel from the bulk to the surface) induced by interaction of the tin dioxide solid with oxygen is the initial electronic situation a gaseous species encounters if converging to the sensor surface. Depending on the reactivity of the remaining surface sites as well as the adsorption of gaseous species on the metal oxide one of the following will result:

- Molecular (non-dissociative) adsorption, in which the interaction is mainly by σ-donation and/or π-bonding interaction
- Dissociative adsorption, in which a molecule dissociates homolytically or heterolytically upon adsorption. Usually an anion-cation coordinatively unsaturated pair site is required. Dissociation of H_2O into H^+ and OH^- is an example of heterolytic dissociative adsorption into charged species.
- Abstractive adsorption, in which the adsorbate abstracts a species from the surface or a previously adsorbed species from the surface. The former is often a proton and commonly occurs on acidic oxides. The latter could be previously adsorbed oxygen.
- Reductive (oxidative) adsorption, in which an adsorbed molecule is oxidised while the surface is reduced, or vice-versa.
- Catalysis, in which the surface acts as catalyst and lowers the activation energy for a reaction between adsorbed species and a previously adsorbed molecule. The surface remains chemically unchanged by the interaction.

As the sensor measures a change in the surface conductivity of SnO_2, only a change of its electronic properties, i.e. a free charge transfer from or to an adsorbed species will result in a sensor signal. Other surface reactions may occur that do not influence the surface band bending. Examples include surface reactions that do not involve the solid and dipole-dipole-interactions with adsorbed hydroxyl groups. Thereby the electron affinity χ or work function Φ of the sensor surface may be changed without a resulting sensor signal. Therefore, only the reductive/oxidative and abstractive adsorption will result in a sensor signal as defined in this work, i.e. a change of the metal oxide sensors conductivity. Figure 1-10 gives an overview of the possible effects such an adsorption with charge transfer has on the electronic properties of the semiconductor.

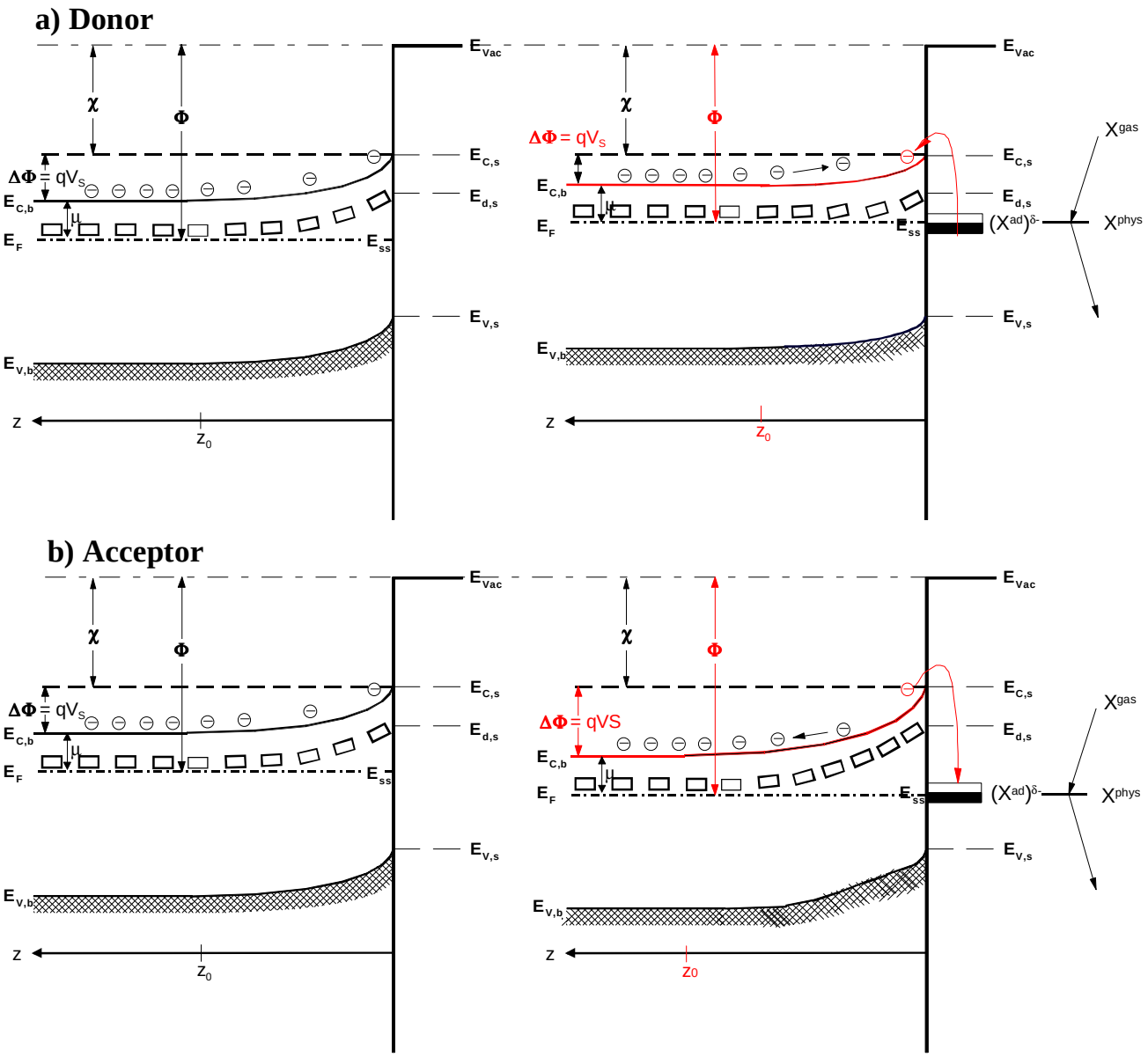

Figure 1-10*:* Adsorption of gaseous species and their effect on the electronic properties of an n-type semiconductor (SnO_2).

A brief guide to Figure 1-10 is in order: a) Gaseous species acts as donor: (left) surface band model, (right) changes to the electronic properties induced by the charge transfer from the adsorbate to the conduction band E_C: decrease of the surface potential barrier qV_S, depth of the depletion region z_0 and work function Φ and increase of free charge carrier concentration. b) Gaseous species acts as acceptor: (left) surface band model, (right) changes to the electronic properties induced by the charge transfer from the conduction band E_C to the adsorbate: increase of the surface potential barrier qV_S, depth of the depletion region z_0 and work function Φ and decrease of free charge carrier concentration.

Gases with low electronegativity can act as donors, transferring electrons to the semiconductor. The increase in charge density will reduce the surface potential barrier, depth of the depletion region and work function resulting in an increased conductivity. However, reducing gases utilised in this work, such as carbon monoxide or hydrocarbons, do not directly interact with the semiconductor. Instead, they react with adsorbed oxygen as mentioned for the abstractive adsorption. The electron previously trapped by the adsorbed oxygen species is released into the conduction band of the metal oxide upon desorption of the reaction product. In this way the electronic properties of the semiconductor are affected indirectly by a surface reaction with the same results as for a donor interaction: increasing in charge density and thereby increasing the conductivity.
Conversely, oxidising gases, such as nitrogen dioxide or ozone, will act as acceptors, trapping electrons from the semiconductor at surface states. The decrease in charge concentration will increase the surface potential barrier, depth of the depletion region and work function resulting in a decreased conductivity just as for the adsorption of oxygen discussed

Adsorption, interaction and reaction of selected adsorbents with SnO_2 Surface

Gas sensors are usually operated under atmospheric conditions which means in a background of oxygen and humidity. The basics properties and characteristics of oxygen and water will be presented in the next two sections. Carbon monoxide will also be detailed as this is our target gas in a third section.

1.4.4 Adsorption of Oxygen (O_2)

Ionosorption of oxygen is of particular importance for gas sensors due to its effect on the charge carrier concentration. However, at present, there is no unambiguous experimental evidence on the forms of oxygen adsorption, at ambient pressure and elevated temperatures, on real sensors/sensor materials.
The following surface oxygen species have been reported, (see Figure 1-11) mainly observed with spectroscopic techniques (TPD [28],[29]and ESR [30],IR [31]) on the surface of tin dioxide: at lower temperatures (<150-200°C) oxygen adsorbs on SnO_2 non-dissociatively in a molecular form (either neutral $O_{2\,(ads)}$ or charged:

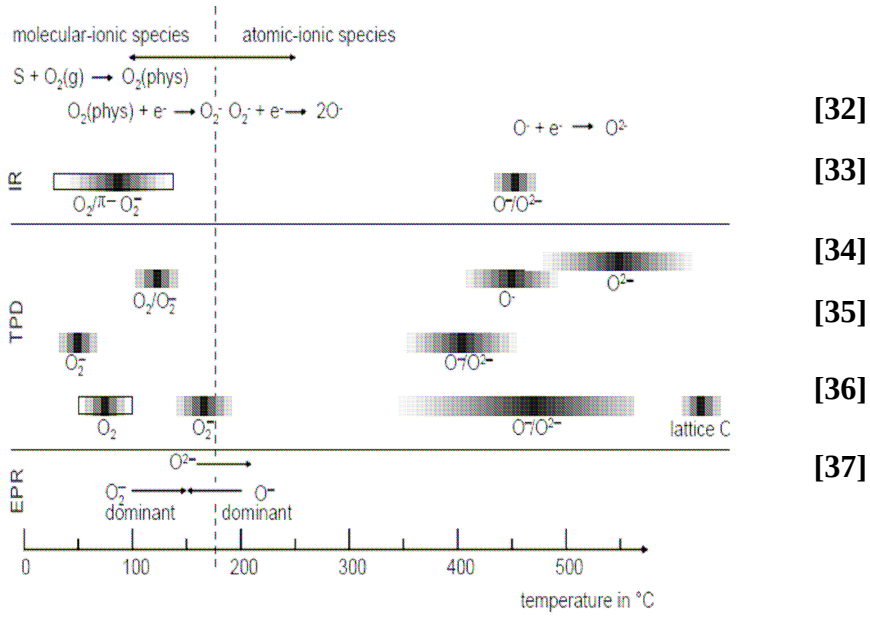

Figure 1-11: Oxygen species detected at different temperature on tin oxide surfaces with IR (infrared analysis), TPD (temperature programmed desorption), EPR (electron paramagnetic resonance).

1.4.5 Water (H_2O)

In nearly every application water vapor is present as an interfering gas. For this reason the interaction of the semiconductor surface with water is of great interest. TPD and IR studies showed, as summarised in Figure 1-12, that the interaction with water vapour results in molecular water adsorbed by physisorption or hydrogen bonding, and hydroxyl groups. Above 200°C molecular water is no longer present, whereby OH groups are continue to exist above 400°C. IR investigations prove the presence of hydroxyl groups. However, the way in which and where the hydroxyl groups are fixed on the tin dioxide is still under discussion. There are publications claiming that the hydroxyl groups are based on an acid/base reaction of the OH^- sharing its electronic pair with the Lewis acid site (Sn) and leaving the weakly bonded proton, H^+, ready for reactions with lattice oxygen (Lewis base) or with adsorbed oxygen [38]. Others assume a homolytic dissociation of water resulting in two hydroxyl groups, an ‘isolated’ hydroxyl bond to Sn and a ‘rooted’ hydroxyl group including lattice oxygen [26][39]

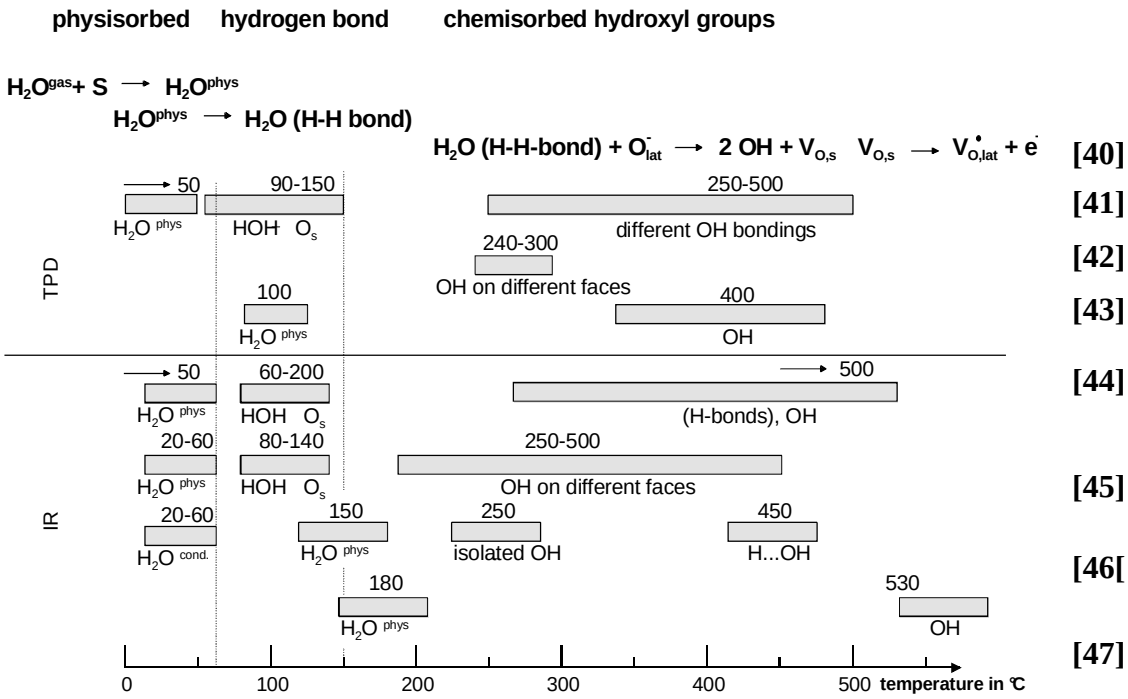

Figure 1-12: Literature survey of water-related species [48] formed at different temperatures at SnO_2 surfaces. Results via IR (InfraRed analysis) and TPD (Temperature Programmed Desorption).

All experiments reported a reversible decrease in the surface resistance in the presence of water. The lessened resistance does not vanish with the molecular water but with the disappearance of hydroxyl groups and could therefore be related to the presence of these hydroxyl groups [49]. Various types of mechanisms have been suggested to explain this finding. Two direct mechanisms have been proposed by Heiland and Kohl [37]. The first mechanism attributes the role of electron donors to the 'rooted' OH group, which includes lattice oxygen according to:

$$H_2O + Sn_{Sn}^{X} + O_o^{X} \rightleftharpoons {}^{-}HO\text{-}Sn_{Sn} + OH_O^{\bullet} + e^{-}$$

$$H_2O + Sn_{lat} + O_{lat}^{-} \rightleftharpoons (HO - Sn_{lat}) + (O_{lat}H)^{+} + e^{-} \qquad \textbf{Eq 1-16}$$

whereby Sn_{lat} and O_{lat} are tin and oxygen atoms in the lattice.

The reaction would imply the homolytic dissociation of water and the reaction of the neutral H atom with the lattice oxygen:

$$H^{+} + O_O^{X} \rightleftharpoons OH_O^{\bullet} + \qquad \textbf{(Eq 1-17)}$$

The second mechanism takes into account the reaction between the proton and the lattice oxygen and the binding of the resulting hydroxyl group to the Sn atom. The resulting oxygen vacancy produces additional electrons by ionisation according to:

$$H_2O + 2\,Sn_{Sn}^{X} + O_O^{X} \rightleftharpoons 2(HO\text{-}Sn_{Sn}) + OH_O^{\bullet} + e^- \qquad \textbf{Eq 1-18}$$

Others [50], [51] assumed that instead of a reaction with the surface lattice, a reaction with chemisorbed oxygen, which results in two hydroxyl groups linked to Sn occurs.
Morrison [52] as well as Henrich and Cox [53] consider an indirect effect, i.e. the interaction between either OH^- or H^+ with an acidic or basic group, which are also acceptor surface states. The co-adsorption of water with another adsorbate, which could be an electron acceptor, may change the electron affinity of the latter. Henrich and Cox suggested that pre-adsorbed oxygen could be displaced by water adsorption. In addition, others have found hints for the influence of water vapour on oxygen chemisorption. Caldararu and others [54 55,56] assume a blocking of the adsorption sites for oxygen by water. For all these mechanisms, the particular state of the surface plays a major role. Surface doping can also influence these phenomena. Egashira et al [57] showed by TPD and isotopic tracer studies that the rearrangement of oxygen adsorbates due to the presence of water vapour depends on surface doping. Williams and Morris et al. also reported that H_2O displaces chemisorbed oxygen by H_2O_{ads} and OH_{ads} producing on SnO_2 a surface electronic state such as a surface hydroxyl species, which has a higher energy state than an oxygen species alone, which is displaced [58].
Clifford and Tuma [59] approximated the influence of water vapour in synthetic air empirically by:

$$R = R_0\left(1 + k_{H_2O} \cdot p_{H_2O}\right)^{-\beta} \qquad \textbf{Eq 1-19}$$

with the water-independent constants R_0, k_{H2O} and β and the water concentration in volumetric ppm pH_2O.

1.4.6 Carbon monoxide (CO)

Carbon monoxide is one of the main gases of interest in the field of gas sensor applications. It is the target in case of fire detection, incomplete burning, etc. as well as an interfering gas because of its high reactivity with semiconductor gas sensors. Because of this, CO is often chosen – even more than H_2 – to typify the performance of sensors. In addition, the physical and chemical properties of CO facilitate investigations, monitoring CO and its

typical reaction product CO_2; with the help of IR one can trace the production of CO_2 by looking at its adsorption wavelength.

In the following a distinction is made between CO interaction with SnO_2 surfaces in the presence of oxygen, which is well characterised and in its absence (no UHV conditions), where not much data is available.

- **In the presence of O_2**

Carbon monoxide is considered to react with pre-adsorbed or lattice oxygen [60]. IR studies identified CO-related species i.e. unidentate and bidentate carbonate between 150°C and 400°C and carboxylate between 250°C and 400°C. A summary of the IR results is presented in Figure 1-13. Moreover, the formation of CO_2 as a reaction product between 200°C and 400°C was identified by FTIR.

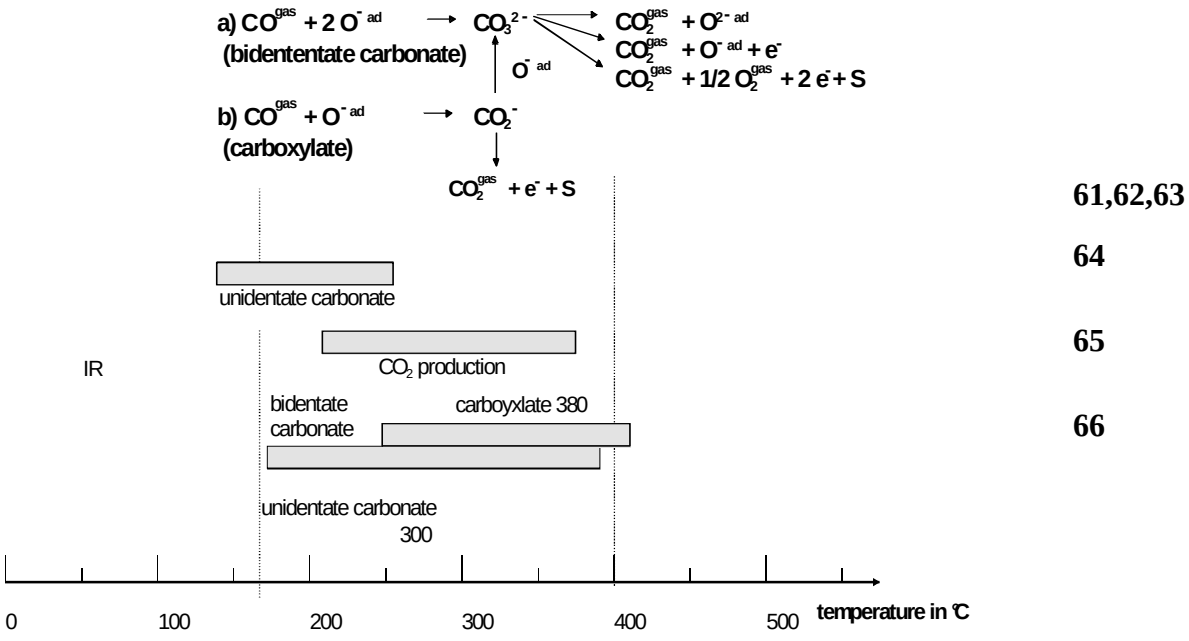

Figure 1-13: Literature survey of CO-related species found by means of IR (infrared analysis) at different temperatures on a (O_2) preconditioned SnO_2 surface. For details, see listed references.

All experimental studies in air at temperatures between 150°C and 450°C report an increase in the surface conduction in the presence of CO. It is generally accepted that the CO reacts with ionosorbed oxygen species and thus releases electrons in the conduction band.

Morrison derived – using a simplified model – the dependence of the resistance on the partial pressure of CO [67]. He assumed that oxygen is present as O_2^- and O^- at the sensor surface according to:

$$e^- + O_2 \rightleftharpoons O_2^-;\ e^- + O_2^- \rightarrow 2O^- \qquad \textbf{Eq 1-20}$$

Hereby the reaction on the left (Eq 1-20) is neglected due to the small probability of such a reaction, which is of a second order in O^- concentration. In addition, he assumed that due to the high reactivity of O^-, the reaction of O_2^- with CO could be neglected. The reaction is:

$$CO + O^- \rightarrow CO_2 + e^- \qquad \textbf{Eq 1-21}$$

The detailed description of how the resulting steady state equation can be solved is given in [68]. An overview of the various conductance dependencies found is presented in **Table 1-2**.

Table 1-2: **Equations describing the dependence of conductance on CO concentration as derived empirically or from theoretical calculations.**

Equation	**Comments / Assumptions**	**Literature**
$G \sim n_S \sim p_{CO}^{2\beta/(\alpha+1)}$ $G \sim n_S \sim p_{CO}^{\beta/(\alpha+1)}$	L_D>r: reactive oxygen species: $O_\beta^{\alpha-}$; β=1, 2; α=1, 2, i.e. O_2^-, O^-, O^{2-} L_D<r: reactive oxygen species: $O_\beta^{\alpha-}$; β=1, 2; α=1, 2, i.e. O_2^-, O^-, O^{2-}	[69]
$G \sim p_{CO}^{0.5}$	empirical	[70]
$G = G_0 + A_1 p_{CO}^{1/2}$	rate equations + SC[1] physics	[71]
$G = G_{air} + A_1 p_{CO}^{n}$	empirical	[72]
$G \sim (A_0 + A_1 p_{CO}^{m})^{0.92}$	SC physic	[70]
$G^2 - G_{air}^2 \sim p_{CO}$	rate equation and SC physic	[73]
$G^\beta - G_{air}^\beta \sim p_{CO}$, $\beta \geq 2$	rate equations and SC physics	[74]
$G \sim 1/A \sim \ln(p_{CO})$ $n_S \sim n_b \exp(-eV_S^{eff} / kT)$	open neck closed neck	

[1] semiconductor

It is well known that the presence of water in the ambient atmosphere has a strong influence on CO detection. The fact [75, 76] that water enhances the interaction of CO has been observed. Three models have been proposed which may account for this observation. On one hand, it is assumed that water enhances the reaction with oxygen [77]. On the other hand, a reaction of CO with hydroxyl groups [78] , [79], [80] is proposed. Various equations have been derived for the sensor conductance in the presence of CO and water vapour. Kappler et al. reported that an increase in humidity leads to an increase in the number of oxygen vacancies (equation 12) [78]. The oxygen vacancies enhance the chemisorption of oxygen and form specific oxygen sites [81], [82]. The increase in the number of available oxygen reaction partners for CO leads to an enhancement of the sensor signal

A summary is given in Table 1-3. Moreover, in some cases a correlation between ageing and the irreproducibility of sensors and the presence of water-related species could be found [83], [84].

Table 1-3: Equations describing the dependence of conductance on the CO concentration and the water vapour pressure as derived empirically or from theoretical calculations.

Equation	**Comments / Assumptions**	**Literature**
$G \sim (1+k_{CO}\, p_{H_2O}\, p_{CO})^{\beta}$	Empirical	[85]
$G \sim (p_{CO}\, p_{H_2O})^{1/3}$	rate equations and SC physics	[86]
$G \sim p_{CO}/p_{0,CO})^{\beta CO}(p_{H_2O}/p_{H_2O,0})^{\beta H_2O}$	rate equations and SC physics	[87],[88]

- **CO interaction in the absence of oxygen**

There are only a few papers dealing with gas interaction of semiconductor SnO_2 gas sensors in the absence of oxygen. The few relevant for this thesis are listed below.

Safonava at al. studied the mechanism of CO sensing in nitrogen for nanocrystalline undoped and Pd doped SnO_2 by Mössbauer spectroscopy and conductance measurement [89]. The conductance measurements were coupled with Mössbauer spectroscopy [90] and carried out at different temperatures (50 – 380°C) and at a constant CO concentration of 1% in nitrogen. With the help of the Mössbauer spectroscopy the reduction of Sn(IV) to Sn(II) in the presence of CO was studied. They found that the electrical response of 1% w.t. Pd doped and undoped SnO_2 at temperatures between 125°C and 380°C is associated with the process announcing

the beginning of Sn (IV) to Sn(II) transition. Accordingly, CO reacted with lattice oxygen, but, as no metallic tin was detected in the spectra, Sn is not completely reduced.
In situ Electron Paramagnetic Resonance spectroscopy (EPR) confirmed the change of chemisorbed oxygen O_{2S}^{-} and single ionized oxygen vacancy $V_O^{\bullet}$ concentration in SnO_2 during the interaction with CO/N_2 gas mixtures [91]

1.5 Conduction model in the sensitive layer

The sensitive layer of thick film sensors is very porous and consists of numerous interconnected metal oxide grains. They can be either single crystals or polycrystalline agglomerates. The high porosity enables the ambient gases to access these intergranular connections. Because of this, a depletion layer is created around the grains, the extension of which is determined by the partial gas concentrations and the bulk characteristics of SnO_2. Therefore, grain boundaries, as bottlenecks for electronic grain-grain transfer, play an important role in the sensing layer conduction and therefore, in the detection mechanism.
If the grains are punctually connected and the depletion layer depth λ_D is much smaller than the grain radius r, a grain bulk area unaffected by the gas will still exists. In order to contribute to electronic conduction, the electrons originating from the “bulk” must overcome these depletion layers and the related potential barriers with the barrier heights eV_S at the intergranular contacts. This is equivalent to a significant resistance increase of the sensitive layer.
As discussed before, the overall resistance R is a function of the contributions of the bulk and the surface of SnO_2 grains, the electrode contacts and the intergranular contacts. The properties of the bulk, i.e. the part of the grain, which is not depleted, are not influenced by surface phenomena due to the rather low operation temperatures (≤ 400°C). The resistance contribution of the electrode contacts, which is related to Schottky barriers between the sensing layer and electrodes, depends on the contact material. Electrodes might also show a gas dependent catalytic effect. The resistance contribution of intergranular contacts is related to the gas dependent barriers, which have to be overcome for the numerous intergranular contacts between the electrodes. In most cases, the resistance contribution of the numerous intergranular contacts dominates the other contributions.
Then the conduction of thick film sensors can be approximated with the help of the Schottky model by:

$$G = G_o(T) \cdot e^{\frac{-eV_S}{kT}} = G_o'(T) \cdot e^{\frac{E_F - E_C}{kT}} \cdot e^{\frac{-eV_S}{kT}}$$ **Eq 1-22**

where G_0 and G_0' depend on the temperature and geometric properties of the layer.

1.5.1 Compact and porous layers

The differences in compact and porous layers are schematically sketched in Figure 1-14. In compact layers, the interaction with gases takes place only at the geometric surface. In porous layers, the volume of the layer is also accessible to the gases and in this case, the active surface is much higher than the geometric one. Porous layers are characteristic for thick film preparation techniques and RGTO (RHeotaxial Growth and Thermal Oxidation, [92]).

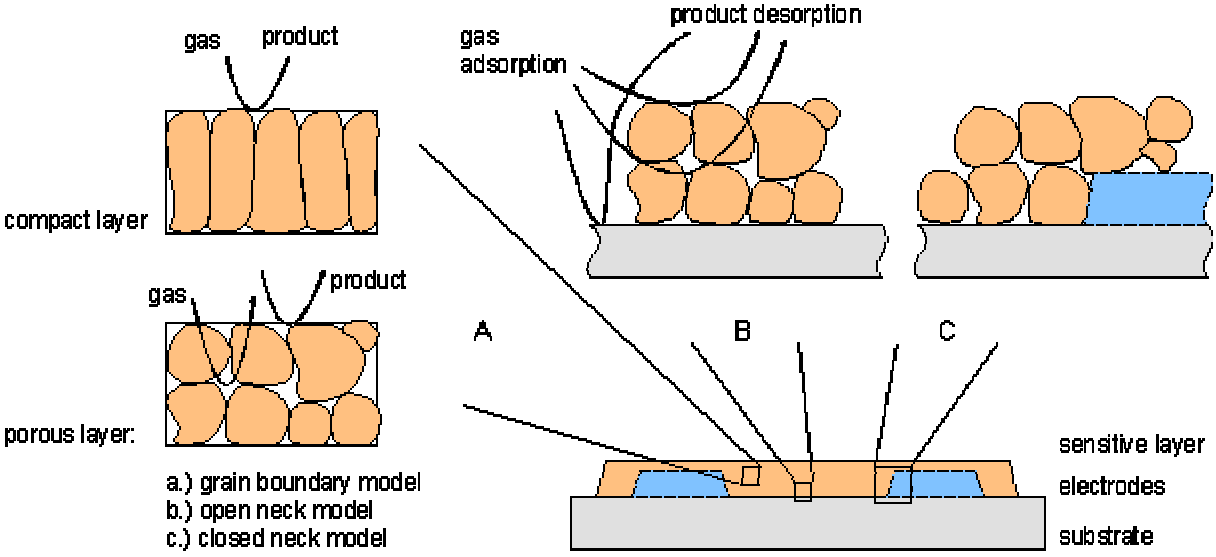

Figure 1-14: Schematic layout of typical resistive SnO_2 sensor. The sensitive metal oxide layer is deposited over the metal electrodes onto the substrate. In case of compact layers, the gas cannot penetrate into the sensitive layer and the gas interaction is only taking place at the geometric surface. In the case of porous layers, the gas penetrates into the sensitive layer down to the substrate. The gas interaction can therefore take place at the surface of individual grains, at grain-grain boundaries and at the interface between grains and electrodes and grains and substrates [Bâr01].

The type of layer determines the conduction mechanism of the sensor. Here, only a small summary is given; for detailed information see [93].

For compact layers, there are at least two possibilities: completely or partly depleted layers[2], depending on the ratio between layer thickness and Debye length λ_D of the electron. For partly depleted layers, when surface reactions do not influence the conduction in the entire

[2] The depletion layer is formed due to gas adsorption like O_2.

layer the conduction process takes place in the bulk region. Formally, two resistances occur in parallel, one influenced by surface reactions and the other not; the conduction is parallel to the surface, and this explains the limited sensitivity of compact layers (see also Figure 1-15) For porous layers the situation can be further complicated by the presence of necks between grains. It may be possible to have all three types of contribution in a porous layer: surface/bulk (for large enough necks, layer thickness > thickness of depletion layer), grain boundary (for large grains not sintered together), and flat bands (for small grains and small necks). For small grains and narrow necks, when the mean free path of free charge carriers becomes comparable with the dimension of the grains, a surface influence on mobility should be taken into consideration. This happens because the number of collisions experienced by the free charge carriers in the bulk of the grain becomes comparable with the number of surface collisions; the latter may be influenced by adsorbed species acting as additional scattering centres [94].

Figure 1-15 illustrates the way in which the metal-semiconductor junction, built at electrode-sensitive layer interfaces, influences the overall conduction process. For compact layers they appear as a contact resistance (R_C) in series with the resistance of the SnO_2 layer. For partly depleted layers R_C could be dominant, and the reactions taking place at the three-phase boundary, electrode-SnO_2-atmosphere, control the sensing properties.

In porous layers, the influence of R_C may be minimized due to the fact that it will be connected in series with a large number of resistances, typically thousands, which may have comparable values (R_{gi} in figure). Transmission Line Measurements (TLM) performed with thick SnO_2 layers exposed to CO and NO_2 did not result in values of R_C clearly distinguishable from the noise [95], 96], while in the case of thin films the existence of R_C was proved [97].

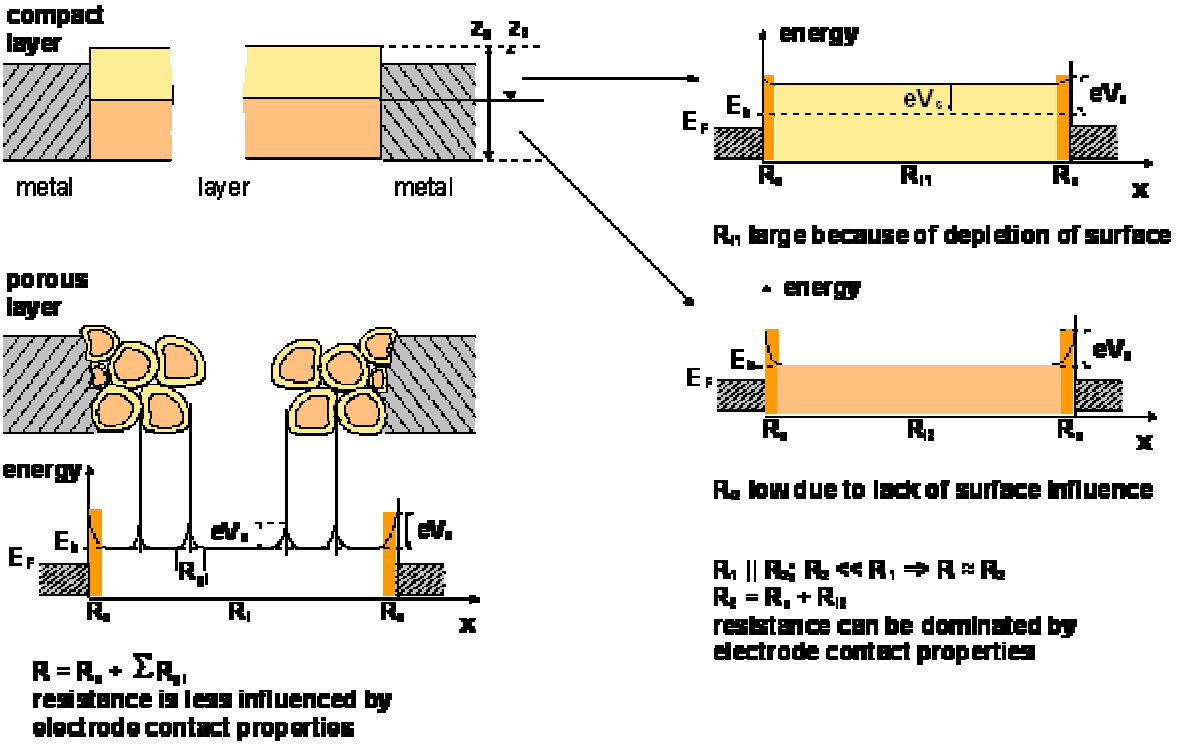

Figure 1-15: Schematic representation of compact and porous sensing layers with geometry and energetic bands, which shows the possible influence of electrode sensing layers contacts. R_C resistance of the electrode-SnO_2 contact, R_{l1} resistance of the depleted region of the compact layer, R_{l2} resistance of the bulk region of the compact layer, R_1 equivalent series resistance of R_{l1} and R_C, R_2 equivalent series resistance of R_2 and R_C, R_{gi} average intergrain resistance in the case of porous layer, E_b minimum of the conduction band in the bulk, eV_S band bending associated with surface phenomena on the layer, and eV_C also contains the band bending induced at the electrode-SnO_2 contact.

1.5.2 Effect of the electrodes

In the different part of the sensor, it is important to consider the role played by the electrodes, whose impact on the response of sensing layer is generally neglected. However, most often used electrode materials in gas sensors, such Au and Pt, are also used in the sensitive layer as catalyst (in particular Pt [98]). It is possible that the electrodes which form the electrode-semiconductor interface can play also a catalyst and has a contribution to the overall resistance of the sensor. This part of the first chapter is dedicated to a review of the work already done about this topic.

As already seen, the contacts between semiconductor sensing material and metal electrodes also have some impact on the sensor resistance and sensing performance. If a metal and a semiconductor are brought into contact, electrons are transferred until the Fermi levels of both materials are equilibrated. If the Fermi level of the metal is above the Fermi level of the semiconductor, electrons are transferred from the metal to the semiconductor. A positive

charge layer at the metal surface and a negative one near the semiconductor surface are created. Band bending and an electric field result. The electrical contact is quasi-ohmic for n-type semiconductors. If the Fermi level of the semiconductor is above the Fermi level of the metal, electrons are transferred from the sensing material to the metal. A depletion layer is created in the n-type semiconductor, an electric field appears and the bands are bent upwards. The resulting potential barrier which electrons have to overcome to contribute to the electronic conduction is determined from the difference in Fermi energies E_F. In this case the resulting Schottky contact shows diode-like behaviour and the resistance is increased. Both situations are sketched in Figure 1-16.

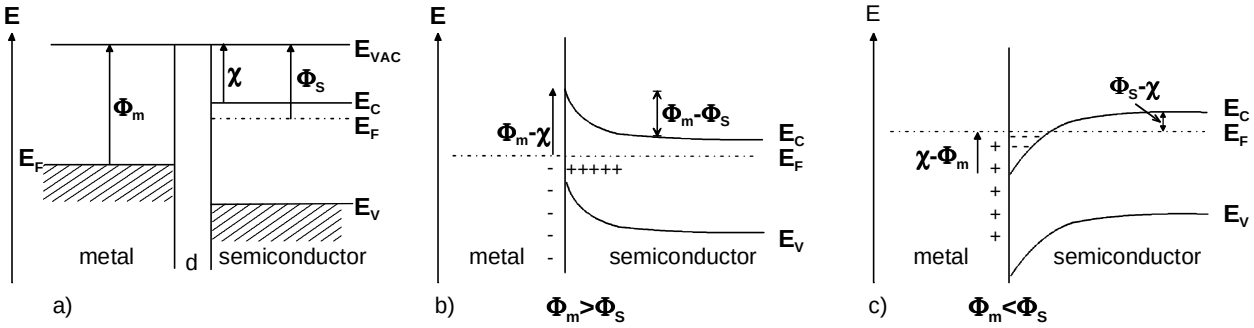

Figure 1-16 : Metal-semiconductor contact. a) Band structure of metal and semiconductor ($\Phi_m>\Phi_s$) before contact. b) Metal–semiconductor contact ($\Phi_m>\Phi_s$). Electrons are transferred from semiconductor into the metal until the Fermi levels are equilibrated. A depletion layer and an energy barrier result. The resistance behaviour of such a contact is diode-like. c) Metal–semiconductor contact ($\Phi_m<\Phi_s$). Electrons are transferred from the metal into the semiconductor. A small enrichment layer at the interface inside the semiconductor results. The resistance behaviour is quasi-ohmic.

In the case of porous metal oxide films, the gas may also reach the metal electrodes. Hence the contacts can additionally have a catalytic effect and may support the interaction for a particular gas.

1.5.2.1 Effect of the metal inside the sensitive layer in semiconductor

Sensitization with noble or alkali metals is often used to improve the performance of the dioxide sensors: it enhances the stability, response and recovery times, and it decreases the cross sensitivity to water vapor (Pd) and the operating temperature. Although the expression ‘doping‘ is in common use, it is, in most of the cases, not doping in the classical semiconductor physics sense but rather a loading of metallic clusters onto the surface of metal oxide grains (Figure 1-17).

In general, upon exposure of as-prepared sensors to target gas the metal clusters at the surface of metal oxide can:

- react directly with the target gas, catalyzing its conversion without interaction with the supporting metal oxide;
- react directly with the target gas, where the target gas removes electrons from the metal. The metal, in turn, compensates the lose of electrons by withdrawing them from the semiconductor which leads to the formation of the depletion layer and band bending - *Fermi level control* mechanism;

- increase the concentration of reaction partners at the reaction site. The metal can dissociate the reactant i.e. O_2 [99, 100] ,H_2 [101] and *spillover* the resulting species at the surface of the metal oxide;

More detail can be told about the spill over effect. The O_2 molecule can dissociated in contact with a catalyst metal. After the dissociation of the O_2 molecule, the oxygen atom can migrate to the surface of oxide and take one electron from the oxide to be stabilized one the oxide site. This effect changes the depletion layer of the oxide. The following equation summarize the spill over effect

$$O_2\,(gas) + 2\,s_M \rightarrow 2\,O\text{-}s_M$$

$$O\text{-}s_M + e_{OX} + s \rightarrow O^-\text{-}s + s_M$$

s_M adsorption site of the metal

s adsorption site of oxide

The presence of catalytic metal makes easier the regeneration of O-s species

In presence of a gas(R) two possibilities can be mentioned:

The first one is the Dissociation of R on the catalytic metal and then a reaction with O-s. The typical example is H_2:

$$H_2\,(gaz) + 2\,s_M \rightarrow 2\,H\text{-}s_M$$

$$H\text{-}s_M + s \rightarrow H\text{-}s + s_M$$

$$2\,H\text{-}s + O^-\text{-}s \rightarrow H_2O\,(gaz) + e_{OX} + 3\,s$$

In this case, the consummation of the oxygen species gives the evolution the electrical properties [102]

In this first mechanism, the oxidation of the gas R doesn't take place directly on the surface of the catalyst. Here the catalyst favours simply the dissociation of the different gas. This effect is called "chemical sensibilization" and a good dispersion is necessary to get the better effect.

The second mechanism is simply catalysis on the metal.

- locally increase the temperature in the vicinity of the metal center leading to an enhanced catalytic activity [103].

Within this study the Pd additive was used. Pd additive in SnO_2 is foremost known for enhancing sensitivity to CO in the presence of water vapor.

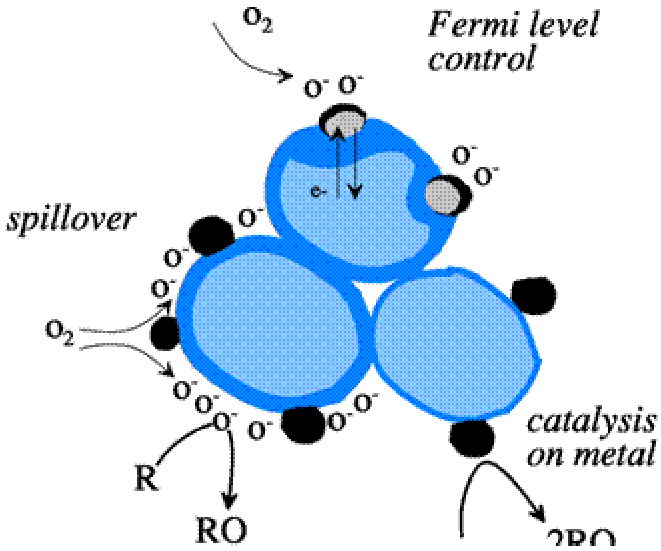

Figure 1-17 : Effect of loading of the metal cluster at the surface of the metal oxide.

There is no common agreement on which of the two mostly accepted models (spillover or Fermi level control) is responsible for Pd activity. The early investigation on well defined Pd clusters on SnO_2 suggests the Fermi level control mechanism [104]. Having also in mind that Pd clusters under atmospheric conditions are fully oxidized this suggestion seems sound: PdO has much large work function and thus causes an electron depletion zone in the SnO_2.

1.5.2.2 Effect of the nature of the electrode

In 1986, C. Pijolat & Al [105] revealed an influence of the electrodes on SnO_2 based sensor for the detection of Benzene. Figure 1-18 the main results are illustrated; depending of the nature of the electrodes (gold or platinum), the conductance as a function of the temperature under Benzene is plotted. The maximum of the peak is shifted. The performance of the sensor against this gas could be governed by the nature of the electrode and the operating temperature. This author introduced the importance of the metal-semi-conductor interface and the band-bending where the height is managed by the nature of the metal.

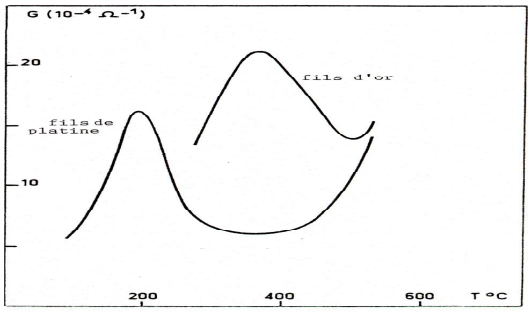

Figure 1-18: Influence of the type of metal wires on the temperature-conductivity curve [78].

Few years after, Schweizer-Berberich [106] tested the impact of the electrodes on gas sensing properties of nanocrystalline SnO_2 gas sensors. A clear trend, in Figure 1-19 was found showing an enhancement of the sensor response with Pt electrodes and all the differently materials (undoped and doped SnO_2). In fact for undoped SnO_2 or Pt doped SnO_2, the effect of the electrodes is observed. This sensitization effect occurs in addition to the effect of the doping.

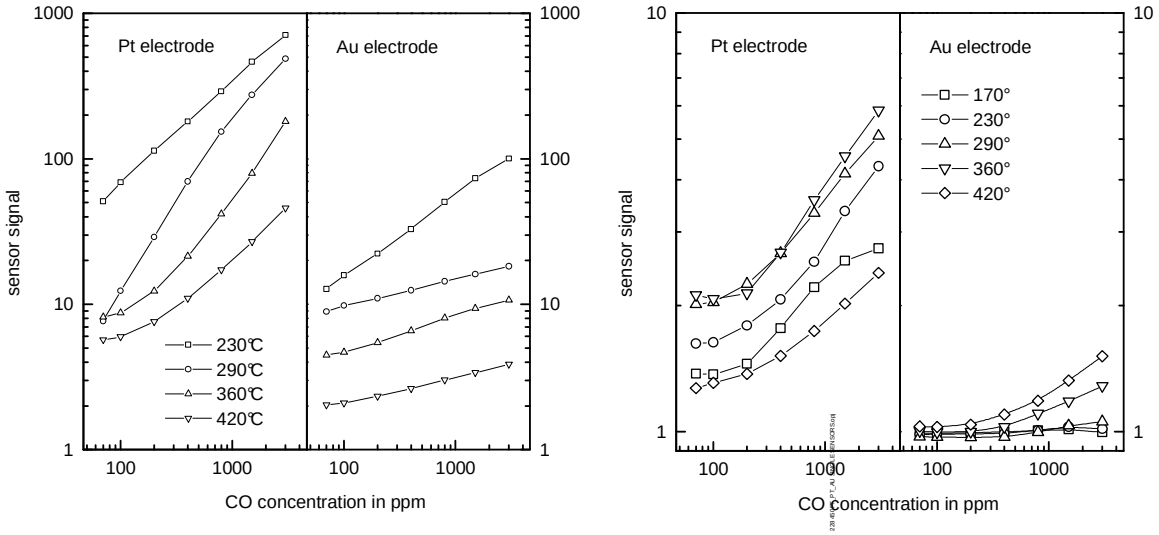

a) Pt doped SnO_2 b) undoped SnO_2

Figure 1-19 : (a)-Calibration curves at several operation temperatures of 450°C annealed Pt doped SnO_2 powder on substrates with platinum electrodes (right) and gold electrodes (left). (b)-Calibration curves for CO at several operation temperatures of pure SnO_2 powder (112 nm) on substrates with platinum electrodes (right) and gold electrodes (left)

S.M.A Durrani [107] used four different natures of electrodes Ag, Al, Au, and Pt. A big difference appears between Ag and Al which are less sensitive whereas Au and Pt are more sensitive.

Lantto [108], in Figure 1-20 shows the conductance of three similar SnO_2 thick Film sensors (doped with 100 ppm of Sb), having Au, Pt and Au/Pt (one Au and the other Pt) electrodes, as a function of inverse temperature between 200 and 450°C in air with a humidity concentration of 1000 ppm. In the case of the sensor with Au/Pt electrodes, conductance values are given for both the polarization directions Au+/Pt- and Au-/Pt+. It is possible to conclude from these results that a contact resistance with some rectification characteristics is present at the Au/SnO, contact. The positive voltage at the Au electrode corresponds to the forward direction of an Au/SnO_2, Schottky diode. Many peculiarities, however, relate to the rectification property of the contact;

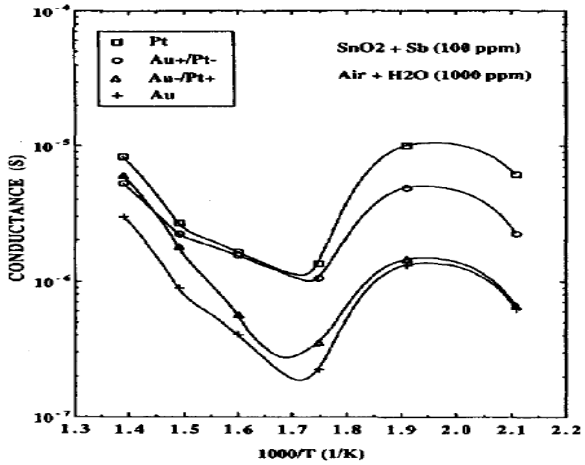

Figure 1-20 : Conductance of three similar Sb-doped (100 ppm) SnO_2, thick-film sensors with Au, Pt and Au/Pt electrodes as a function of inverse temperature in air containing 1000 ppm of H_2O. In the case of the Au/Pt sensor, results are given for both polarization directions of voltage (Au+/Pt- and Au-/Pt+).

SAukko [109] also studied the impact of the electrodes materials on the performance of sensor provided by Pt or Au electrodes. He shows that in some case the energy barrier between electrode and the sensing semiconductor could be significant compared to the energy between

the semiconductor grains. Sample with Pt electrode was more sensitive to H_2 whereas Au seems to give a better response to CO.

1.5.2.3 Effect of the geometry of the electrodes

1.5.2.3.1 Position

In addition to the type of metal used as contact, several authors note the significant effect of the position of the electrodes. S.M.A Durrani [110] and X.Vilanova [111] show an unexpected result that the electrodes placed on the top or side give a higher sensitivity, but electrodes placed on the bottom are the most interesting in terms of selective U.Jain[112] found the same conclusion using a numerical model with a slight difference: the relativity reactivity of the gas. The back contact sensor will be more selective for moderately reactive gases compared to less or more reactive ones, which is in general agreement with the observations made on Figaro gas sensors.

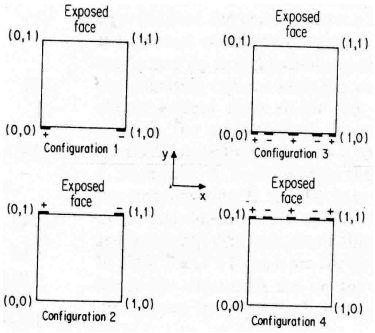

Figure 1-21: position study by Jain [84]

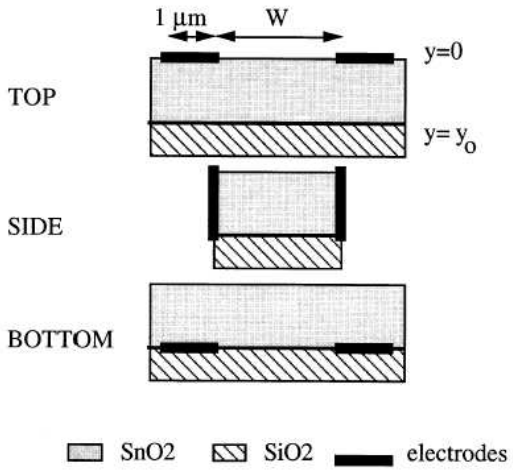

Figure 1-22; Structure simulated: A SnO2 active layer on a SiO2 substrate. Zero thickness ideal electrodes have been considered (Duranni) […]

1.5.2.3.2 The width between the electrodes

S. Capone [113] made some investigations about the influence of the spacing between the two electrodes; see Figure 1-23 and the nature of the electrodes (Au and Pt).The author

showed that the sensor with the shorter finger separation show a higher response to CO with Pt electrodes. The sensor provided with gold electrodes suffer from diffusion of metal into the the sensitive layer. The reason could be a higher collection efficiency of the electrical signal, due to the fact that the current, crossing short path is no too much influenced by charge trapping or barrier limited conduction. Sensors prepared with Pt electrodes have shown a higher resistance compared to sensors equipped with Au electrodes. Finally, she shows that the humidity enhances the response of CO greater in the case of gold than platinum. In other paper[114] […] she also demonstrates that the ageing of the contact is a major cause of the drift of the sensor.

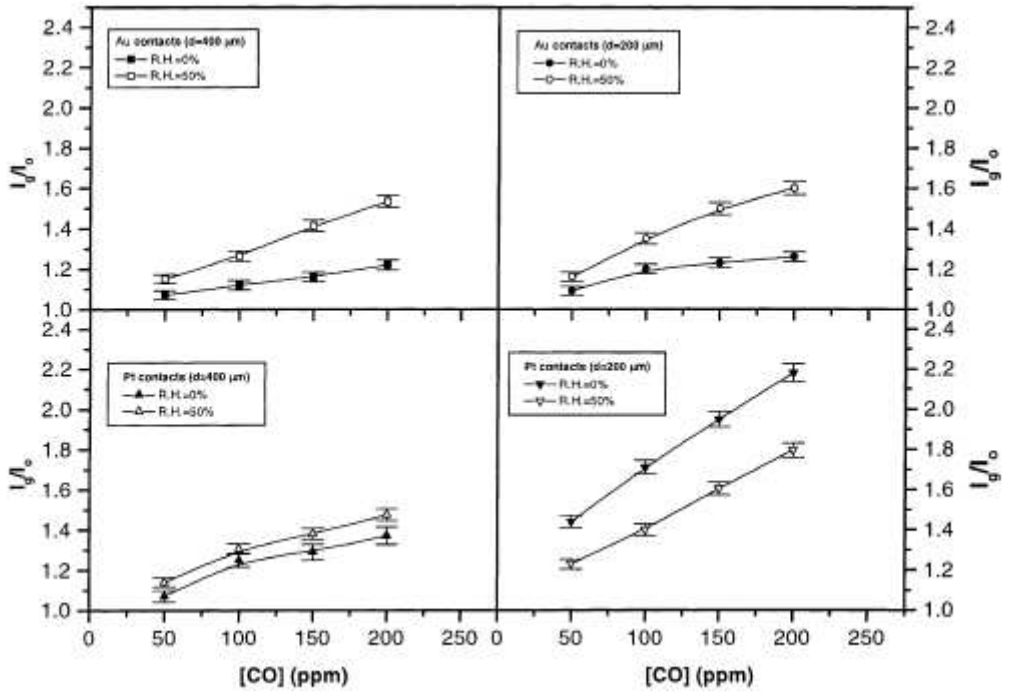

Figure 1-23: Calibration results for all types of electrodes configurations both in dry and wet air (50%)

U. Hoefer[115] uses the TLM, “Transmission line model”, to characterise the contribution of the electrodes in the overall resistance of the sensor. In Figure 1-24, under gas, this author shows that mainly the resistance near the electrodes is affected where in the same time the others are not.

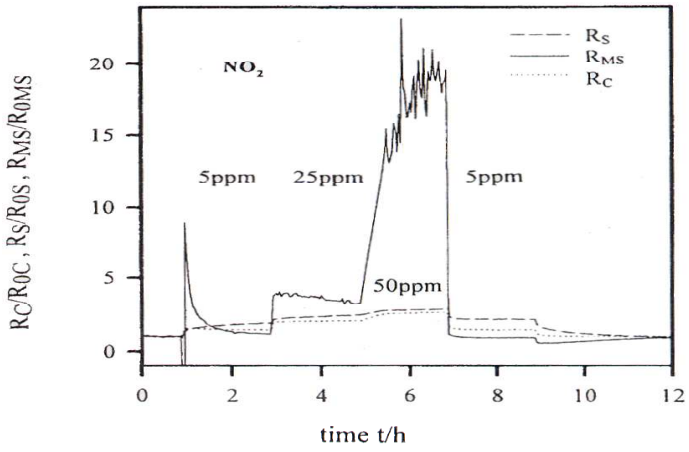

Figure 1-24 : NO_2 effect on the contact R_c, sheet resistance R_s and modified sheet resistanceR_{ms} of non catalysed TLM sensors Vs measurement time, T=300°C, 50 %RH.

1.5.3 Model of conduction

- Various approach

Various authors have tried to explain the role of the electrodes. Udo Weimar [116] showed by impedance spectroscopy that the essential of the phenomena seems to be localized near the electrodes. This author introduced the notion of the three boundary point (semiconductor/the metal/the gas) which seems to play an important role. The extraction of electrons from the depleted region causes a larger effect as compared to the changes in the "bulk" material between the contacts. K. Varghese[117] attributes the occurrence of the capacitance to the accumulation of adsorbed oxygen ion species at the sample-electrode contact region, Figure 1-25. This result confirms the main role played by the three boundary point.

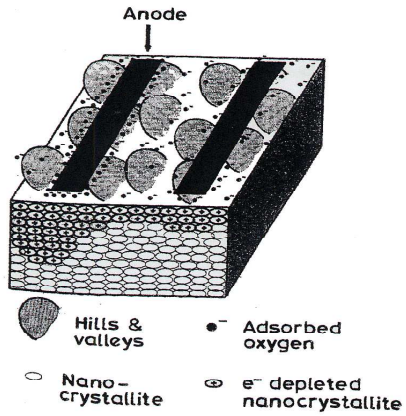

Figure 1-25: Schematic diagram showing accumulation of (O_{ads}^-) ions at the electrode-sample contact region and its effect on depletion layer width [...].

- Model of P Montmeat, basis of this study

In M.I.C.C. department in St Etienne, during the previous thesis of P Monmeat, the role of metal (gold) on the electrical response on tin oxide sensor was investigated thanks to the development of a particular test bench (Figure 1-27): it allowed separating the atmosphere surrounding SnO_2 region in contact with gold electrodes from the atmosphere in the area between electrodes.

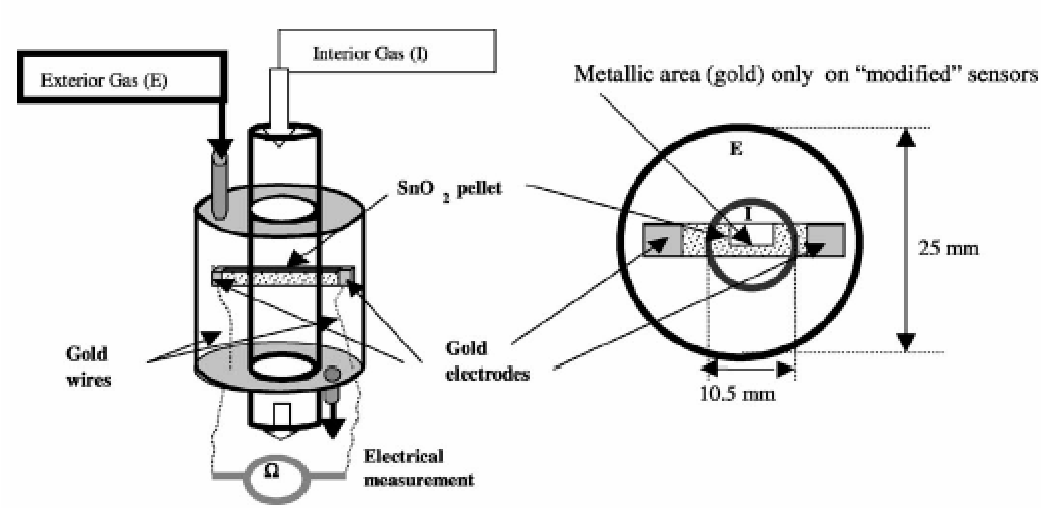

Figure 1-26 : Schematics of the test bench to generate different atmospheres: exterior gas (E) in contact with gold electrode areas, interior gas (I) in contact with only tin oxide for standard sensors and with tin oxide and the centered metallic area for modified sensors.

The action of oxygen and thus of a reducing gas such as CO, Figure 1-27, was under focus and is greatly enhanced in the region containing gold. This result associated with calorimetric tests, Figure 1-28, indicates the creation of specific oxygen species at the metal–oxide interface.

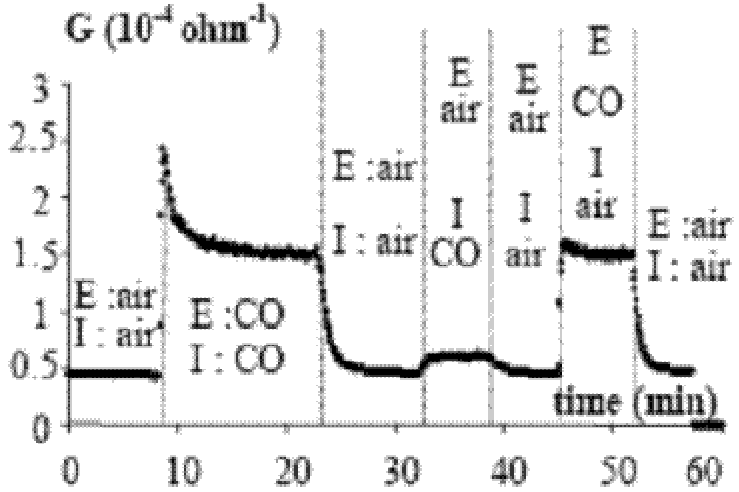

Figure 1-27: Electrical response of a sensor to CO (300 ppm) at 450 ◦C in a test bench with separate atmospheres (E: SnO_2/electrode area; I: SnO2 area).

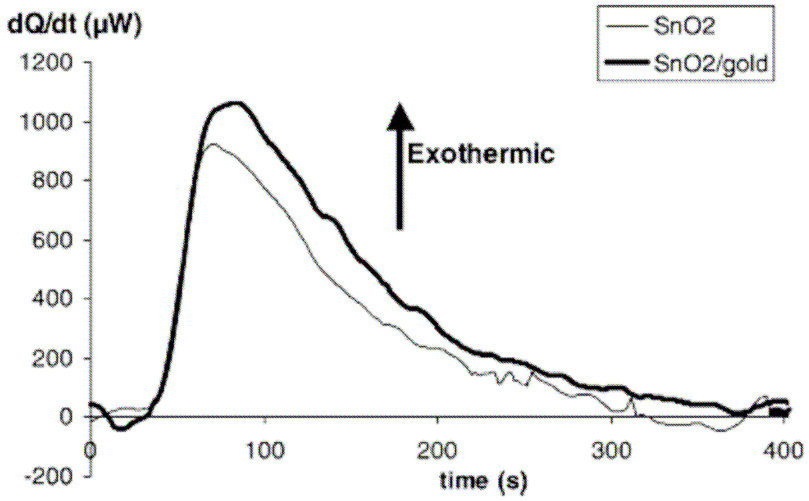

Figure 1-28 : Calorimetric signal obtained at 400 ◦C for an increase of oxygen pressure from 0.1 to 50 mbar for a pure SnO2 material and on SnO2+gold material.

A qualitative physico-chemical model, in Figure 1-29, based on the electronic effect of different oxygen adsorbed species, resulting in the increase of space charge area was proposed, more detail in [118].

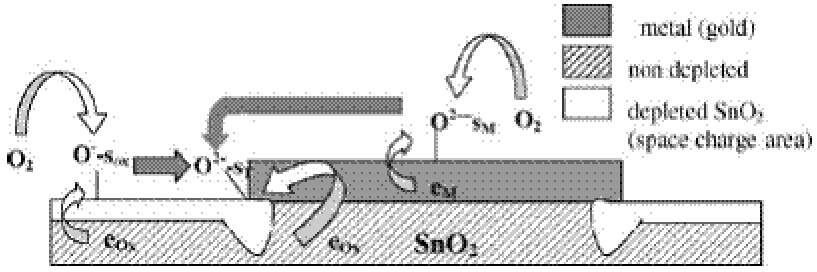

.

Figure 1-29: Proposed mechanism based on space charge area at the three boundary point (gas-metal-oxide) to explain metal effect on tin oxide electrical conduction, from [116].

Taking into account the previous physico-chemical mechanism, a geometrical model based on space charge area is proposed in order to quantify the influence of the sensor thickness. In agreement with the schematic representation of the model in Figure 1-29, it was considered that sensor is constituted of depleted areas located at the sensor surface and under the electrodes (three-boundary point) due to oxygen chemisorptions at these particular points, and of non-depleted area. At the moment, no experimental results bring information concerning the shape of the depleted area at the three boundary point. In order to simplify further calculations, it was considered a rectangular shape centered under the three boundary point Figure 1-30(a)). Then, it was supposed that the resistivity ρM of the not depleted area is constant and independent on the atmosphere. This hypothesis is supported by the experiments with separate atmosphere (Figure 1-26), as the gas has a negligible action in the inner area which only contains SnO_2 and is not under the influence of the three boundary point. Concerning resistivity ρS under air of the depleted area under the surface, it was assumed that it is constant within a weak thickness Figure 1-30 (a).

The result and the different parameters used are shown Figure 1-30 for SnO_2 based sensor in the presence of carbon monoxide and ethanol, for thickness varying from 10 to 80 µm.

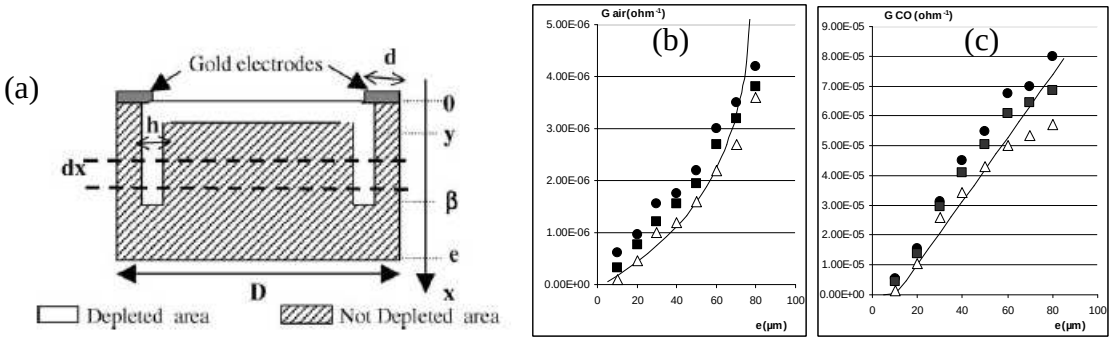

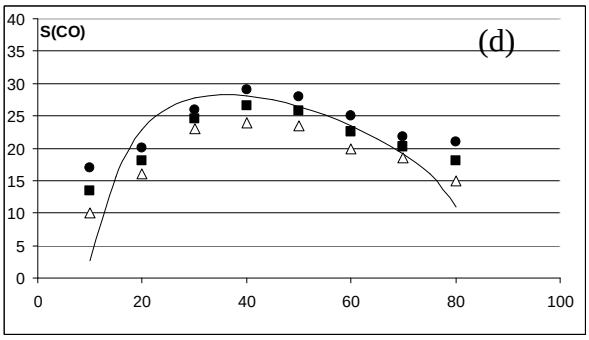

Figure 1-30: (a) Geometrical model of conductance with depleted area under the comparison between experimental measurements and simulated curves for conductance under air (b) , CO (c) and for the sensitivity (d). […].

Summary of the bibliography

The aim of this first chapter was to remind the general properties of the tin dioxide and especially which can be useful to understand our results.

In the SnO_2 used as sensor different contributions from the grain, the grain boundary can be clearly identified. Most of authors suggest an important role of the electrodes but a few of them have an explanation. The possibility of a particular zone called three point boundary that could play an important role on the detection is one of the justifications.

Due to its localization and the difficulties to get rid of the other contributions, it is difficult to have some proofs about the real possible existence of this region.

This study will try to add a contribution to understand the role play by the electrodes

CHAPTER 2

2 Material, sensors preparation and electrical measurements

Les méthodes de préparation relatives à la réalisation de nos échantillons seront présentées dans ce chapitre. Les différents montages électriques utilisés dans cette étude seront également décrits. Quant aux résultats obtenus sur l'influence de la nature des électrodes, nous les présenterons dans une dernière partie

.

The influence of electrode material on the properties of oxide semiconductor gas sensor was not often studied. Contact resistance or depletion layer that is formed in the electrode–semiconductor interface can in some cases have significant contribution on the response of the sensors, as reported by P Montmeat (cf. previous chapter). It is extremely difficult to characterize this region because it is generally "hidden" by the resistance of the sensitive layer (like SnO_2). By increasing the contacts between electrodes and SnO_2 grains, the energy barriers in the electrode–semiconductor interfaces would have a greater significance in the sensor response. In this work, the influence of the electrodes on the properties of SnO_2-based gas sensors was studied by comparing samples with different electrodes materials, namely Au and Pt. To enhance the electrodes influence, metal particles were dispersed in the sensitive layer in order to increase the metal/SnO_2 contact. Electrodes are mainly obtained from screen printing technology.

This chapter contains two parts: firstly, the preparation of the different samples used and the sensor fabrication are described; secondly, the electrical characterization of the influence of the electrodes nature is presented.

2.1 Material and sensors preparation

2.1.1 Powder and ink preparation.

2.1.1.1 Pure SnO_2 powder

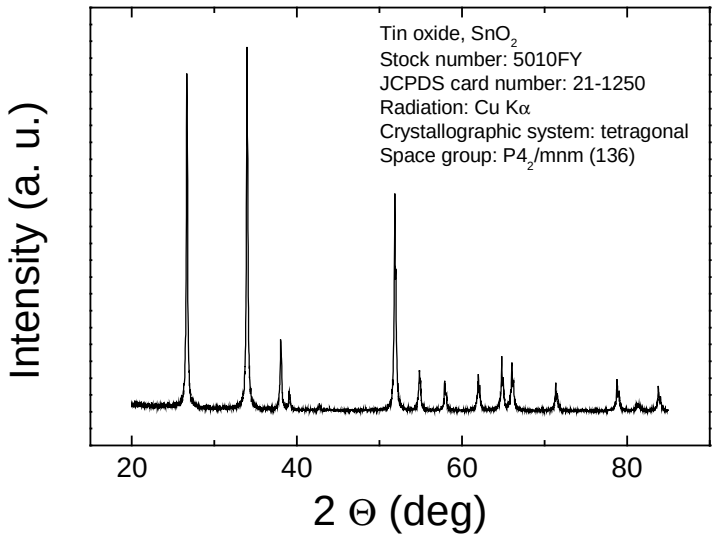

Figure 2-1: XRay diffraction pattern of the SnO2 nanoamor powder

All sensors investigated have been obtained by using a commercial powder of SnO_2 from Nanoamor®. As shown in Figure 2-1, the SnO_2 powder is perfectly crystallised and has a high specific area around 30m²/g corresponding to a grain size of approximately 30nm. Nevertheless, SEM picture (Figure 2-2) reveals that this SnO_2 powder can agglomerate with agglomerates of few micrometers (1-5µm). The sensor sensitive layer results from a paste obtained from this powder. The paste is obtained by mixing an organic binder and an organic vehicle from ESL® with SnO_2 powder. The details of the proportion are summarized in Table 2-1.

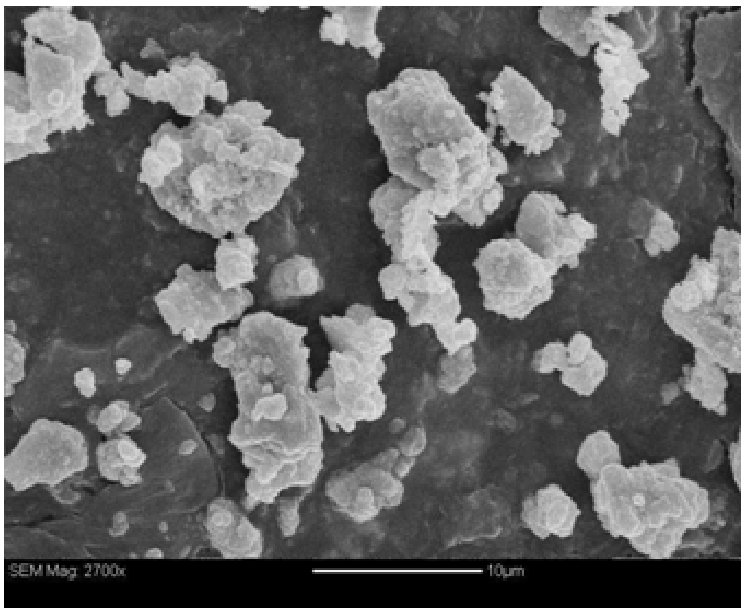

Figure 2-2 : SEM Picture of the particle of SnO2 Nanoamor®. Particles have a tendency to agglomerate

Table 2-1 : composition of the SnO_2 paste

Component	Quantity
SnO_2 (Nanoamor®)	4 g
Organic binder(ESL)	1.7 g
Organic solvent (ESL)	20 drops

This composition has been determined [119] in the laboratory of St Etienne to have an adequate Rheological characteristic for the screen printing technique.

2.1.1.2 "Mixed SnO_2" preparation.

To amplify phenomena which can occur at the metallic electrode-SnO_2 interface, "mixed powders" have been prepared from the SnO_2 nanoamor® powder mixed with commercial metal (Au or Pt) powders. The size of the metallic particles is bigger than the one of SnO_2 powder, around 1 µm. The aim is to disperse the metal into the sensitive layer to increase the metal/semiconductor contact and try to keep the massive metal proprieties. Figure 2-3 exhibits the SEM pictures of metal particles. The morphology is different between gold and platinum powders. In fact, a homogenous round grain is observed for the gold whereas some cavities and porosity are observed for the platinum particles.

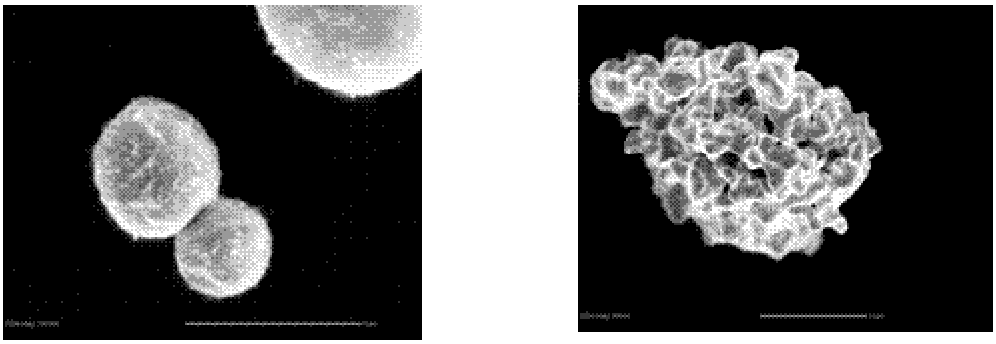

Figure 2-3 : SEM pictures of the metal particles included in the SnO_2 layer; (left) gold particle (right), platinum particles

The preparation process is quite simple (Figure 2-4). The SnO_2 powder and 1% wt (weight) metal powder have been mixed and finely grinded by using mortar and pestle. Secondly, a paste has been obtained by adding the same solvent and the binder as before.

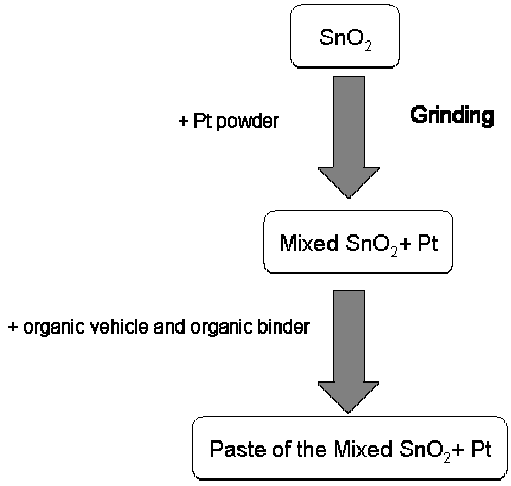

Figure 2-4 : Schematic of "mixed" tin dioxide powders preparation techniques.

The metal particles are visible to the naked eye. The XRD analysis confirms the presence of the metal into the paste. The example for platinum is shown in Figure 2-5.

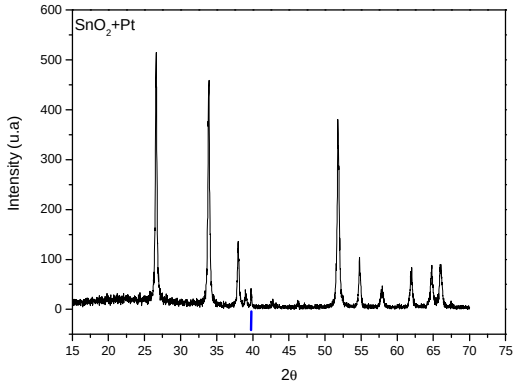

Figure 2-5 : XRD of SnO_2 mixed with platinum particle. The Band marks with a blue line prove the presence of the platinum into the sensitive layer.

2.1.2 Sensors fabrication

2.1.2.1 Deposition on the substrate.

All devices have been mainly obtained by using screen printing technique.

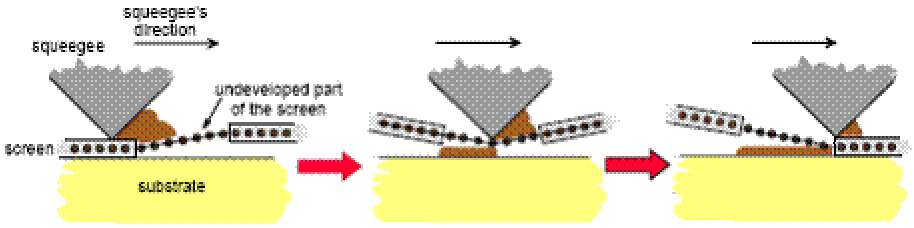

Figure 2-6 : Principle of screen printing. A rubber squeegee presses the viscous paste through. the undeveloped part of the screen onto the substrate.

For the transfer of the paste onto ceramic substrates, screen-printing is used. Hereby, a rubber squeegee presses the paste through the undeveloped part of the screen, which works as some kind of mask for the paste transfer, onto the substrate (see Figure 2-6). By this method, SnO_2 layers can be adjusted with a thickness of a few micrometers to around 100µm. The thickness value depends on the chosen screen, the paste viscosity and the screen-substrate distance. For the herein discussed sensors, a semi-automatic screen printer (Aurel Model C890, Figure 2-7) was used. The screen is made from stainless steel and has a mesh count of 300.

Figure 2-7 : Screen printing machine Aurel Model C890

After screen printing, the substrate stays some minutes at room temperature to allow the paste to settle. Afterwards, the substrate is put into a drying oven (MEMMERT UM/SM 100) to dry the paste at 80°C. Finally, the substrate is inserted into an oven. During the final annealing, the so-called "firing", the organic binders of the film are removed. The layer gets mechanically stable and is firmly bond to the substrate. The used oven (Thermolyne Type F48000 Models) has the possibility to control the ramp and the dwell (delay).

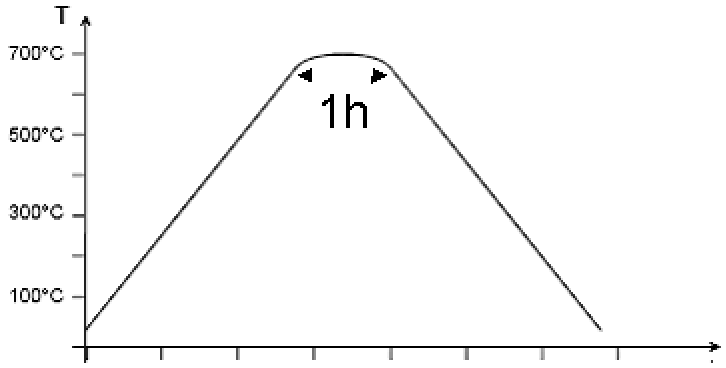

Figure 2-8 : Typical firing profile for a thick film paste. The temperature is raised slowly to the maximum temperature, where it is kept for 10 minutes, afterwards a controlled cooling takes place.

The firing profile was adjusted in such a way, that a gradual heating from room temperature to the maximum firing temperature (700°C) and a gradual cooling back to room temperature was achieved (see Figure 2-8). The operation takes place in air for the firing step. The thickness of the finally resulting SnO_2 layer for the discussed sensor types was around 20µm.

2.1.2.2 Geometry designs for substrates, heaters and electrodes for DC measurement and DRIFT analysis

The planar substrates are tiles made out of alumina (Al_2O_3, purity of 96%) with a lateral dimension of 2inch x 2inch and a thickness of 700µm. These tiles are predicted and provided with Pt or Au interdigited electrodes on the front side for measuring the sensor resistance and Pt heaters on the back for keeping the sensors at the operating temperature (Figure 2-9). The measuring electrodes have the typical shape used for conductivity sensors, namely 2 combs opposed one to the other, the so-called interdigital structure. The width of the fingers of the electrodes is 0.2mm and the gap between the fingers is also 0.2mm. The electrodes material is additive free gold or platinum which required e.g. a firing of the substrates with screen printed Pt electrodes and heater structures at 1600°C (constructor information) and 980°C for gold. Each substrate holds twenty sensors. Due to predicing they can easily be separated at the end of preparation.

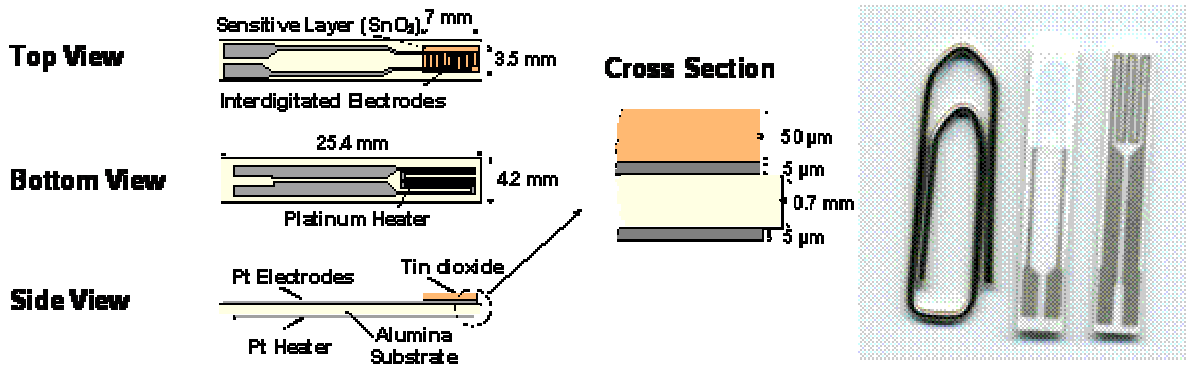

Figure 2-9 (same as Figure 1-15): Layout of the planar alumina substrate with Pt electrodes and Pt heater. The SnO_2 layer is printed on top of the interdigitated electrodes. The heater on the back keeps the sensor at the operation temperature.

The sensors obtained by such technique will be used for DC characterisation and DRFIT analysis.

2.1.2.3 Specification for the TPD samples

Temperature programmed desorption (TPD) technique was used in order to investigate the desorbed species from the different SnO_2 powders. Due to some limitation of the DRIFT technique (mainly, the impossibility to observe the oxygen at the surface), it was interesting to associate TPD investigation with DRIFT analysis. The aim of this study, developed in the chapter 3, is still to understand how the electrodes can disturb the surface species. Due to the experiment set up, it was not possible to work directly on sensors but on powders. The

powders were obtained by following the same procedure to obtain the sensitive layer for the gas sensors. Starting from the paste of pure SnO_2 and mixed metal SnO_2, they were screen printing on Teflon substrate. After 10 min drying, the layer is removed from the Teflon substrate and grinded again to obtain a powder. These powders were annealed in the same condition as gas sensors device. Finally 3 types of powders were obtained:

- Pure SnO_2
- Mixed SnO_2 + 1%wt Pt
- Mixed SnO_2 + 1% wt Au

2.1.2.4 SnO_2 sensitive layer characterization on sensors

- Pure SnO_2 layer 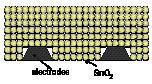

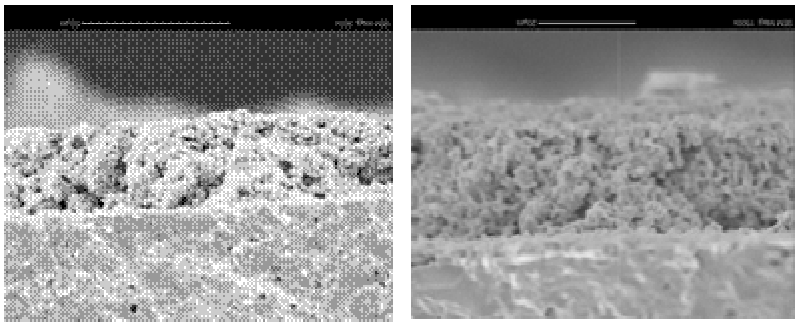

Au **Pt**

Figure 2-10 : SEM picture of the sensor with gold electrodes and platinum electrodes prepared by screen-printing

Figure 2-10 shows the SEM of the deposition of pure SnO_2 on the top of Au or Pt electrodes. The SEM pictures indicate a thickness of 20µm and a good adhesion with the substrate. No crack has been observed. The layer can be considered equal regard to the electrodes nature.

- Mixed sensitive layer 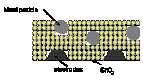

The metal particles are naked eye visible. The optical microscopy images (Figure 2-11) prove the presence of well dispersed metal particle in the layer

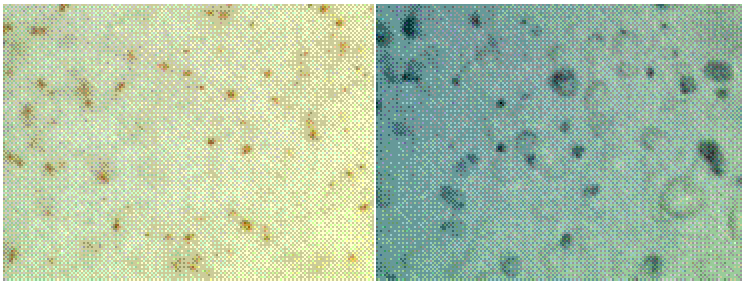

"Mixed Au"=SnO_2+Au **"Mixed Pt"=SnO_2+Pt**

Figure 2-11 : Optical microscope picture of the sensor with gold electrodes and platinum electrodes prepared by screen-printing

2.1.2.5 Calibration of the heating of the sensor

Tin dioxide sensors are operated at elevated temperatures in the range 200°C and 400°C. To keep the sensor at the operation temperature, a power supply is used to ensure a constant voltage drop over the platinum meander on the rear side of the alumina substrate. In order to calibrate the platinum heater, i.e. to obtain the relationship between the applied voltage and the thereby adjusted temperature, an infrared pyrometer (Maurer KTR 2300-1) was used. The measurement set-up is sketched in Figure 2-12. The pyrometer detects the infrared emission from a measurement spot of 3mm² (the area of the sensitive layer is 7mm x 3.5mm) and calculates, using the specific emission coefficient ε of the material (ε_{SnO2} = 0,75), the temperature of the sensitive layer. The pyrometer is kept at room temperature and can be used for detecting temperatures from 200°C to 500°C. The resulting calibration curve of the platinum heater for temperatures from 200°C to 400°C is given in Figure 2-12.

.

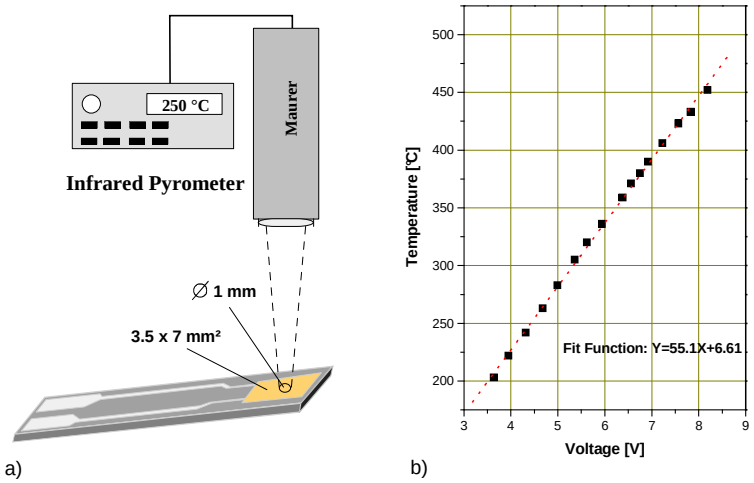

Figure 2-12 : Calibration of the Pt heater. In a) the measurement set-up is sketched. The resulting calibration curve b) can be nicely approximated by a linear fit.

2.2 Electrical measurements

2.2.1 Test Bench presentation

The sensors were mounted on a Teflon chamber and heated by a power supply. The resistance was measured with a scanner multimeter (Keithley DMM 199 or DMM 2000, Germany). The gas mixtures were adjusted by a gas mixing system. In order to be absolutely sure that thermodynamic equilibrium was reached for the various surface complexes associated with water adsorption, the sensors were kept in an atmosphere of constant humidity for 10h after every variation in humidity, and before the test gas was introduced. The sensor signal was investigated for CO and CH_4 exposure. The sensor was purged with a flow of synthetic air for 1h between every two successive gas concentrations.

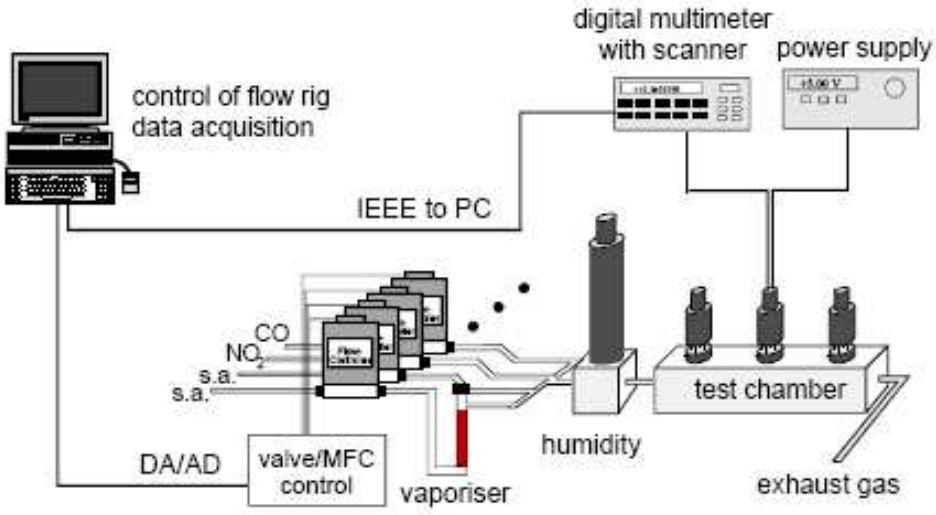

Figure 2-13 : Experimental set-up which was used for DC characterisation of gas sensors. A computer is used to adjust the ambient gas atmosphere of the sensors by means of a gas mixing bench and to acquire the sensor resistance data via a digital multimeter and IEEE card. A power supply keeps the sensors at operation temperature

- **Mixing and monitoring of gases**

In order to provide the desired gas atmospheres, gas mixing systems are used. A typical gas mixing system consists of PC controlled mass flow controllers (MFC) and valves. The gas mixing, Figure 2-14, system is operated by home made software called POSEIDON. The software via A/D card not only controls the actual gas flow through the mass flow controllers but it can also (at the same time) record the resistance of the sensors and other parameters like humidity or oxygen concentration

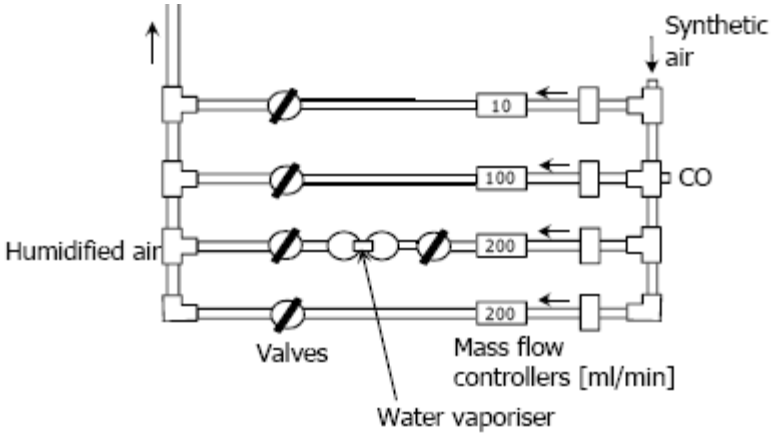

Figure 2-14 : Schematic picture of a four-channel gas mixing bench. Test gas is introduced either from gas cylinders or added by flowing synthetic air through vaporisers. The latter is used to adjust the relative humidity.

2.2.2 Results and discussion

2.2.2.1 Metal Nature influence

In humid or dry condition, three types of SnO_2 sensor have been studied under different concentration of CO (90, 160, 230, 300 ppm). 2 sensors were obtained from the same SnO_2 ink but the nature of electrodes is different:

SAu: pure SnO_2 + gold electrodes

SPt: pure SnO_2 +platinum electrodes

Moreover a third sensor is studied,

S (Au) Pt: mixed SnO_2 + %1 Au particles and screen printing to substrate provided with platinum electrodes.

S (Pt) Pt: mixed SnO_2 + 1% Pt particles and screen printing to substrate provided with platinum electrodes. Due to the lack of time, only few experiments was done with this sample.

The main results obtained are shown in the following.

2.2.2.1.1 In dry air

For 3 different temperatures 200°C, 300°C and 400°C, the responses and the sensor signals are shown in Figure 2-15. As expected, with the rise of the temperatures, the values of the baselines resistances decrease. For example for SPt, the value is 135M at 200°C and goes to 1.8M at 400°C. It is well-known that the reaction at the surface with the gas phase and the semi-conductor is fundamental for the value of the resistance. With the temperature, the

chemistry of the SnO_2 surface is different, especially the chemisorption of oxygen species, water and hydroxyl groups which can be bond in several ways as a function of temperature (see chapter 1). Samples SPt and S(Au)Pt provided with platinum electrodes always show higher values of resistance than gold ones. At elevated temperature, the differences between the resistances of each sample become more pronounced. At 200°C, the resistances of each sample are in the same range of MΩ. Focusing on pure SnO_2 based sensors provided with gold and platinum electrodes, only 15MΩ separates these two types of sensors. At 400°C, the difference becomes larger, around one order of magnitude. These results clearly confirm the role played by the electrodes nature, even under air. Sample provided with platinum electrodes but with a different sensitive layer, SPt and S (Au)pt, exhibit also interesting results. S(Au)Pt which is loaded by 1% wt Au shows the highest resistance for each working temperature. The behaviour of S(Au)Pt is very close to the behaviour of SPt . The density of Gold particle/SnO_2 contacts is more important than platinum electrodes/SnO_2 contacts. Results of pure SnO_2 provided with gold electrodes show the lowest resistance. So, by adding gold particle inside the sensitive layer, S(Au)Pt , we could expect that the resistance of such example would be lower compared to the one of SPt sample. However, experiments show opposite results which mean that the platinum electrodes have the dominant effect.

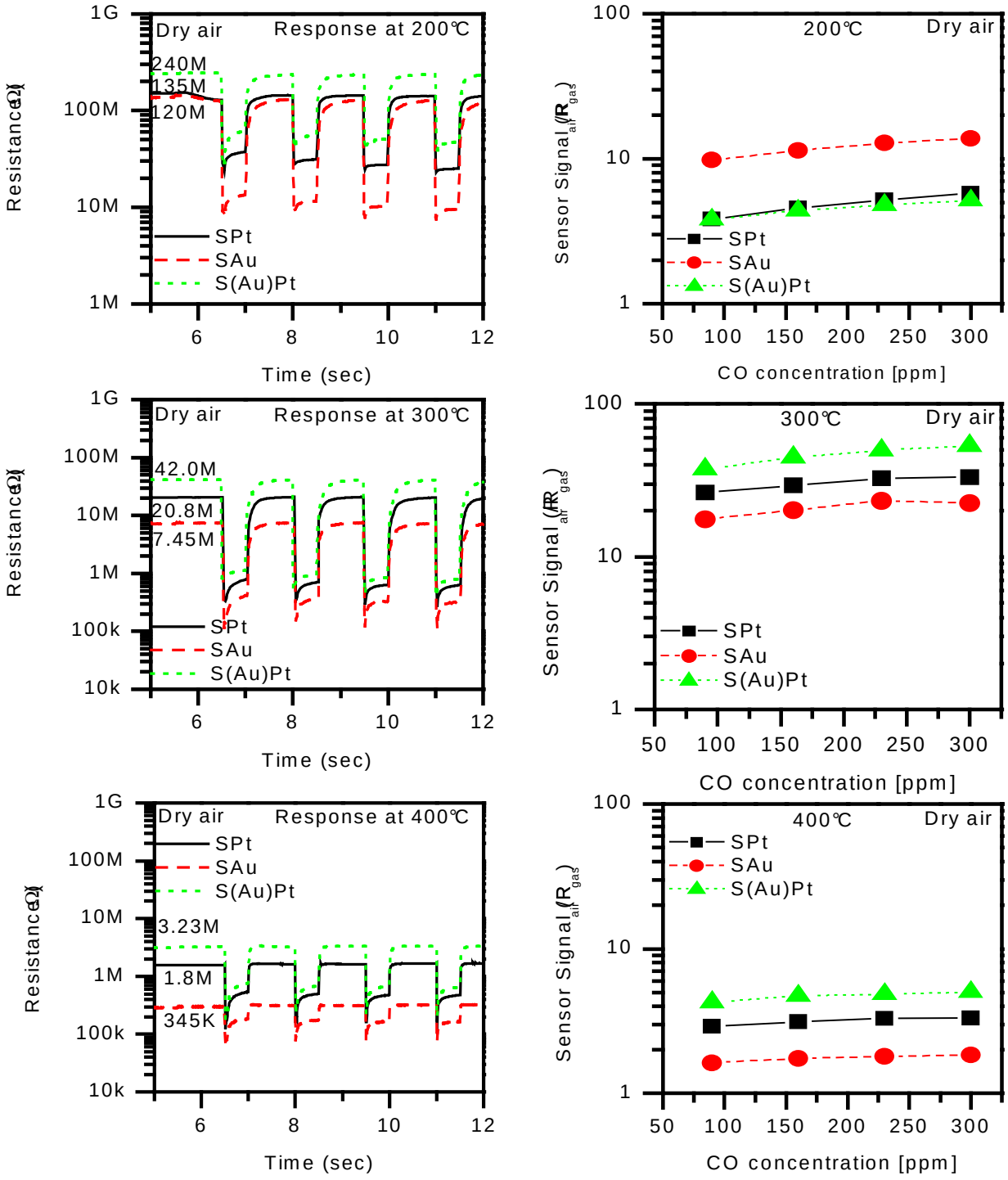

Figure 2-15 : Response (a) and sensor signal of SnO_2 sensor provided with gold electrodes(SAu) or platinum electrodes (SPt) and SnO_2+1%Au sensor based provided with platinum electrodes (S(Au)Pt) to CO (90,160,230, 300 ppm)in dry air at 200°C, 300°C and 400°C

When sensors are exposed to CO gas, as expected to n-type semiconductor, the resistance decreases due to the interaction with the reducing gas CO. The sensor signals (R_{air}/R_{gas}) are shown in Figure 2-15(b). For all sensors, with the increase of CO concentration, the sensor signals increase. As expected, for undoped SnO_2, the sensor signal is low, around 10 (doped with Palladium for which the value can go to more than 100[…]).Gold particles inside the sensitive layer S(Au)Pt increases a little bit the sensitivity, but only at high temperature (300-400°C). The value of the sensitivity is still low with gold particle inside the layer, which proves that the material is not doped. The metal is just dispersed in SnO_2 layer as required.

At 200°C, the sensor signal is much higher for sensor with gold electrodes than the one with platinum electrodes. The sensor signal of S(Au)Pt is close to SPt. With gold electrodes the sensor signal is the best, but with gold particles included in the sensitive layer (which means more gold/SnO_2 contact) the sensor signal is the same as SPt. This result matches with the observation already mentioned in air. Predominant effect of the electrodes in opposition with the effect of a metal dispersed in the sensitive layer is revealed. By increasing the temperature to 300°C or 400°C, SPt and S(Au)Pt, become the most sensitive sensors to C Oand SAu the lowest. The difference between the SPt and S(Au)Pt is difficult to explain by only electrical measurements but these result confirm that the presence of electrodes modified the sensitivity of the gas sensor.

2.2.2.1.2 Humidity effect

For the present study, the influence of humidity has been investigated at 10 % relative humidity (RH) and 50% RH. The sensor is exposed to different CO concentrations from 90 ppm to 300 ppm. The temperature of the sensor varies from 200°C to 400°C. The results obtained in dry air are inserting for comparison with humid air. The results for 200°C, 300°C and 400°C are shown in Figure 2-16, Figure 2-17 and Figure 2-18 respectively.

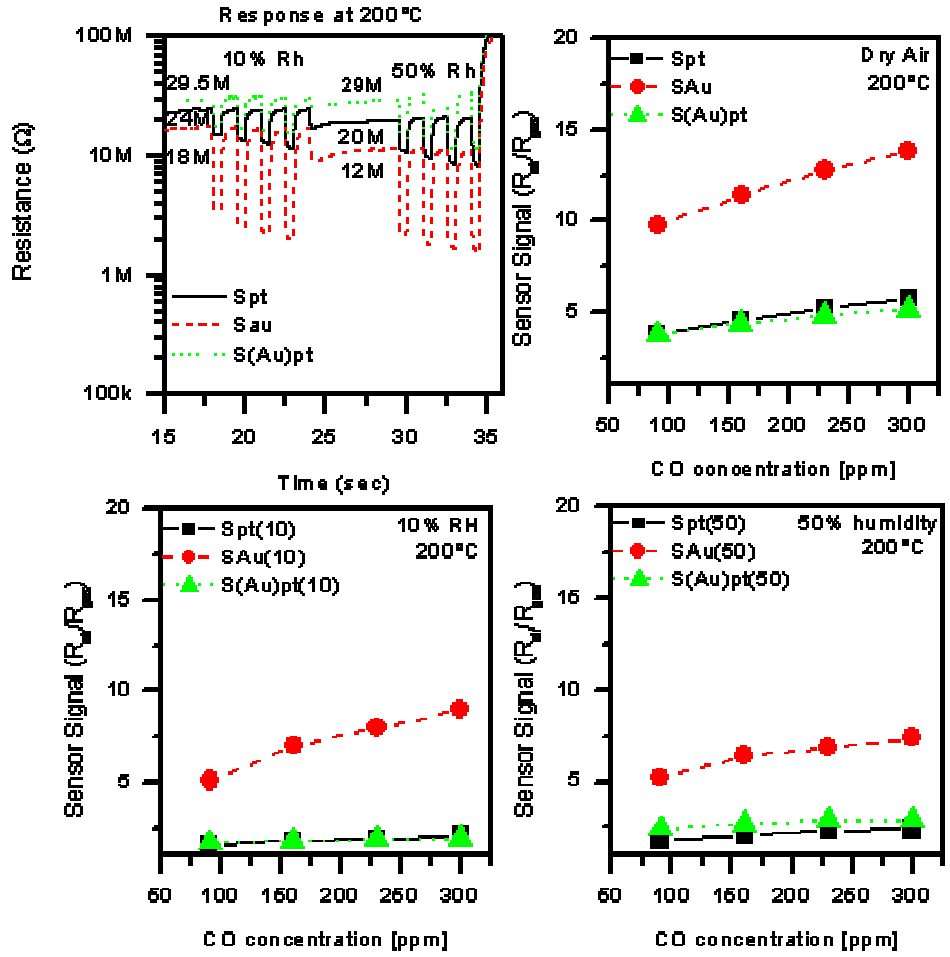

Figure 2-16 : Response and sensor signals of the sensors for SPt, SAu, S(Au)Pt ,at 200°C, at different level of humidity (dry air, 10 or 50 %RH) .

In dry air, at 200°C, the sensor with gold electrodes is the most sensitive to CO. Both sensors with platinum electrodes are the less sensitive. The performance of the gold electrodes sensor is still the best in humid conditions. For all sensors the sensors signals are twice lower than in dry condition. For SPt and S(Au)pt, it clearly appears that CO detection is blocked by the presence of humidity. In presence of humidity, the performances in terms of sensor signal are slightly decreased with the increase of humidity level from 10 to 50%RH. They are not too much sensitive to the humidity level at this temperature. The baseline resistances at 10%RH and 50%RH are quite similar.

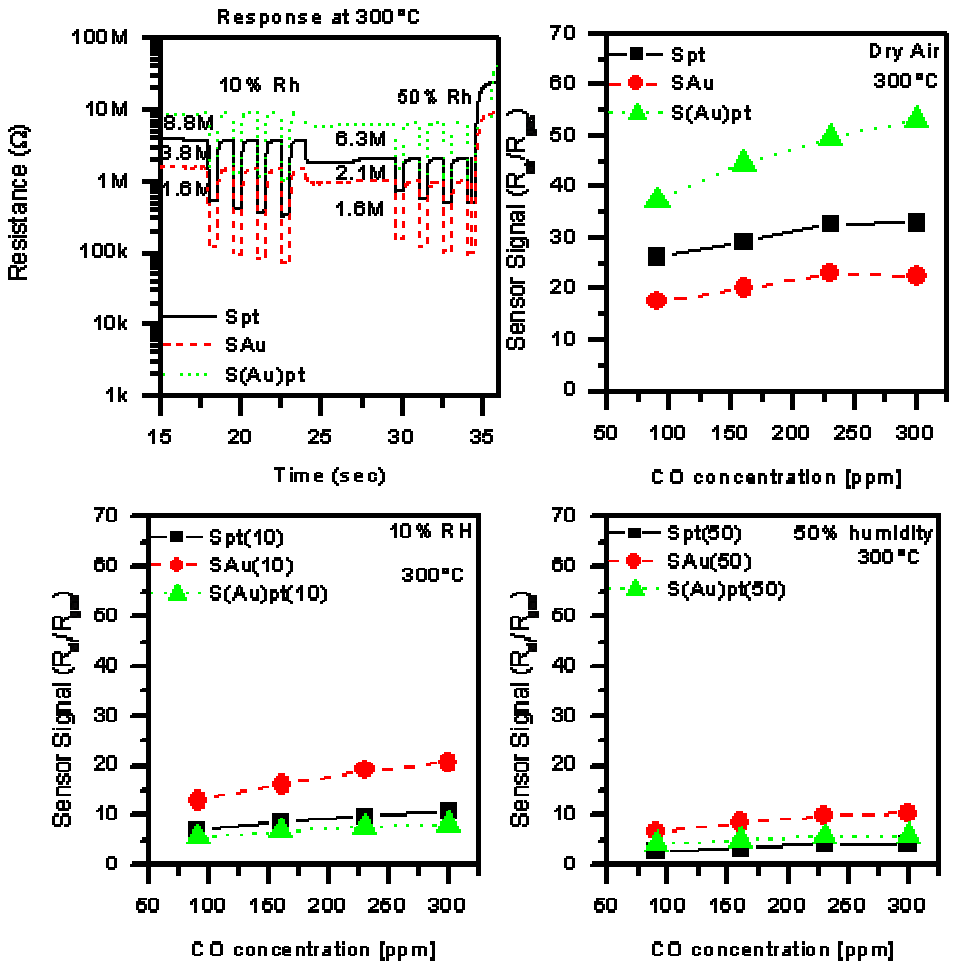

Figure 2-17 : Response and sensor signal of the sensor for SPt, SAu, S(Au)Pt at 300°C at different level of humidity (fry air, 10 or 50 %RH) .

At 300°C, it was already mentioned that the sensors provided with platinum electrodes are the most sensitive in dry air. The presence of humidity affects the performance of all sensors but in particular sensor provided with platinum electrodes. Sensors with platinum electrodes are the most altered, see Figure 2-17. The sensors are 4 times less sensitive in 10% RH than in dry air. In fact, at 300°C, in humidity, the sensor with gold electrodes is the most sensitive which means that the sensor is less disturbed by humidity. Here, the interesting facet is the reverse effect in function of the electrode nature. At 300°C, in dry air, sensors provided with platinum electrodes are the most sensitive whereas in humid condition the gold one exhibits the higher sensor signal.

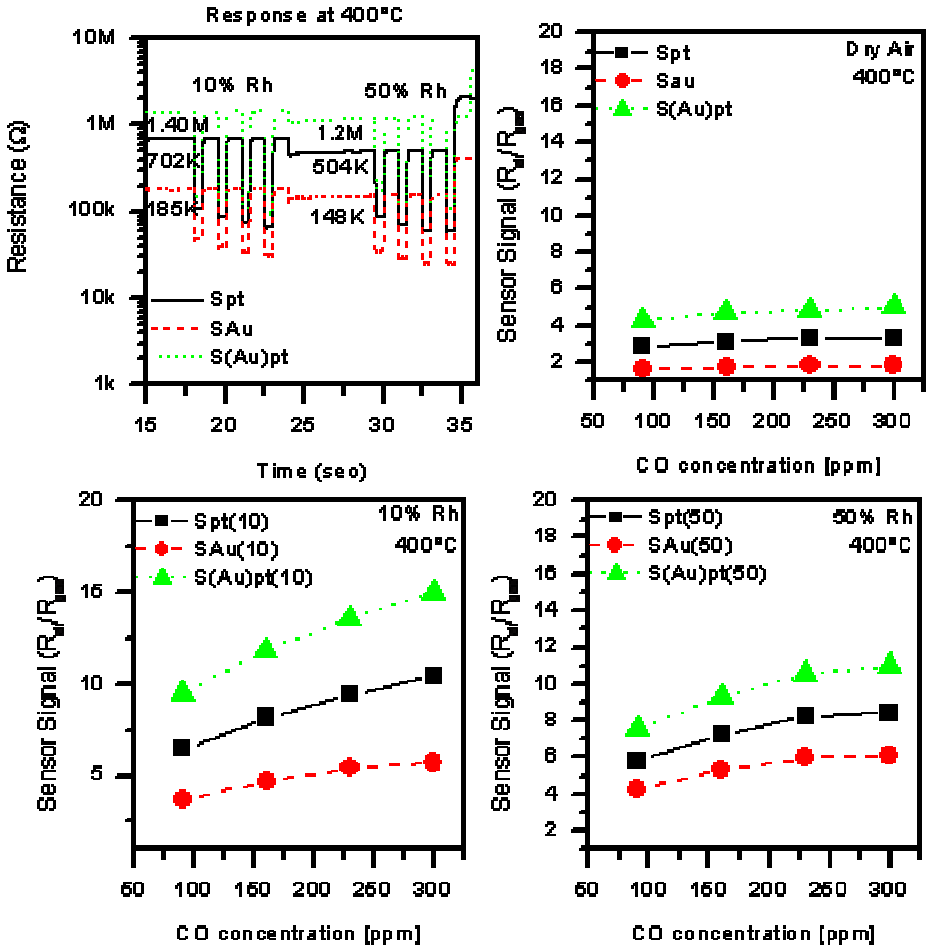

Figure 2-18: Response and sensor signal of the sensor for SPt, SAu, S(Au)Pt at 400°C at different level of humidity (10 or 50 % RH) .

At 400°C, Figure 2-18, the performance in dry air is very low for all sensors. In this range, the platinum electrodes are the most sensitive. In presence of humidity, at 400°C, the performance increases to a factor 2.5 in 10% RH but less than 2 in 50% RH. On opposite to 200°C and 300°C, the presence of humidity enhances the CO detection for all sensors. Sensors provided with platinum electrodes are the most sensitive.

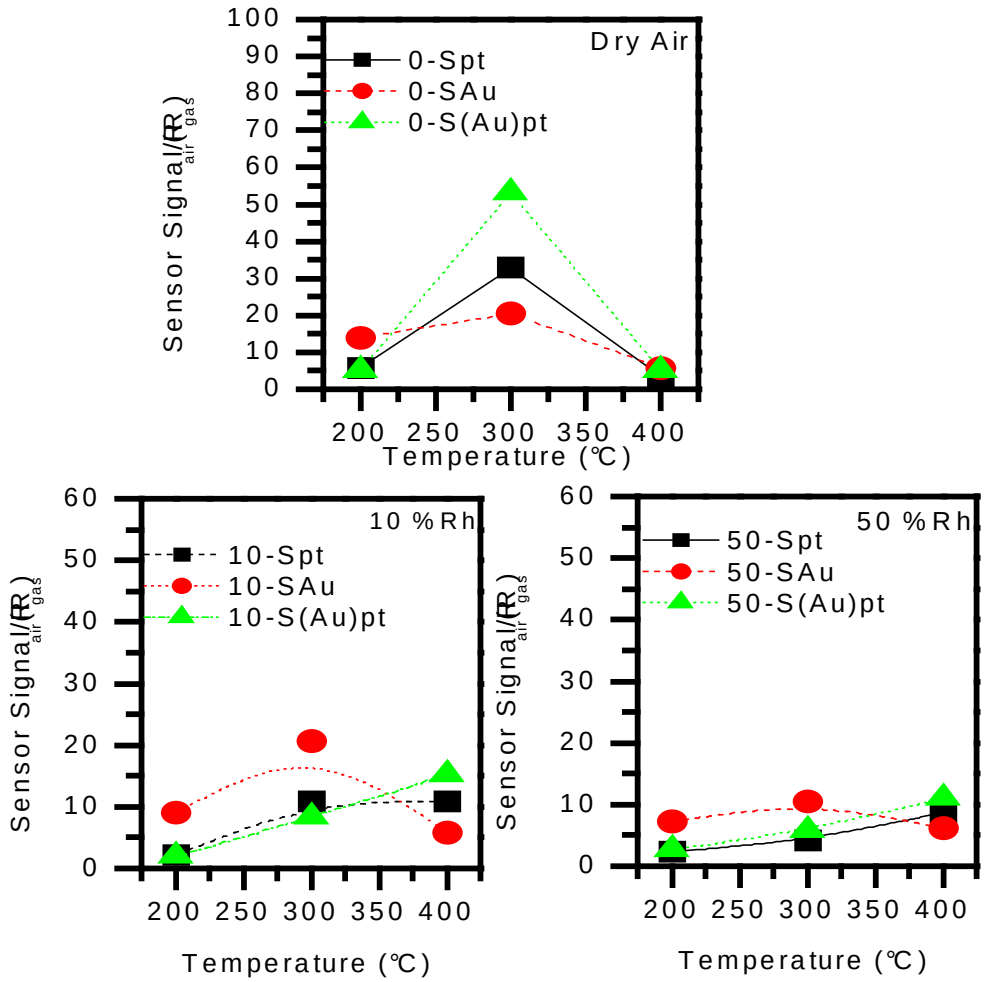

Figure 2-19 : Sensor signal for the sensor SPt, SAu, S(Au)Pt in dry air, 10%RH and 50%RH as a function of the operating temperature in 300ppm CO.

Figure 2-19 shows the results of the CO detection obtained at a fixed concentration (300ppm) in dry and humid conditions as a function of the working temperature. In dry air, the curve shows a maximum detection for 300°C. With humidity, the shape of the curve depends on the type of used electrodes. With the gold electrodes sample, the shape is conserved, but the sensor signal decreases slowly with the increase of the humidity level. At 300°C, with platinum electrodes, the CO detection is blocked by the presence of water. In fact, the sensor signal is extremely altered. The CO sensitivity increases linearly with the temperature without any maximum at 300°C. At elevated temperature (400°C) and for a high level of humidity, all sensors can be considered equal.

2.2.2.1.3 Comparison between S (Au) Pt and S (Pt) Pt

Due to the lack of time, only few experiments were done with the sample S (Pt) Pt. Figure 2-20 illustrates the comparison between S (Au) Pt and S (Pt) Pt. The resistance and the sensor signal for both types of sensors, SnO_2 mixed either gold or with platinum are relatively close.

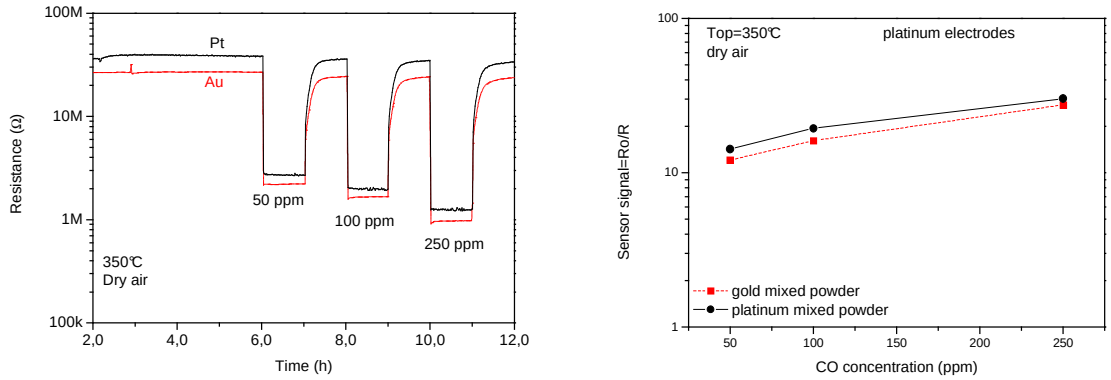

Figure 2-20 : Resistance and sensor signal dependence on the CO concentration in dry air at 350°C sensors working temperature. "gold or platinum mixed sensor" provided with platinum (Pt) electrodes

As follow, the characteristic are:

- Identical performance is observed for both types of mixed SnO_2 based sensors.
- The baseline resistance for sensor contain Platinum mixed sensitive layer is little higher than mixed Gold device.

2.3 Conclusion

The role of the electrode could be expected to only collect the output signal resulting from the transduction of chemical reaction at the surface of the sensitive layer. As mentioned by many authors, we check that the electrode nature plays an important role on sensors performance. For the detection of CO, it is pointed out that sensors provided by platinum electrodes are the best in dry air however water alters the sensor with platinum electrodes. The performances are driven by the electrodes. For different types of mixed sensitive layers but with the same type of platinum electrodes, the performances are quite close. The role of metal dispersed in SnO_2 layer is not clearly explained.

Chapter 3

3 Investigation of the surface reactions by DRIFT analysis and TPD

Les mesures électriques ont certes permis de mettre en évidence les effets des électrodes sur les réponses électriques des capteurs SnO_2. Cependant, les causes n'ont pu être clairement identifiées. Afin de comprendre les effets des électrodes sur la détection des capteurs de gaz, une approche originale a été utilisée. L'implication de l'électrode dans les réactions de surface a été étudiée à l'aide du DRIFT (réflexion diffuse en Infrarouge en transformée de Fourrier), simultanément avec la mesure de la réponse électrique. Cette méthode permet d'analyser la surface tout en considérant les changements électriques. Afin de mieux comprendre les réactions à la surface, une étude par thermodésorption (TPD) a été élaborée. En effet, il s'est avéré que la chimisorption de l'oxygène à la surface du SnO_2 est primordiale. Le dispositif mis en place avec le DRIFT ne nous permet pas de suivre l'oxygène et donc la TPD s'est révélée complémentaire pour cette étude.

.

3.1 Introduction

The influence of the nature of the electrodes over the detection performances of semi-conducting metal oxide based gas sensors was recognized and experimentally proven in the previous chapter. This one is divided in two parts with a spectroscopic approach for the investigation of the electrodes role:

The first one deals with DRIFT (Diffuse Reflectance Infrared Fourier Transform) performed simultaneously with DC measurement on CO sensing. In fact, the electrical measurements input are insufficient when one aims to understand the electrodes role. Many approaches can be used. In situ DRIFT analysis is a powerful method to study the adsorbed species at the surface of the sensing element and thus to understand the implication of the electrodes on the CO sensing mechanisms. Infrared spectroscopic technique is a standard method for analysis adsorbed species and surface reactions. The common transmission infrared spectroscopy is not applicable for gas sensors because of the opaque substrates (Al_2O_3…). The first spectroscopic investigations on sensors under operating conditions were conducted only recently by Benitez and Pohle [120; 121]. In case of Benitez studies, DRIFT analysis of the reversibility of CdGeON sensors towards oxygen exposure was performed. Their interest was directed more towards the bulk material changes as a result of O_2 reaction. Pohle et al. studied adsorption of water vapour and oxygen on different metal oxides (Ga_2O_3 [122], WO_3, $AlVO_4$, and Co_3O_4 [123]) thick film gas sensors in various operating conditions using IRES (Infrared Emission Spectroscopy). Among others, they found from the spectroscopic and electrical measurements a correlation between water adsorption and the evolution of the surface hydroxyl group concentration, and in this way, it was proved that IR spectroscopy is applicable for the study of surface reactions on sensors. Since Benitez, the SnO_2 were intensively explored by this technique […] to understand the sensing mechanism of gas sensor.

In the second part, a powerful method to analyse the surface reaction in combination with DRIFT analysis is the Temperature Programmed Desorption (TPD). With DRIFT analysis, it is not possible to observe directly oxygen because the vibration of the bond between the surface and the oxygen physisorbed/chimisorbed are in low wave number close to the limit of the detection of our system. The role of metal on the ionosorption of oxygen is ambiguous. TPD studies of oxygen adsorption-desorption behaviour at SnO_2 surfaces have been reported earlier by several authors [124,125,126,127]. Based on these studies, it is interesting to

observe how the metal modifies the adsorption and desorption of oxygen. This part reports the study of the oxygen adsorption on our powder and the interaction of oxygen with others interfering gas. The implication of gold and platinum on the chemisorptions is also pointed out.

3.2 DRIFT

3.2.1 Theory of Diffuse Reflectance [128]

3.2.1.1 The ideal case

The phenomenon of Diffuse Reflectance from mat surfaces is observed in everyday life. It was, for the first time, mathematical described by Lambert [129]. The intensity of radiation reflected (re-emitted) from a completely mat surface is everywhere of the same intensity, independent on angle of observation ϑ and incident α (Figure 3-1). The flux of the remitted radiation I_r in area df and solid angle $d\omega$ is a function of the cosine of the angle of incident and the angle of observation:

$$\frac{dIr/df}{dw} = \frac{CS_0}{\Pi}\cos\alpha \times \cos\beta = B\cos\vartheta$$

Where S_0 is irradiation intensity, B is the radiation intensity of surface brightness, and the C is a constant smaller than 1.

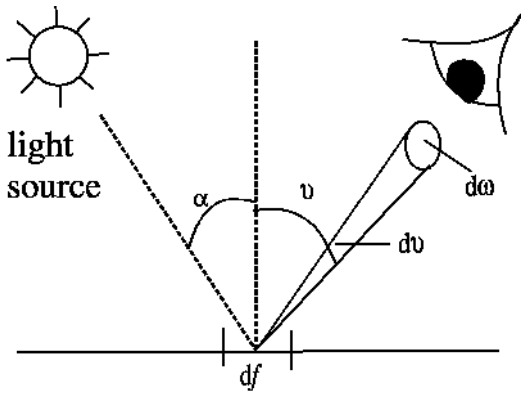

Figure 3-1: Diagram showing the variables used in the Lambert cosine law.

According to Kortüm [130], the model is rigorously valid only for black body radiator acting as an ideal diffuse reflector. However, an ideal diffuse reflector has never been found

and numerous experimental investigations suggest that the law is true only when both the angle of incident and the angle of observation are small.

3.2.1.2 The real case

In the real case, an incident radiation can be absorbed, directly reflected, internally reflected or finally diffused in all directions (see Figure 3-2). The light directly reflected (externally) by the surface, or multi-reflected at the surface of particles (internally, also named volume specular reflectance) give rise to specular reflection. Both specular components are functions of refractive index and absorbtivity of the material and considered being unwanted effects in Diffuse Reflectance Spectroscopy. The later one, diffusion in all direction, is a consequence of IR light penetration into one or more particles and its diffusion in the sample. The light which travels though the particles contain information about the absorption properties of the material and, in this way, the measured spectra is similar to transmission spectra. This is the component of interest in Diffuse Reflectance Spectroscopy.

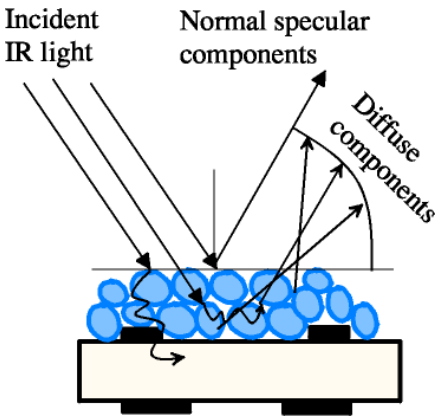

Figure 3-2 : Mechanism of generating the Diffuse Reflected spectrum of sensor.

There are two ways in order to diminish external specular reflectance:

- The first one is to use one of commercial available optics: Praying Mantis (Harrick Scientific Products, Inc.), Collector (Spectra Tech) or Selector (Specac Ltd.) - which minimizes the flux of specular reflectance.
- The second deals with sample preparation: particle size should be smaller than the wavelength of the incident radiation. In this work both approaches have been realized practically: (a) in-situ chamber for sensors measurements

was built in Praying Mantis Optics (Figure 3-5), (b) the grain size of SnO_2 was in 50 nm range which is several orders of magnitude smaller than the wavelength in MIR range.

The internal specular reflectance exists at any angle of observation and therefore it cannot be optically separated from diffuse reflection. But in general specular reflectance is relatively small in the material with low absorptivity [131]. The qualitative analyzes have been of interest within this work. However, for the sake of completeness a brief description of the quantitative approach will follow. There are two approaches in the qualitative treatment of diffuse reflection: the continuum and discontinuum theories. The former one is expressed in terms of continuous sample having certain absorption and scattering coefficients, whereas the last one is expressed in terms of absorption, reflection (re-emission), and transmission of certain layer of sample.

3.2.1.3 The continuum theory

The theories which describe the diffuse reflectance are in general based on solving of the radiation transfer equations [132].

$$-dI = \kappa.p.I.ds \qquad (3.1)$$

It describes the changes of the light intensity *dI* of a given wavelength on the path length *ds* in a sample whose density is ρ and κ. is an attenuation coefficient (due to scattering or absorption). Schuster [133] solved the problem by simplifying the assumptions of using two oppositely directed radiation fluxes. The flux *I* directed in the direction of the incident beam and the flux *J* in the opposite direction. Accordingly, Schuster derived the following differential equations:

$$\frac{-dI}{d\tau} = (k+S)I - SJ \qquad (3.2)$$

$$\frac{-dJ}{d\tau} = (k+S)J - SI \qquad (3.3)$$

By setting the boundary conditions

$$I = I_0 \text{ and } \tau=0$$

$$I=I_{\tau=0} \rightarrow \infty; J=0 \text{ at } \tau= \tau \; \tau \rightarrow \infty$$

The differential Eq. 3.2 and Eq. 3.3 can be solved to give reflectance at infinite depth:

$$\frac{(1-R_\infty)^2}{2R_\infty} = \frac{k}{S} = \frac{2\alpha}{\sigma} \qquad (3.4)$$

The constant terms *k* and *S* are defined by Schuster as adsorption and scattering coefficient for single scattering.

However, the most widely accepted and commonly used model is the one proposed by Kubelka and Munk [134] where k and S are defined as absorption and scattering coefficient for densely(thickly) packed sample as whole and made the following assumptions:

- the radiation fluxes (I and J) travel in two opposite directions (perpendicular to surface plane);
- the sample is illuminated with monochromatic radiation (I_0);
- all regular (specular) reflection is ignored;
- the particles are randomly distributed through the layer;
- The particle size is smaller than the wavelength of the incident radiation which ensures that the scattering coefficient will be independent of wavelength. However, this is relevant only for non monochromatic light;
- The scattering particles are distributed homogeneously throughout the entire sample.

On their bases Kubelka and Munk developed two fundamental simultaneous differential equations:

$$-dI= - (K+S)\, I.dx – S.J.dx \qquad (3.5)$$

$$dJ= - (K+S).J.dx - S.I.dx \qquad (3.6)$$

Where K = 2k (k - the absorption coefficient of material) and S = 2s (s - the scattering coefficient of material) and dx the deepness. By setting several simplifications one obtains:

$$I\left(r^2 - 2ar + I\right)^{-1} dr = SIdx \qquad (3.7)$$

Where $a = 1 + \frac{K}{S}$ *and* $r = \frac{J}{I}$

Eq. 3.7 integrated in the given boundaries:

For x=d=∞: $\left(\frac{J}{I}\right)_{x=d}$ =R_g=0 reflectance of the background

For x=0: $\left(\frac{J}{I}\right)_{x=0}$ =R reflectance of the sample

The solution can be found

$$\frac{(1 - R_\infty)^2}{2R_\infty} = \frac{k}{S} = \frac{2\alpha}{\sigma} = \frac{(\ln 10)ac}{S} \qquad (3.8)$$

Absorption (α) and scattering (σ) coefficients per unit path length and c is the concentration of absorbance particle in the defined section.

Which is similar to the one first derived by Schuster. Accordingly the reflectance which is measurable is a function of the ration of constants, K and S, and not their absolute values.

3.2.1.4 The discontinuum theory

The discontinuum theory models the sample as a series of parallel layers with assumption that radiation moves: in two directions, the direction of the incident beam and in the opposite direction (two flux model) or in three directions, forward, backward and perpendicular to the incident beam (three flux model) [135]. In the plane parallel layer model sample consisting of particles of different size and compositions is described as a collection of identical layers, each representative of the sample as whole. Thus it is possible to assign measurable spectroscopic properties to the composition of complex system. The incident radiation may be absorbed, may be transmitted forward into the next layer, or may change the direction and be re-emitted (diffuse and specular reflection) into the previous layer: $A_d + R_d + T_d = 1$. The absorption/re-emission function *A (Rd, Td)* based on this model

will be valid for sample of any thickness *d.* In theory for d_∞ where there is no transmission, the Dahm[112] equations become equivalent to the Kubelka Munk equations:

$$A(Rd,Td) = \frac{(1-R_d)^2 - T_d^2}{R_d} = A(R_\infty,0) = \frac{(1-R_\infty)^2}{2R_\infty} = \frac{2K}{B} \qquad (3.9)$$

K and B are the linear absorption and reemission coefficient. However, the practical application of this model requires the transmission and reflection measurements performed on the same sample on an absolute scale. Although, the model fits in principle better to the sensors geometry (see chapter 2,) it cannot be used in practice because the reliable transmission measurements are impossible.

3.2.1.5 Free carriers' absorption - theory and application in sensing

Absorption on free carriers *(α)* is characterized by a monotonic function proportional to wavelength (λ^p). An absorption process for a photon of energy $h\upsilon$ must involve intravalley transition of an electron to a higher energy level [136,]. Such a transition requires additional interactions in order to fulfil the conservation of the momentum. The change in carrier momentum must be larger than the photon momentum itself and may be achieved by an interaction with the lattice (phonons) or scattering on ionized impurities. The dependence of the absorption coefficient *(α)* on wavelength *(λ)* differs for various kinds of electron scattering

$$\alpha \approx \lambda^P = A\lambda^{1,5} + B\lambda^{2,5} + C\lambda^{3,5} \qquad (3.10)$$

Where A, B, C are constants.

The solution of the acceleration of free carriers in a semiconductor by the oscillating electrical field, within the framework of classical electrodynamics, derives [137] the following dependence between the absorbance coefficient *(α)* and free carriers concentration (n)

$$\alpha = \frac{\sigma_0}{n' C\varepsilon_0 (1+\omega^2\tau^2)} \qquad (3.11)$$

where: ε_0 is permittivity of free space, ω - frequency, τ - relaxation time (factor sensitive to the temperature and purity in any substance), c - light velocity in free space, n' - real part of the complex index of refraction.

Limiting the consideration to IR wavelength range, where $\omega\tau >> 1$ Eq. 3.11 can be reduced

$$\alpha = \frac{\sigma_0}{n' C\varepsilon_0 (\omega^2\tau^2)} = \frac{n'\lambda_0^2 e^3}{4\pi\varepsilon_0 m^{*2} c^3 n\mu} \qquad (3.12)$$

Where: μ is the mobility, m* is the effective mass of the free carriers, λ_0 is the wavelength in free space, n_e - concentration of the electrons per unit volume. According to the Eq. 3.12 the absorbance of a material at a given wavelength is directly related to its electrical conductivity.

This property was used to determine the type of conduction (n or p) in the case of gas sensors (SnO_2, n-CuO/$BaTiO_3$) under oxidizing or reducing gases [138, 139]. A gas adsorbing on to the sensors surface modulate the free carrier density which leads to a variation of the infrared energy transmitted by nanoparticles. The transmitted energy plotted versus gas concentration was directly related to the electrical response of the real sensor.

The influence of the change of free carrier density was also studied by means of IR reflectance spectroscopy [140]. In general, the reflectance (R) is related to absorptivity (see Eq. 3.12) by the Fresnel equation

$$R = \frac{(n+1)+\kappa^2}{(n+1)+\kappa^2} \qquad (3.13)$$

Where κ is the index of absorption.

Infrared reflectance spectra of solid oxides depend critically upon the electronic properties of the material. For non-metallic oxides the reflectivity is: low above the frequency of phonon modes and high between longitudes optical (LO) and transverse optical (TO) phonon frequencies (Reststrahlen spectra). The carriers in metallic materials screen out the coupling between lattice vibrations and external fields. However, the screening is not perfect due to the non-zero screening length, allowing a weak structure to appear close to the LO phonon frequency in IR reflectance. The formation of the carrier free surface layers (depletion layer), associated with chemisorption influences the infrared reflectance spectra of metallic oxides by allowing the coupling of IR radiation to phonons within the ’unscreened’ layer.

The influence of the surface depletion layer on infrared reflectance spectra of Sb:SnO_2 and Na*x*WO3 has been explored using model calculations on a two layer system and compared with IR reflectance experimental data [141]. For Sb:SnO_2 it was shown that with increasing doping levels (increase conductivity) changes in reflectivity at phonon frequency are superimposed on a background reflectivity that becomes stronger and flatter. Other authors [142] attempt to correlate increases of Sb concentration in SnO_2 with four points sheet resistance measurements with reflectivity in MIR range. It was shown that the optical

properties do not fully support the results of the resistance measurements. However, both studies show the potential of IR reflectance studies in this area.

Within this study, the main interest is in diffuse reflectance, which, by itself, is not directly depending on the absorptivity of the material. However, as it was discussed above, the specular components of radiation cannot be fully eliminated and therefore it is necessary to point out how they will influence the diffuse reflectance spectra.

The radiation internally reflected is just directionally scrambled (diffuse) specular reflection and it can be also described by the Fresnel equation (Eq. 3.13). For bands with high absorptivity the reflectance is high. Only light that was not specularly reflected from the sample can enter the sample and hence be adsorbed by it. An increased level of specular reflectance counteracts the absorption by the sample and as a result, strong absorption peaks degenerate into spurious doublets (Reststrahlen bands) [143].

As it was discussed above the increases of the conductivity of $Sb:SnO_2$ increase the background absorbance. This fact has to be taken into consideration when discussing the changes of the conductivity and optical properties of tin dioxide base sensors upon exposure to reducing/oxidising gases. In the relatively high resistance range (>MΩ) this effect can be neglected. But for the sensors with relatively low baseline resistance (<kΩ) the strong changes of baseline reflectance mask the absorption bands and the total reflectance become uninterpretable

3.2.2 DRIFT on sensor- set up and measurement protocol

The quantitative theories of diffuse reflectance assume either 100% reflecting reference material or the layer of infinite depth (continuum theory) or require the transmission and reflection measurements performed on the same sample on an absolute scale (discontinuum theory). In practice, none of them is applicable to sensors.

The IR penetration depth is larger than the thickness of the layer, which makes that the absolute diffuse reflectance spectrum (single channel), contains information from the SnO_2 layer and the alumina substrate. The optical properties of the SnO_2 based sensors (as a whole) change with the temperature. Therefore in order to separate changes at the SnO_2 surface, the reference other than the usual absolute one (i.e. mirror, KBr) has to be used.

Within this work, the differential (relative) approach with the reference spectra recorded directly before gas exposure, also on sensors, is applied. The determined absorbance will be

named the apparent absorbance in order to distinguish between the absolute absorbance measured in transmission mode and relative absorbance measured in diffuse reflectance mode. In the same way, the single channel spectra recorded directly before gas exposure is used as a reference for the transformation to the Kubelka and Munk units. The as-obtained KM relative spectra contain only information on the surface species actively taking part into the sensing: the ones which appear or change their concentration during exposure to gases.

Recently, a similar sampling (referencing) technique was applied for obtaining spectra of unknown samples [144]. There, a relatively IR inactive abrasive is used. However, both cases do not fulfil to the KM prescription of qualitative diffuse reflection spectroscopy.

3.2.2.1 Setup of the DRIFT and electrical measurement (Tubinguen)

- **Mixing and monitoring of gases**

In order to provide the desired gas atmospheres, gas mixing systems are used. A typical gas mixing system consists of PC controlled mass flow controllers (MFC) and valves. The gas mixing(Figure 2-14), system is operated by home made software called POSEIDON. The software via A/D card not only controls the actual gas flow through the mass flow controllers but it can also (at the same time) record the resistance of the sensors and other parameters like humidity or oxygen concentration. Our aim is to observe the surface, mainly in dry air. To do that, the control of the humidity level is crucial. In order to keep the humidity background constant while mixing carrier and target gases a humidity trap was used. It was built out of a folded stainless steel pipe (5 m long) placed in a stainless steel dewar partly filled with liquid nitrogen. The pipe was cooled down by vapour of liquid nitrogen and not directly liquid nitrogen itself, in order to freeze only water and prevent the condensation of oxygen. The trap allows keeping the humidity level constant at 3 ppm ± 1 ppm. To control such level of humidity, a dew point (DS 100 Alpha Moisture System) meter was used. The measured humidity is displayed on the instrument indicator in Celsius degree (°C) and is recorded as output current

Dew point meter Humidity was measured by using a dew point meter (DS 100 Alpha Moisture System) based on capacitance changes measurements. The sensor is a variable capacitor, which capacitance is directly affected by changes of partial pressure of water

vapor and that are proportional to the dew/frost point temperature. The measured humidity is displayed on the instrument indicator in Celsius degree (~C) and is recorded as output current.

Dp (°C) =-105.12399+6.26044*1000* I

I is the output current from the dew point meter.

DP, °C	ppm_V
-150	9,2E-12
-140	3,9E-7
-130	9,2E-6
-120	1,2E-4
-118	2E-4
-116	3,3E-4
-114	5,4E-4
-112	8,7E-4
-110	0,00141
-108	0,00222
-106	0,0035
-104	0,00543
-102	0,00837
-100	0,0127
-98	0,0192
-96	0,0287
-94	0,424
-92	0,0622
-90	0,0905
-88	0,1305
-86	0,1869
-84	0,2655
-82	0,3742
-80	0,5238
-78	0,728
-76	1,005
-74	1,378
-72	1,878
-70	2,543
-68	3,425
-66	4,583
-64	6,099
-62	8,072
-60	10,626
-58	13,916
-56	18,132
-54	23,513

-52	30,329
-50	38,961
-48	49,816
-46	63,408
-44	80,368
-42	101,43
-40	127,51
-38	159,64
-36	199,12
-34	247,37
-32	306,32
-30	377,76
-28	464,34
-26	568,82
-24	694,34
-22	845
-20	1025
-18	1239
-16	1494,74
-14	1796,05
-12	2152,63
-10	2573,68
-8	3067,11
-6	3646,05
-4	4322,37
-2	5110,53
0	6027,63
2	6963,16
4	8025
6	9226,32
8	10585,53
10	12117,1
12	13839,47
14	15773,68
16	17940,79
18	20365,79
20	23072,37

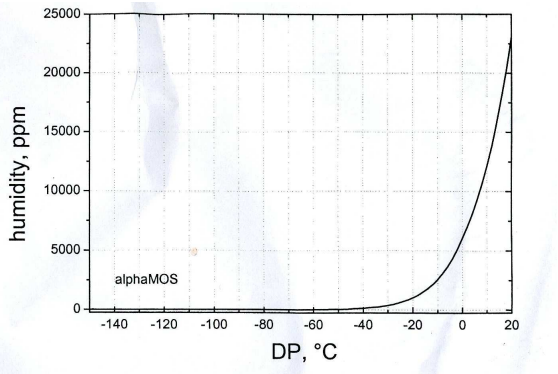

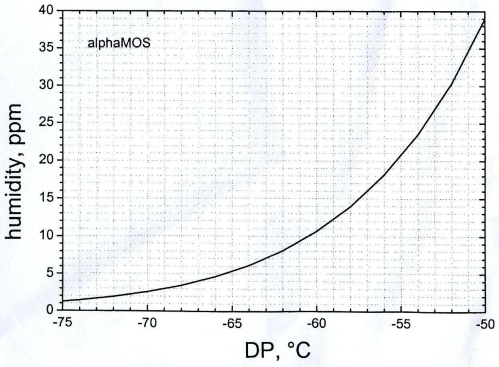

Figure 3-3 : Correspondence Table for the dew point sensor

FTIR Spectrometer. Figure 3-4 shows the complete experimental set up that has been used to simultaneously perform Diffuse Reflectance Infrared Fourier Transformed Spectroscopy (Bruker 66v FTIR spectrometer) and resistance measurements. For measuring resistances digital multimeters (Keithley DMM 199 or 2000) are used. In the case of highly resistive sensors (>200 MW) an digital electrometer (Keithley EMM 617) is needed. The multimeter measures the voltage drop over a reference resistance and sensor resistance and based on the voltages ratio, the sensor resistance is determined. An electrometer is a highly sensitive electronic voltmeter which input impedance is so high that the current flowing into it can be practically considered to be zero. Additionally to the instrumentation used in the characterisation of sensors performance the system is equipped with the Bruker 66v FTIR spectrometer. The diffuse reflectance is collected with the Praying Mantis (fig. 3-5) optics (Harrick Scientific Products, Inc.). The measurement chamber (fig. 3-6) is equipped with:

two NaCl mirrors (which allows the access and afterwards the collection (already diffusely reflected) IR radiation); the sensor holder with 4 electrical outputs (for supplying voltage on the Pt heater and the read out the sensor resistance). The chamber is placed on x, y, z position stage and the whole is built in the optical unit. Around the Drift cell where the sample is positioned, the vacuum is done in order to prevent any interaction with the surrounding atmosphere of the cell.

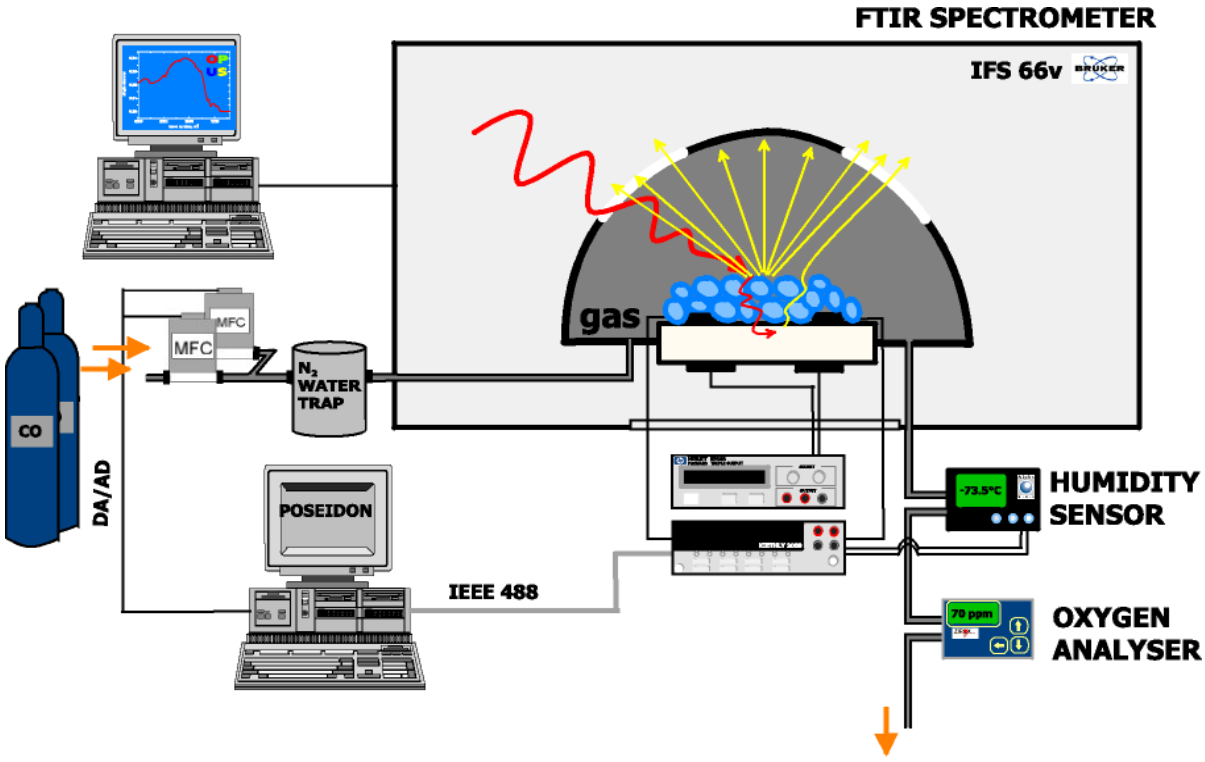

Figure 3-4°: The experimental setup for simultaneous DRIFT, resistance and combustions measurements

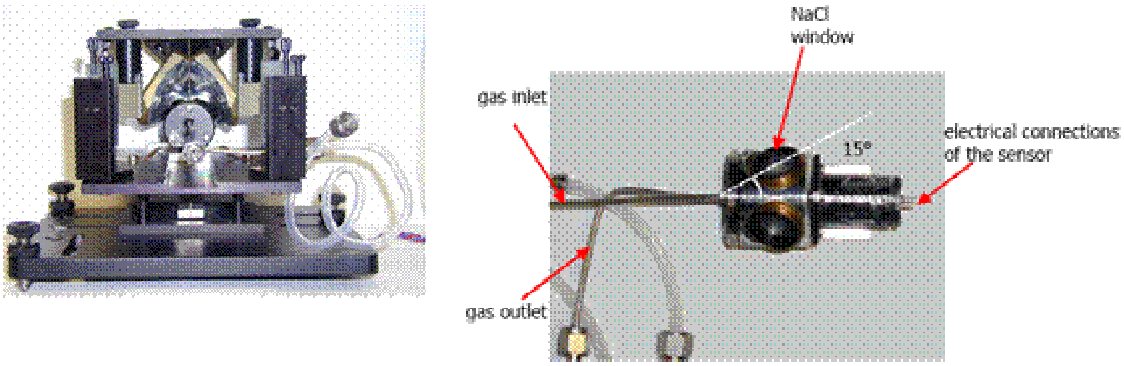

Figure 3-5 : (left) DRIFT-unit "Praying Mantis" with sensor chamber. Two ellipsoidal mirrors collect diffuse reflection. These two ellipsoidal mirrors are positioned on the principle of "off axis" which minimizes direct reflection. (right) Sensor chamber.

To avoid misunderstanding, the single channels are presented. The reason for this is the difficulty to find a common reference like KBr. For a good comparison, we have to know the characteristic of the spectra in dry air of our different sample.

3.2.2.2 DRIFT on powders (St Etienne)

The spectrometer at St Etienne. DRIFTS spectra were recorded with a Fourier transform Nicolet 510P spectrometer with a DTGS detector operated at 4-cm^{-1}resolution. The spectrometer was equipped with commercial diffuse reflectance optics (Spectra-Tech 0030-103). 1024 scans were accumulated in each run. Spectra were presented in the Absorbance mode.

The DRIFTS Chamber. Our DRIFTS chamber (Figure 3-6) is equipped with High Temperature/High Pressure Chamber (HPHTC) Model 0030-103, provided by Spectra-Tech. The powder is placed in the cup of the HPHCTC. A ceramic spacer (T) places the sample (S) at the focal point of the diffuse reflectance accessory. Two pieces of sealed ceramic feedthroughs (E) are employed to establish the electrical connections with the power supply. Pair of Vl6-in. stainless steel tubes (I and O) is available for gas supply. The dome of the DRIFTS chamber is equipped with a pair of 13-ram x 3-mm circular KBr windows (W). Before the DRIFTS analysis, the sample was kept under air overnight at 500°C in order to desorb atmospheric impurities and impurities from the serigraphic deposition.. The sensor was then heated up to the working temperature. In this case, it was not possible to put the vaccum around the cell. An constant pure nitrogen atmosphere were maintained

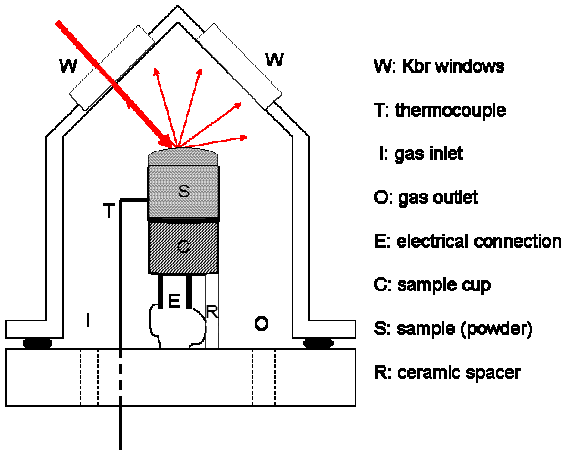

Figure 3-6 : Description of the DRIFT chamber for powder analysis

The gas mixing system. A similar device as the use previously was utilized. In this case, it was not possible to check the level of humidity but we assume that the level is inferior to 10 ppm (air bottle specification)

3.2.3 Band Analysis

The bands in the IR spectra can be fitted by Lorenz, Gauss or Voigts functions. The latter one consist of a Gauss and Lorenz part and is the most suitable function for the bands obtained in an IR spectrum, since the curve form of the IR bands are influenced by homogeneous and heterogeneous band broadening. Homogeneous broadening (broadening through the Experimental Section impulse) correspond to a Lorenz profile, heterogeneous broadening corresponds to a Gauss profile.

In this work, the best results were obtained by applying Lorenz and Voigt functions. For most of the bands, a Lorenz function was used.

For the curve fitting, a small spectral range was selected and on this spectral range a baseline correction was performed. Through the baseline correction, the wings of the Lorenz curve are cut. The error is calculated and can be found in the literature. The error is between 10 and 20%. In this work the error bars are calculated for 10%.

3.2.4 Specific bibliographies on adsorbed species from CO gas.

3.2.4.1 Description of the CO reaction pathways

The person who reads this section has to have some knowledge about the CO reaction pathways in addition of the bibliography offer in chapter 1. One generally agrees that the ionosorbed oxygen species are CO reaction partners and final gaseous reaction product is CO_2. Different carbonates and carboxylates which are often leave out are reaction intermediates. There are different reaction mechanisms leading to such conversion and depending on the temperature. The general reaction can be denoted as follow:

$$nCO + \sigma\text{-}O_n^{\beta-} \rightarrow nCO_2 + \sigma + \beta e^-$$

σ represents absorption sites (various possible sites)

When oxygen is adsorbed on SnO_2 based sensor, the oxygen ionosorption will be formed and one electron becomes localized. The form of the reactive species has to be considered as dependant on the temperature (chapter1, oxygen adsorption). In our range of studies 200°C-400°C, we can consider the form of reactive oxygen according to the following schema:

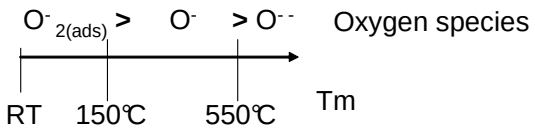

This schematic is also based on TPD measurement (see the section 3.3.2) and helps us to know the major species at the surface of SnO_2. T_m represents the maximum temperature desorption of the species. The maximum desorption for O_2^- is 150°C which not means that above this temperature this species doesn't exist, but it just means that this one is not the major species above 150°C.

The change of the baseline resistance in any SnO_2 based sensor in dry air as a function of the temperature can be related to different oxygen species formed at the surface of the SnO_2. So, in presence of CO, the oxygen species influence the pathways.

The CO conversion in CO_2 is not a direct reaction and some intermediates can be formed at the surface of SnO_2. These species are even not mentioned because they are only stable at the surface of the material and people are usually observed educts and products of the system. In our case which is the study of the surface of SnO_2, these "intermediate" species are crucial the CO sensing.

On Figure 3-7, a sketch of CO reaction pathway is summarized. It describes the formation of the main species observed during the reaction of CO with the surface oxygen species. In the following, possible reaction mechanisms are established on the basis of the correlations described in our own experiments and in the literature [145]. Cartoon presentations are given for a better description of the possible reaction mechanisms. The first aim was not to study the CO mechanism at the SnO_2 surface but to understand how the presence of the metal electrodes can altered the surface reaction.

The sketch in Figure 3-7 demonstrates that the product of CO reacting with the surface is always CO_2. It is assumed that CO_2 which will be observed by DRIFT analysis will be localized in the pore of the SnO_2 matrix. In fact, it was shown that the distance between the two branches of CO_2 bands can change in function of the support. It was observing [146] compared to the free CO_2 (gas phase), the CO_2 present in the pores presented a shorter distance between the branches. One can imagine that the rotation of the molecules is hindered like in viscous media. Moreover, the amount generated at the surface of the SnO_2 is too low in such small chamber.

The starting point of this sketch is CO which reacts with "O^- ". For simplicity on the sketch, only "O^-"is considered to be formed at the surface of SnO_2 during the oxygen ionosorption which is not valid. More details will be brought during the explanation of each species in the following.

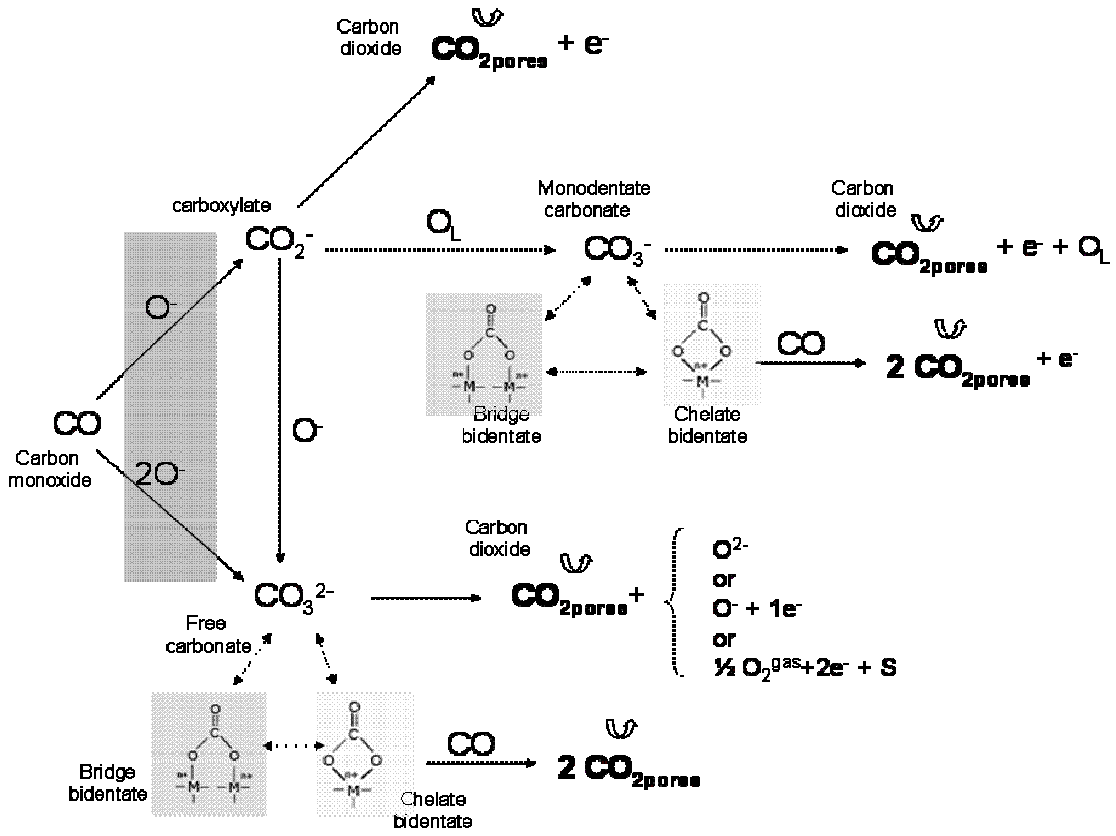

Figure 3-7 : Schematic of CO possible pathways on the surface of tin dioxide

3.2.4.2 Formation of the main intermediates

- **Formation of the carboxylate (CO_2^-):**

The first intermediate species easy to form is the carboxylate. As regards to the oxygen species considered, two possibilities are offered to form the carboxylate (CO_2^-) with reactions with O^-(1) or O_2^-(2) It desorbs to CO_2 in final by the equation (3). Only in the last step (eq. 3), an electron is released to the bulk, which causes change of the conductivity.

$$CO + O^- \leftrightarrow CO_2^- \qquad (1)$$

$$2CO + O_2^- \leftrightarrow 2CO_2^- \qquad (2)$$

$$CO_2^- \leftrightarrow CO_2 + 1e^- \qquad (3)$$

Reaction (1) and (3) pathways are presented in Figure 3-8. First, CO reacts with O- and form the carboxylate which is not stable at the surface. An electron is released to form

CO_2. Reaction with O_2^- (reaction (2)), at least two molecules of CO are needed with one O_2^- to create two carboxylates. The carboxylate species is easiest to create but is relatively not stable at the surface because of the weakest of the bond between the molecule and the surface. It desorbs rapidly CO_2 and release one electron.

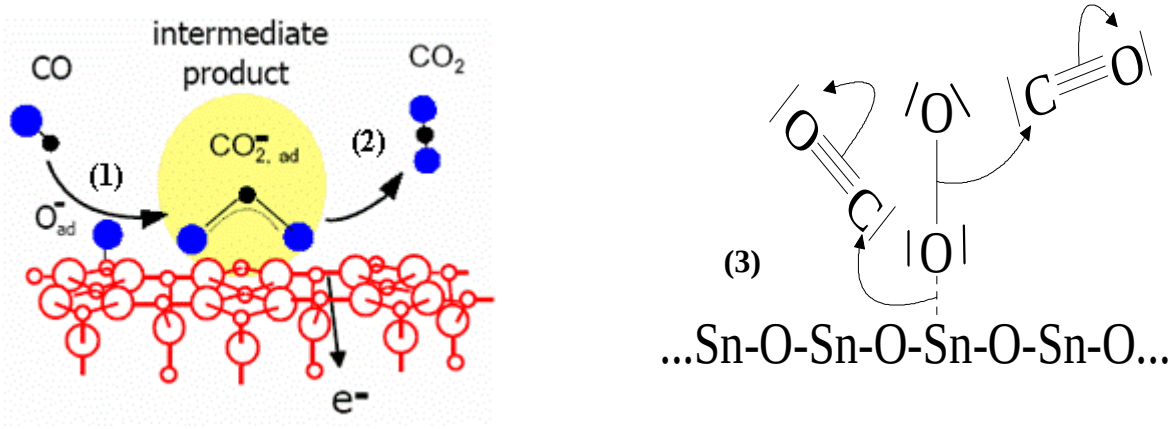

(a) Two steps reactions **(b) one step reaction**

Figure 3-8 : Cartoon of the formation of CO_2^-

In IR, the domain of vibration depends on the coordination of the molecules at the surface of the tin dioxide surface. Table 3-1 shows the frequencies depending on the structure of the molecules at the surface.

Table 3-1 : Structure of differently bound carbonate carboxylate species and their characteristic frequencies in the IR spectra

	Structure	Observed frequencies [cm^{-1}]
I	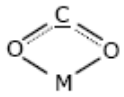	1520-1560 (ν_{as}) 1300 (ν_s)
II	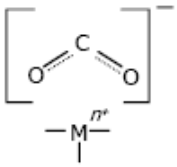	1630-1560 (ν_{as}) 1420-1350 (ν_s)

- **Formation of the free carbonate(CO_3^{2-}):**

Another possible intermediate species is CO_3^{2-}. Three reactions can give the free carbonate:

$$CO + O^- \leftrightarrow CO_2^-$$

$$CO_2^- + O^- \leftrightarrow CO_3^{2-} \qquad (4)$$

$$CO + 2O^- \leftrightarrow CO_3^{2-} \qquad (5)$$

$$CO + O_2^- + 1e^- \leftrightarrow CO_3^{2-} \qquad (6)$$

This species can result from CO_2^- itself which reacts a second time with "O^-"according to reaction (4) and shown in Figure 3-9. It is possible to make a distinction between reaction (4) and (5) where for the reaction (5) CO reacts directly with $2O^-$ without the formation of the carboxylate. Reaction (6) is also theoretically possible but, in this case, a second electron should be extract from the material. Reaction (6), due to the need of a second electron is not favoured, the electron is mainly localized on oxygen species and to catch another one, the required energy would be important. Furthermore, such reaction will have a bad influence on the sensor by reducing the sensor signal. It is assumed that this reaction can be neglected.

One can imagine a possible reaction with O^{2-}.For this, we have to consider that CO reacts with O^{2-} and in the same time with O_L (lattice oxygen).

$$CO + O^{2-} + O_L \rightarrow CO_3^{2-}$$

In this case, CO_3^{2-}do not give vibrations of free carbonate as oxygen is linked to the lattice but the vibration of monodentate carbonate CO_3^-. It is not possible to obtained free carbonate with O^{2-}.

The reaction with a second CO molecule should be considered to be the easiest way to give the final CO_2 product.

$$CO_3^{2-} + CO \leftrightarrow 2CO_2 + 2e^- \qquad (7)$$

It assumes that the stability of the free carbonate is not too much important and the free carbonate can react itself as follow:

$$CO_3^{2-} \leftrightarrow CO_2 + \begin{cases} O^{2-} \\ O^- + 1e^- \end{cases} \qquad (8)$$

$^1/_2O_2 + 2e^- + s$

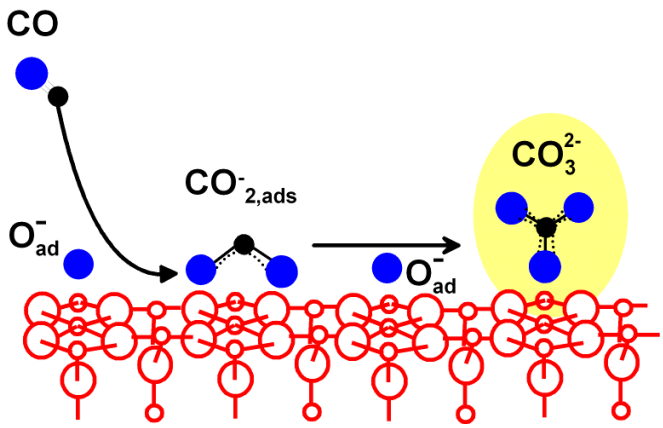

Figure 3-9 : Formation of CO_3^{2-}

- **Formation of the monodentate carbonate (CO_3^-):**

In this work, CO_3^- ions can be also identified as intermediate products. CO_2^- can react on a specific site on SnO_2 and give one of the most stable intermediate at the surface; the stability is due to the delocalization of the electron, the cloud of electron is deformed and stabilizes this entity. The formation could be:

$$CO_2^- + O_L \leftrightarrow CO_3^-(9)$$

Another possibility to form CO_3^- is the possibility to free carbonate CO_3^{2-} to lose one electron and move to a free site at the surface of the SnO_2:

$$CO + O_2^- \leftrightarrow CO_3^{2-}{}_{(free)}$$
$$CO_3^{2-}{}_{(free)} \rightarrow CO_3^-{}_{(surface)} + 1e^-$$

CO can react with O_2^- to give CO_3^- free at the surface of the SnO_2 and then this species has to found a place to be stable, rather while it become directly CO_2

The desorption process is as follow:

$$CO_3^- \leftrightarrow CO_2 + 1e^- + O_L$$

A cartoon presentation is given in Figure 3-10. Experiments made with CO_2 as educts give mainly this intermediate species.

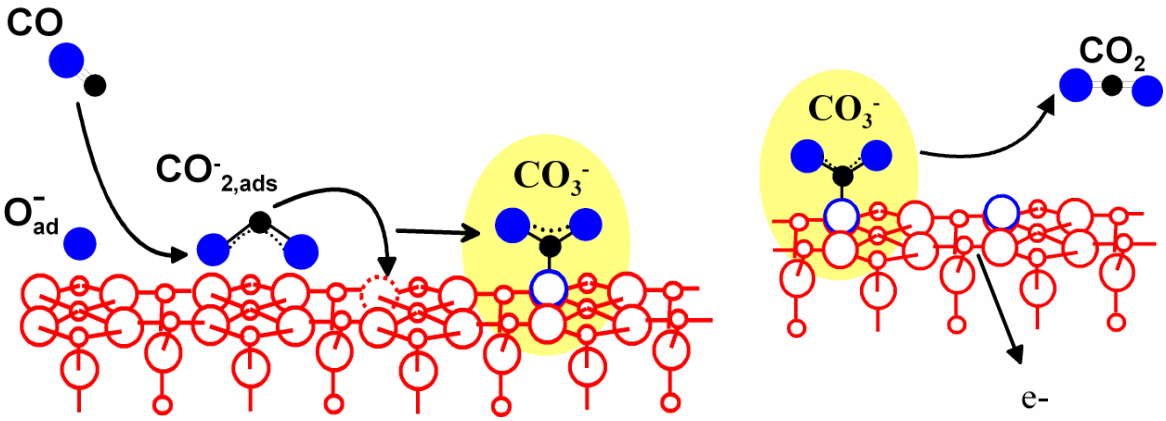

Figure 3-10 Formation of the monodentate carbonate

- **Formation of the bidentate (chelate and brigde):**

It is assumed that the formation of the bidentate (chelate and brigde) is only possible in the pathway of the formation of the monodentate or the free carbonate. These species are more stable at lower temperature and should not be considered at elevated temperature. There are mainly coming from a recombination of CO_3^- or CO_3^{2-} for the chelate bidentate. For the bridge a direct reaction of CO wit $2O^-$ can be also possible.

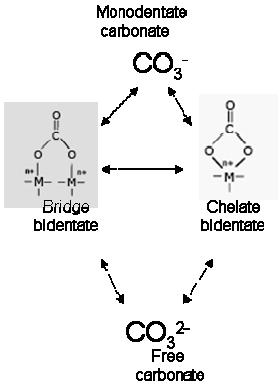

Figure 3-11 : Schematic of the formation of the bidentate chelate and bridge resulting from a rearrangement of CO_2^- and CO_3^{2-}

3.2.5 RESULTS

The aim of this work is to follow the changes of the properties of SnO_2 sensors surface induced by the change of the electrodes material (Au or Pt). How the electrodes can handle the modification of sensitivity towards CO and the modification of the reaction mechanisms? Electrical DC measurements conducted in parallel to the DRIFT measurements will be presented in this section.

3.2.5.1 Remind of DC measurement with CO on SnO_2 based sensors with different electrodes (Au and Pt). Position of the problem.

In Figure 3-12, the time dependence of the SnO_2 based sensors resistance provided with two different nature of electrodes (Au or Pt), placed in the DRIFT measurement cell and heated at 350°C, is shown; three CO pulses were applied (50, 100 and 250ppm).

The differences associated to the different nature of electrodes can be summarized as follows:

1. The baseline resistance is higher for platinum (24 MΩ) than gold (1MΩ);
2. The sensor with platinum electrodes presents higher sensor signals toward CO;
3. The shape of the response indicates different kinetics

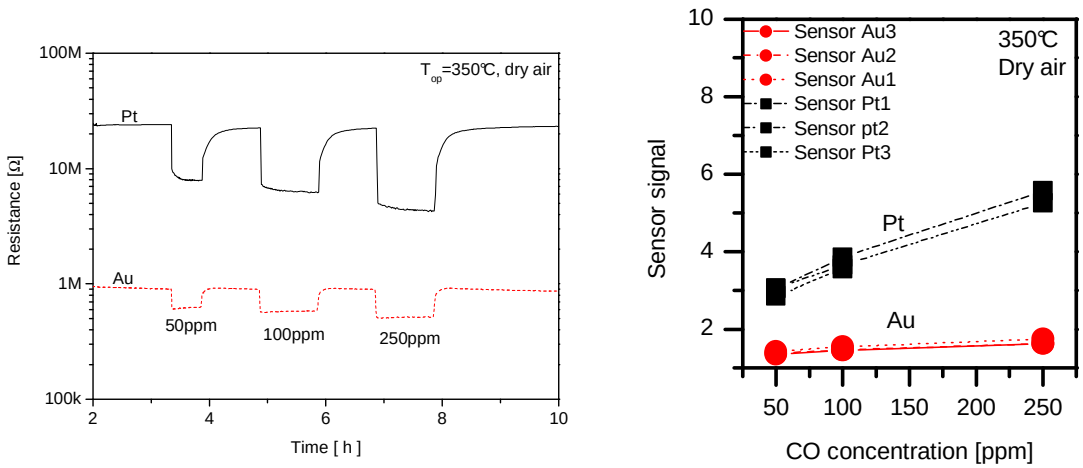

Figure 3-12 : Resistance and sensor signal dependence on the CO concentration in dry air at 350°C sensors working temperature. Sensor provided with platinum (Pt) electrodes and gold electrodes (Au)

At 350°C, the performance and in particular the sensor signals are the most significant in term of the influence of the nature of the electrodes. Figure 3-12 (On the right), the sensor signal for 3 sensors provided with Pt electrodes and 3 other ones with gold electrodes are shown. At this temperature, statistically the platinum presents the higher response to CO in

dry air. The role of the electrodes on the performance of the sensor is difficult to explain looking only the DC measurement

Along the operating temperature of our sensors range, 200- 400°C, the same outcome is found. DC sensing performance is presented in Figure 3-13. According to the results, the most marked difference between the sensors provided with Au and Pt electrodes is observed for both baseline resistance and sensor signal. Along the working temperature, the baseline of the platinum sensor is always higher than that of the gold one. It is nearly 1 order of magnitude at temperature superior than 200°C. At 200°C, for both sensors, the resistances are similar. For all working temperatures, the sensor signal is higher for platinum than for gold. Besides that, at this temperature, both the electrical and spectroscopic results were quite stable and reproducible.

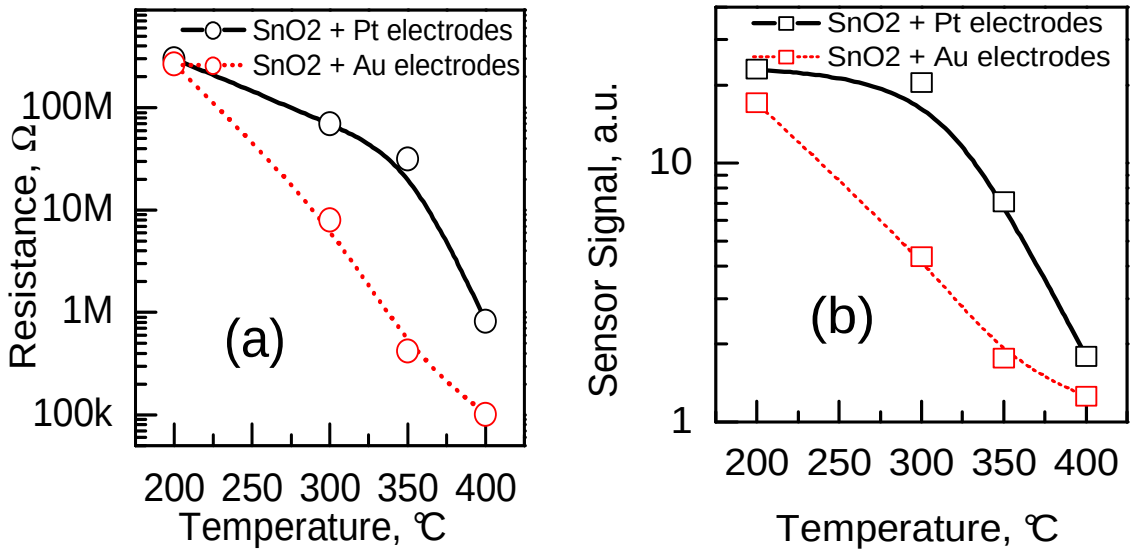

Figure 3-13: Resistance and sensor signal dependence on the 300 ppm CO concentration in dry air for different working temperature. Sensor provided with platinum (Pt) electrodes and gold electrodes (Au)

This behaviour matches with other studies [147]where the authors found also better performances using Pt electrodes. The interpretation of the electrical data is complicated by the fact that the adsorption of both reaction partners, oxygen ions and CO, depends on the temperatures. The reason for such behaviour of the sensors is investigated by simultaneously performed electrical measurement and DRIFT spectroscopy, and will be presented in the following section.

NB: The dependence of resistance and sensor signal on temperature is not exactly similar to the one observed in previous test (cf Figure 2-19, p68): the presence of a maximum is not always observed. The main hypothesis to explain such difference is the presence of residual water, depending on various experiments

3.2.5.2 CO sensing-Impact on the sample' surface

To characterize the impact of the nature of the electrodes during the CO sensing 4 types of sensors have been used; the preparation of each sample was explained in the chapter 2:

a. Conventional SnO_2 sensors: with 2 different natures of electrodes Au, Pt and without any electrodes

b. Powders: Pure SnO_2 and Mixed SnO_2 + metal particles (Au or Pt)

c. Mixed sensors: mixed SnO_2+ metal particles (Au or Pt) as the sensitive layer on alumina substrate provided with heater but where the electrodes were removed.

d. Mixed sensor with platinum electrodes: same sensors in **c** but with platinum electrodes

3.2.5.2.1 Conventional SnO_2 based sensors

3.2.5.2.1.1 Important ranges of DRIFT

Before any descriptions of the results, it is important to define some important range of DRIFT spectra which will be studied in this work. Figure 3-14 shows a typical DRIFT spectra in single channel (raw data), in the IR middle range between 900 and 4000 cm^{-1} for the sensor with platinum electrodes and pure SnO_2 as a sensitive layer. Here, two spectra in single channel are shown in fig3-13(a): one in dry air and the other one where 250 ppm CO was introduced in dry air. To analyse the data is necessary to convert them in Absorbance (fig. 3-13(b)) because it is easier to identify the modification due to the presence of the gas.

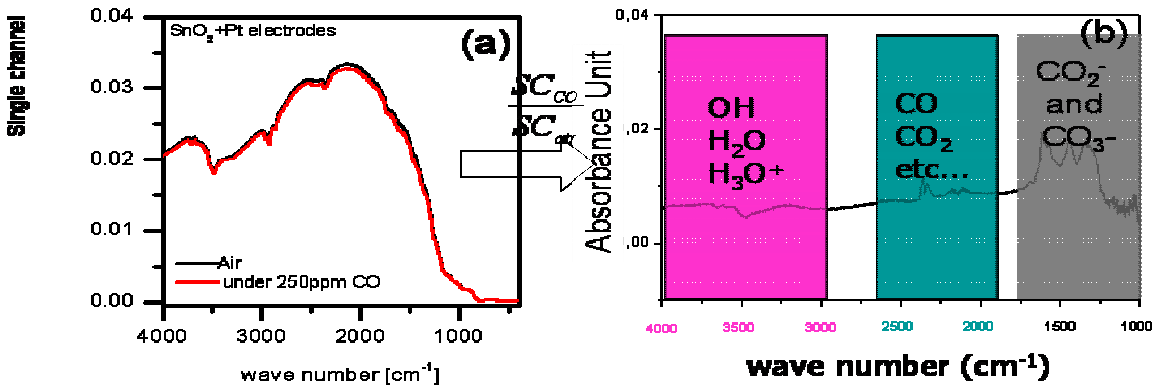

Figure 3-14 : Illustration of the conversion of the single channel spectra (raw data) into the absorbance spectra

In the range of the study, three main regions are affected by the presence of CO:

- 4000 to 3000 cm^{-1}: is the OH region where the vibration of surface OH group and water stretching vibration can be identified.
- 2500 to 2000 cm^{-1}: corresponds to the position of the band of CO_2 and CO.
- 1800 to 900cm^{-1}: Several adsorption bands could be present. These bands are assigned to surface carbonate and carboxylate species, deformation mode hydroxyl group and metal-oxygen. This is the region of all bands corresponding to the different intermediates of "CO_2 reaction" between surface oxygen species and CO.

Limitation and important remark:

Due to the set up of our system, the oxygen study is not possible. In other word, follow the metal-oxygen bond during the gas exposure, its evolution and possible shift are not feasible.

An important remark has to be mentioned. In this study, the carboxylate and carbonate will be mainly study to understand the effect of the electrodes on the surface species. In this region, it is important to note that in our case no new bands appear during the CO exposure. Only a variation of the intensity (increase or decrease) of bands already presented in air is observed. Due to the presence of CO_2 in atmosphere, the carbonate and carboxylate species can be formed during the fabrication process of the sensors or during the time past in atmosphere. Davydov [148] shows that with a CO_2 exposure on SnO_2, the same intermediates species observed with a CO exposure can be present. In this study, the creation of new band in single channel (which means new species) has never been observed.

3.2.5.2.1.2 SnO_2 conventional sensor: DRIFT analysis of devices with Au and Pt or without electrodes under air

Figure 3-15 shows the single channel of pure SnO_2 for gold, platinum and without electrodes in dry air at 200°C. Several adsorption bands can be seen in the spectra range between 4000-3000 cm^{-1} and 1800-900 cm^{-1}. The entire study is a comparison of the different samples used. Here, we illustrate that in single channel, in dry air and without any gas exposure, the surface of sensor is different from one type of sensor to another. The sensors with gold, platinum and no electrodes present some similarities.

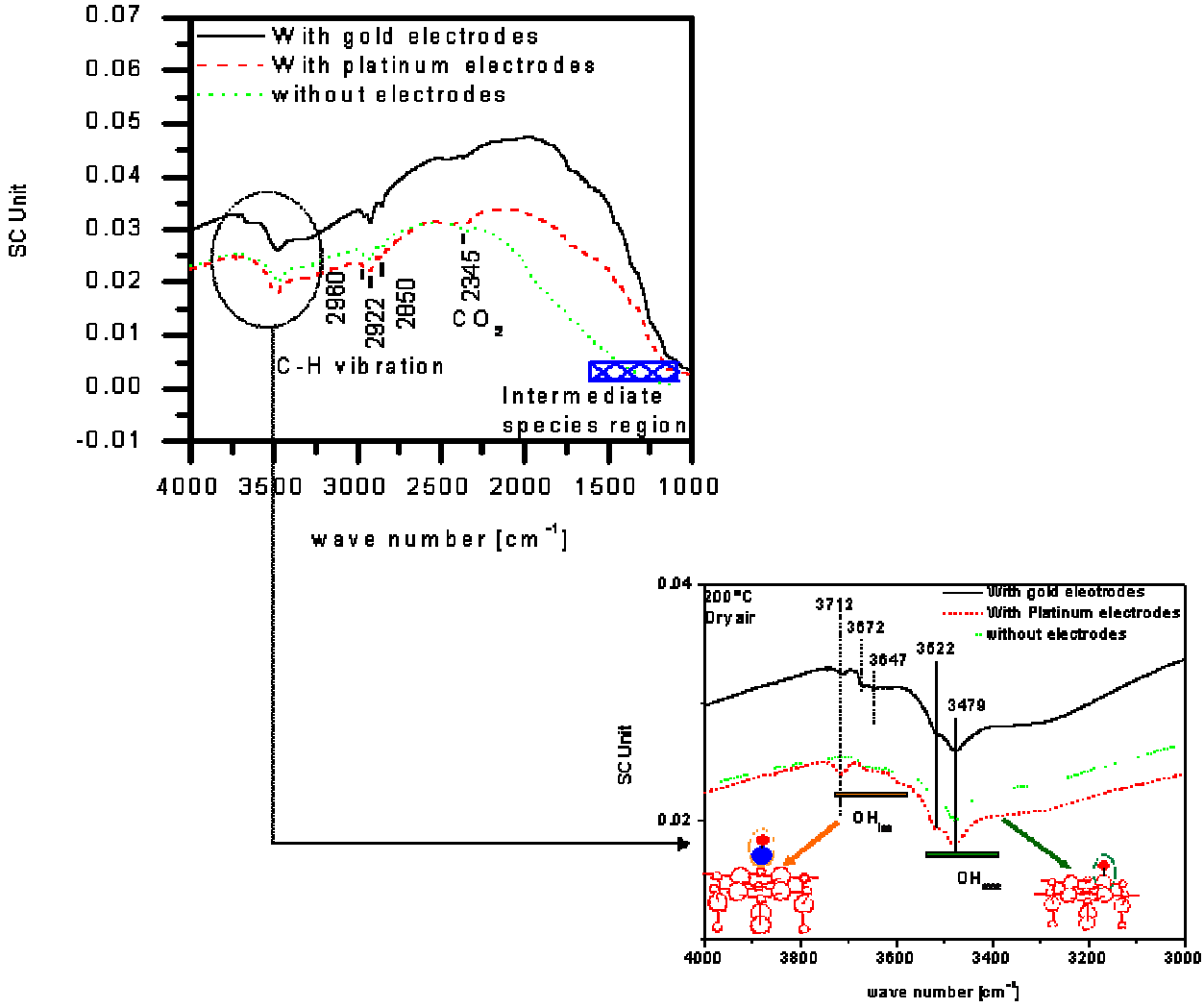

Figure 3-15 : Single channel spectra for pure SnO_2 for gold, platinum and without electrodes recorded at 200°C in the full spectre range (4000-850cm^{-1})

The general shape of single channels spectra is very similar for the three samples. Nevertheless, some difference appears:

- The general absorbance is higher for the gold type whereas for the others they are nearly the same. This effect could be explained by the phenomena of the free carrier charge already mentioned; As mentioned before, the influence of the free carrier charge depend on the resistance of the sensor. The gold resistance is lower so the effect of the free charge carrier can be more important.
- In the region of the intermediate species (1800-900cm^{-1}) the level of pseudo absorbance in single channel (SC) is different. We don't have any convenient explanations.

- A small band is present at 2345 cm^{-1} corresponding to CO_2, resulting from trace of CO_2 in the air flow.
- Three bands are easily identified at 2960, 2922 and 2850 cm^{-1} corresponding to C-H vibration. In fact, in the past, an oil pump was used for the vacuum around the cell. Some traces are still present. However, the level is always constant.
- The main difference between the three samples appears in the range of 4000-3000 cm^{-1}. If we make a zoom, Figure 3-15, at high wave number (4000-3000 cm^{-1}) different characteristic bands are present. Bands at 3712, 3672, 3647 cm^{-1} are assigned to terminal hydroxyl groups and bands at 3522, 3479 cm^{-1} are assigned to rooted OH groups. The band at 3712 cm^{-1} appears only for sensor provided by electrodes. Between 3400 and 3000 cm^{-1} weak broad is present corresponding to molecular water H_2O

- **Effect of the temperature on OH/H_2O species**

In order to determine the influence of the temperature on the surface species in dry air, heating was applied between 200°C and 400°C on conventional SnO_2 sensor provided with electrodes (Au or Pt).

Figure 3-16 shows the single channel spectra recorded at different temperatures in dry synthetic air. With increasing temperature a dramatically change of the spectra is observed over the complete spectral range. Looking over the total spectral range, general changes in the band structure and intensities are observable for both sensors.

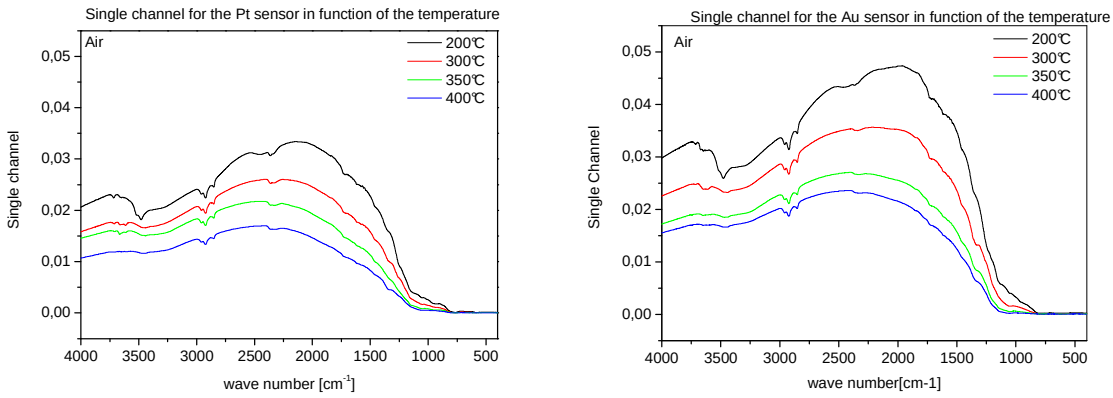

Figure 3-16 : Single channels IR spectra at different temperatures for Pt electrodes and Au electrodes.

The main changes are seen in the region between 4000-3000cm^{-1}. The main affected OH bands are the rooted OH group at 3522, 3479 cm^{-1}, they disappear with the rise of the temperatures. Figure 3-17, focuses on the OH region and compares the influence of the temperature on the visible OH bands between gold and platinum. They are nearly similar with the temperature even if at 350°C the sensors with platinum shown more bands (3710, 3666, 3614 cm^{-1}) whereas only one band is observed with the gold at 3648 cm^{-1}.

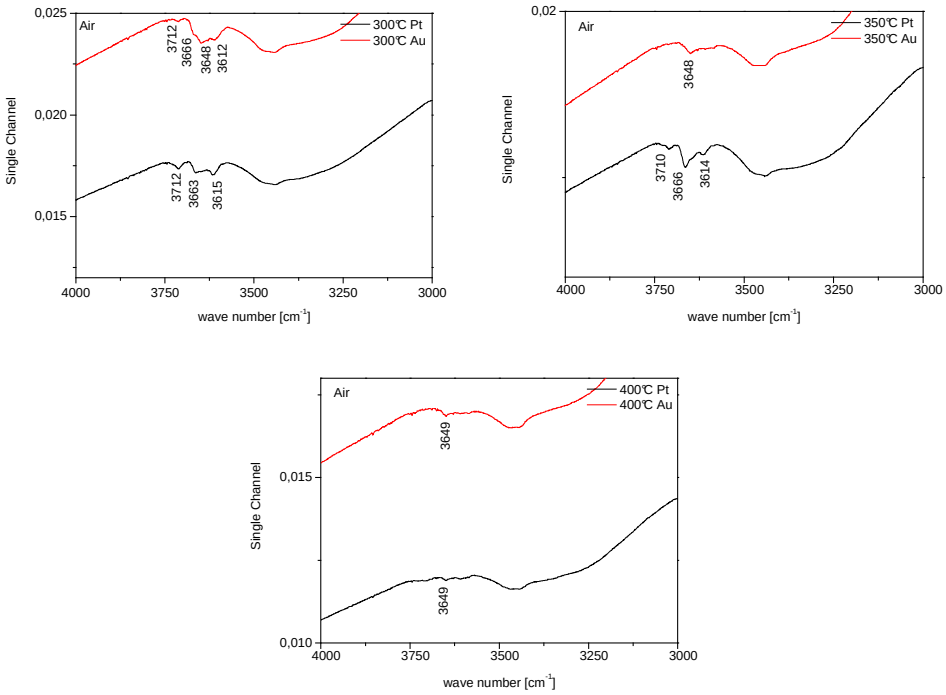

Figure 3-17 : OH/H_2O spectral range recorded at different temperature in single channels spectra for Pt electrodes (black) and Au electrodes (red) SnO_2 sensors.

- **Conclusion of results under air**

Results obtained with the three conventional sensors in dry air as a function of the temperature give us the following information:

- First, no significant difference has been observed to one sample to another in the region of intermediate species (carbonate and carboxylate). It is assumed that region is the same for all the type of conventional sensor in dry air.
- The terminal OH groups, in a certain extent, are different between each sensor at low temperature. With the increase of the temperature, the difference disappears. This result could explain the difference observed in the baseline resistance where platinum exhibit a higher resistance. Along the range of

temperature, the OH group are more stable at the surface of the sensor provided with platinum electrodes.

3.2.5.2.1.3 Interaction of CO on the surface of conventional sensors.

- Global analysis of total spectra 4000-1000cm^{-1}:

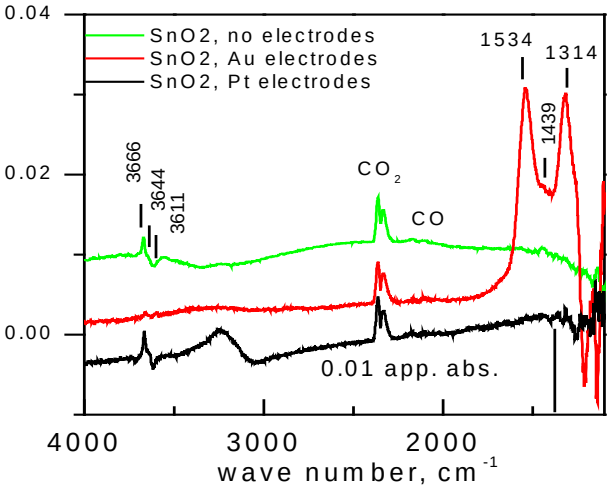

Figure 3-18 : The whole DRIFT spectra of the tin dioxide sensors after exposure during 30min, at 350°C, to 250 ppm CO in dry air with different types of electrodes (-Au,-Pt, -No electrodes).The spectrum recorded before CO exposure was used as a reference for each type of sensors.

The DC measurement was described in Figure 3-12. At 350°C, the effect was found to be meaningful. **This temperature will be considered for all the type of samples the temperature of the study**. DRIFT spectra in absorbance were recorded in the same time of electrical measurement. The results for the type of sensors (Au and Pt electrodes and without electrodes) are shown in the Figure 3-18. Spectral features are different depending on the electrode nature used:

- Formation of CO_2 (band at 2343 cm^{-1}) is observed for each sensor. In the Figure 3-19. The peak area of the CO_2 bands is shown in function of the CO concentration for gold and platinum. The CO conversion seems to be slightly higher with gold. No enough concentration was done with the sample without electrodes to compare with the others.

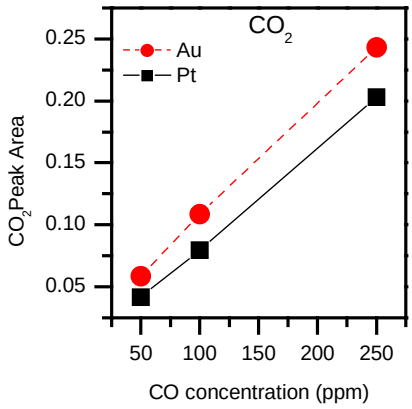

Figure 3-19 : Change of the area of the CO_2 band as a function of CO concentration.

- General overview of the spectra in Figure 3-18 indicates that OH bands are less affected with gold electrodes devices. On the contrary intermediates species between 1800 and 900 cm^{-1} are more present on such devices. Details analysis is exposed hereafter.

- For SnO_2 sensor with Pt electrodes and without electrodes, in the OH-group region, the positive band at 3666cm^{-1} and 3644cm^{-1} prove the increase of isolated group. Negative bands at 3611cm^{-1} has been observed and corresponds to the decrease of isolated OH.

- <u>OH region analysis during the CO exposure for Au and Pt electrodes.</u>

OH region (4000-3000cm-1) is affected during the CO exposure and as a function of the working temperature.

In order to have a clear understanding, the study of this region is developed in this section. Figure 3-20 shows the spectra in the range of 4000 and 3000 cm^{-1} for the conventional sensor provided by gold or platinum electrodes.

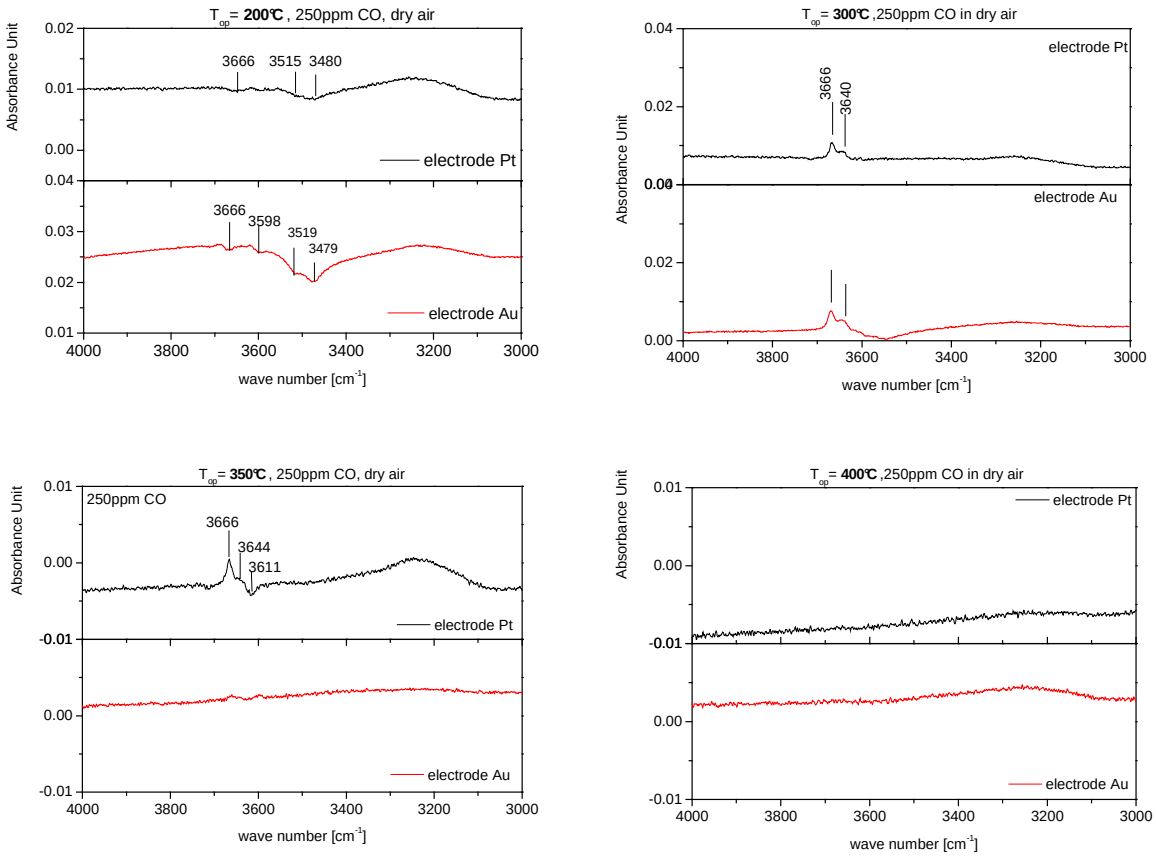

Figure 3-20 : Spectra in absorbance between 4000 and 3000 cm^{-1} of the pt and au electrodes sensors exposed to 250ppm of CO at 2different temperatures. As a reference spectrum in air directly before CO exposure has been used.

- At low temperature, (200°C): for both sensors, the bands at 3666, 3514 and 3480 cm^{-1} decrease which means isolated OH-group (the two first) and rooted group are eliminated or consumed.

- At intermediate temperature elevated (300°C-350°C): the OH bands at 3666 and 3644 cm^{-1} increase whereas the bands at 3611cm^{-1} decreases. This increase of the OH groups is observed for both sensors (Au and Pt electrodes) even if at 350°C for the gold the bands are not very intense.

- At temperature above 400°C: no band appears or disappears; OH groups are not modified in this range of temperature.

Amount of absorbed species dependending on the electrodes nature

Carbonate and carboxylate species analysis:

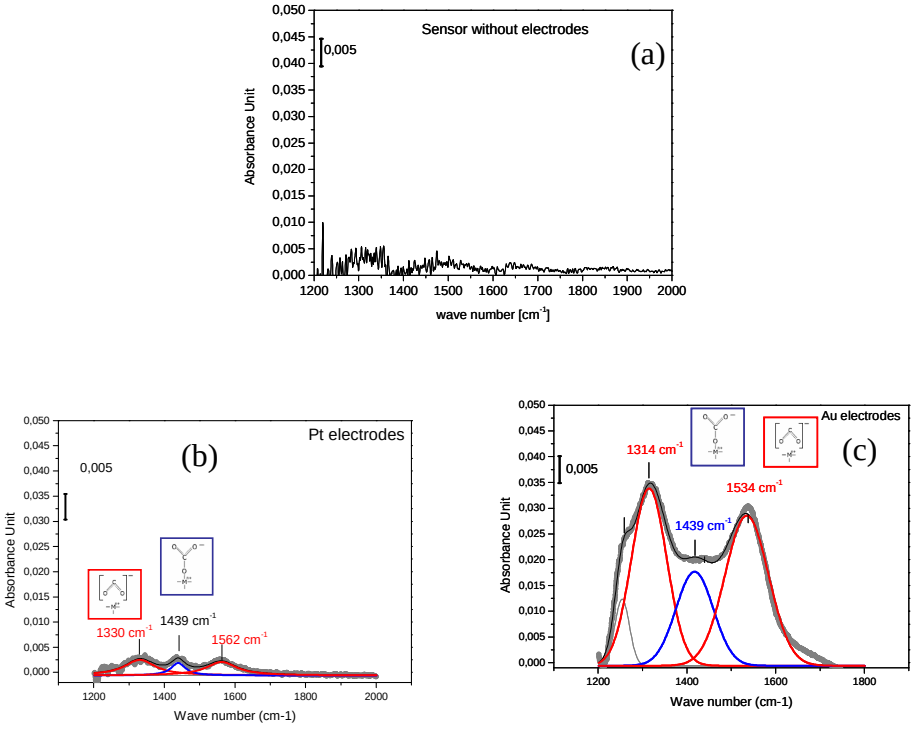

Figure 3-21 : Low wave number analysis DRIFT spectra of SnO_2 sensors recorded at 350°C under 250 ppm of CO. on top: (a) sensor without any electrodes, at the bottom (b) sensor with platinum electrodes (c) sensor with gold electrodes. The spectrum recorded before CO exposure was used as a reference.

It is assumed that the amount of intermediate species decrease with the increase of the temperature. In fact, the stability of the intermediate species is function of the kinetic of the CO conversion which depends also of the operating temperature. On Figure 3-21, for pure SnO_2 sensors without any electrodes, no intermediate species is observed. On the platinum electrodes devices some weak bands is observed at 1562, 1330cm^{-1} and 1439cm^{-1} corresponding to the carboxylate and the monodentate carbonate. The intensity of this bands suggest that the amount of intermediate at the surface of this sample is low and should be consider as traces. On gold electrodes devices, the intensive bands at 1534 and 1314 cm^{-1} attest a large amount of carboxylate present on the surface.

- Kinetic of intermediates species (range 1800-900cm^{-1}) during CO exposure

DRIFT spectra at 300°C in absorbance during 250ppm CO exposure in dry air and link to DC measurement are shown in Figure 3-22 for gold and platinum electrodes.

In DC measurement, it is shown that:

- Baseline resistance is higher for Platinum than gold
- Sensor signal is higher for Platinum than gold
- The response time (95%)is quite similar around the minute
- The recovery time is shorter for Platinum electrodes.

In correlation with the resistance, a special attention has to be taken to the formation of the intermediate species at low waves number (1800 to 900cm^{-1}). The absorbance spectra at 300°C is shown because the formation of band is emphasized and phenomena easy to follow.

With gold electrodes during Figure 3-22 (a):

- The presence of CO_2 is observed immediately in the first spectra (15min), band at 2345 cm^{-1}.
- Formation of bands at 15439 and 1324 cm^{-1} corresponding to the carboxylate are the first intermediate created on the surface (15min).
- With the time (30 min), the formation of the carboxylate is in equilibrium
- During this time, a new band at 1449 cm^{-1} corresponding to the carbonate which was not clearly present before on the spectra at 15min is present.

when CO exposure is stopped, Figure 3-22 (b)::

- Trace of CO_2 is still visible after 15min but disappear after.
- Bands corresponding to caboxylate (1549-1324cm^{-1}) disappear quickly and are not detectable after 15 min.
- The band at 1449 cm^{-1} (monodentate carbonate) takes time to disappear. After 2 hours, it is possible to identify it.

With platinum electrodes during the CO exposure Figure 3-19 (a):

- The presence of CO_2 is observed immediately in the first spectra (15min)
- The intensity of the bands is quite weak is comparison with the sensor provided with gold electrodes

- After 15 min, three bands are identified. They are assigned to carboxylate (1550-1350 cm^{-1}) and carbonate (1449 cm^{-1}). This means that these species appear at the same time.
- The intensity of all the bands increases with time.

When CO exposure is stopped Figure 3-22 (b):

- After 15 min, only carbonate are still present, prove is the band still present.
- After 30min, all bands disappear.

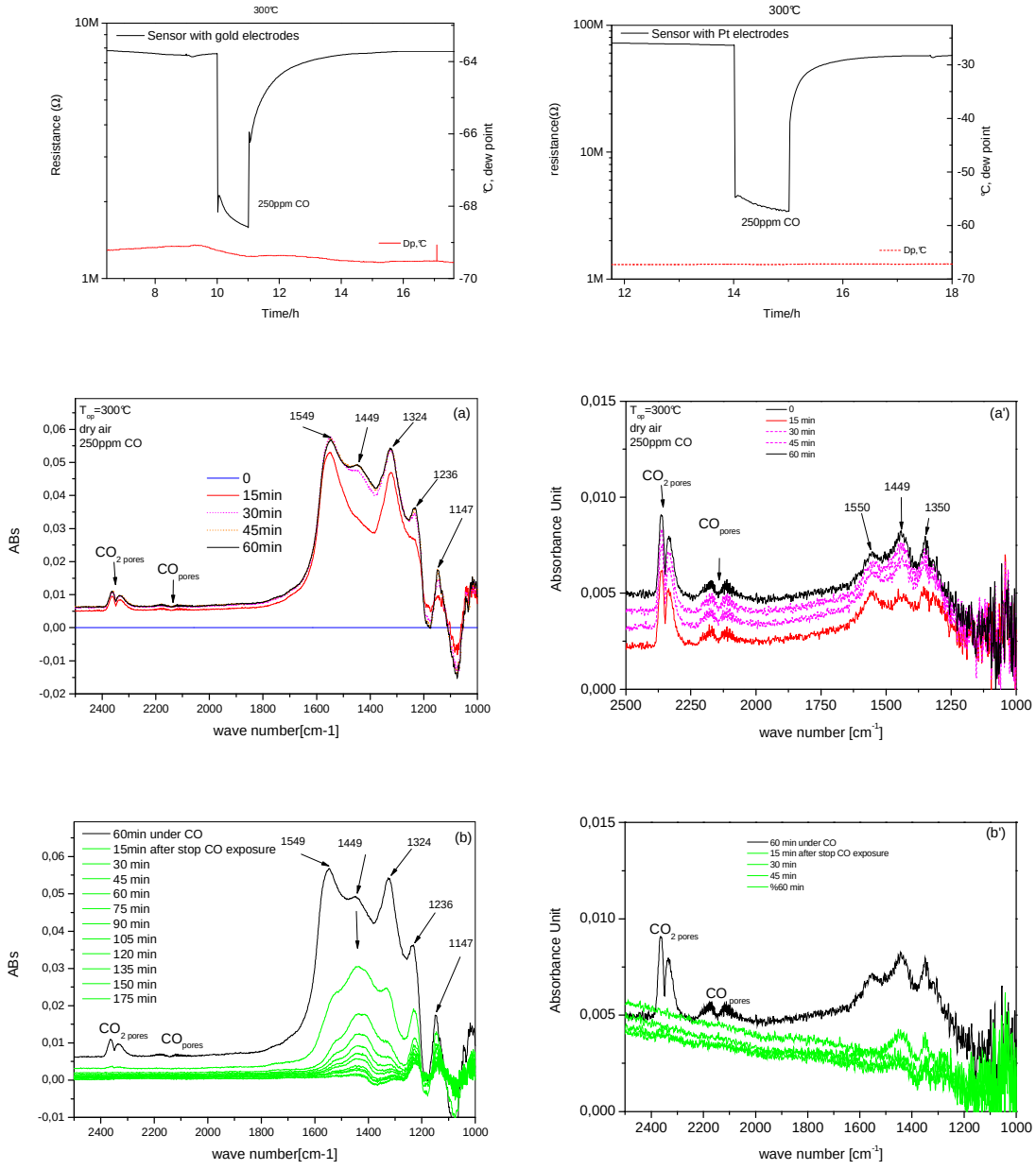

Figure 3-22 : Resistance and DRIFT spectra versus time, measured at 300°C for Au and Pt electrodes sensors: (a) the spectra under CO. (b) spectra recorded after the CO exposure.

3.2.5.2.1.4 Humidity effect on CO sensing

It was important for us to complete the studies by applying water in our system. If we want to talk of real working condition we have to take account of the humidity.

At 300°C, the response of pure SnO_2 sensor provided with gold electrodes and platinum electrodes under CO in 10%RH is shown in Figure 3-23. The simultaneously DRIFT spectra experiment are shown in Figure 3-24 for Platinum and Figure 3-25 for Gold. The performance for each type of sensors, in humidity, is quite closer in term of electrical response. At 300°C the signal (R_0/R) is higher for Pt (26) than for gold (20) device.

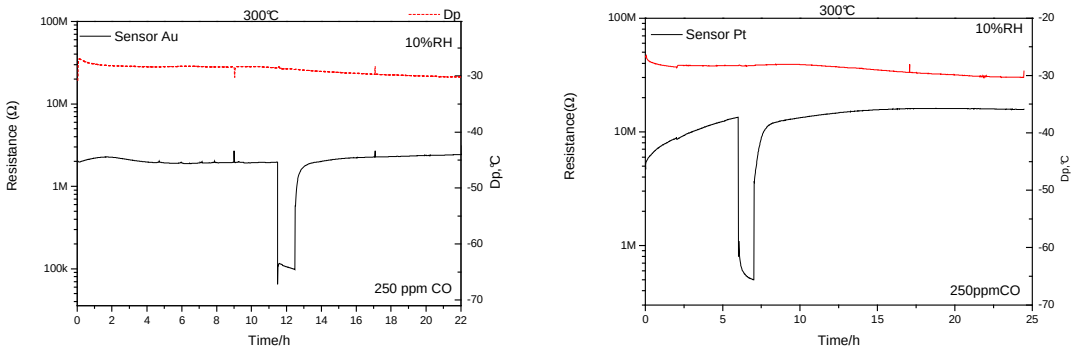

Figure 3-23 : Response of sensors provided with gold electrodes (left) and platinum (right) at 300°C.

DRIFT experiments were also performed in the presence of humidity. The results are presented hereafter.

- With platinum electrodes:

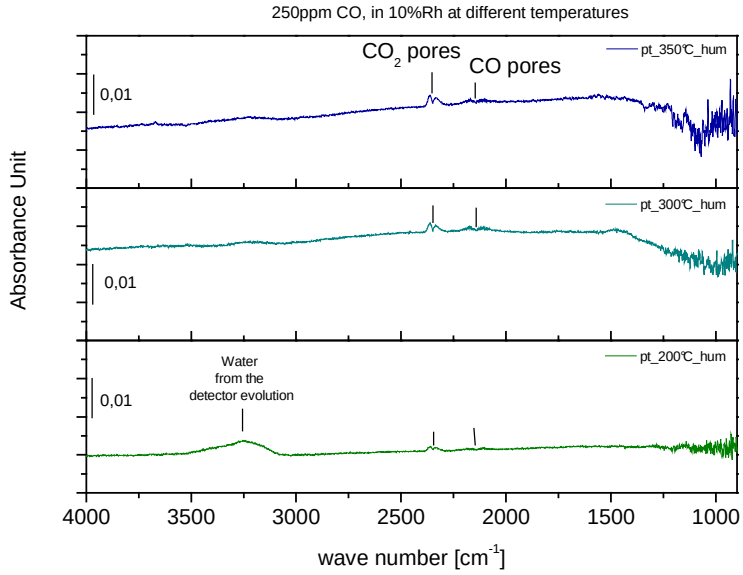

Figure 3-24 : Spectra in absorbance for Pt electrodes sensor exposed to CO at different temperature in 10% of humidity. As a reference, spectrum in air directly before CO exposure has been used.

Figure 3-24 shows the spectra for different temperatures of the Pt electrodes sensors exposed to 250 ppm CO in 10% RH. For all operating temperatures, no band has been observed excepted for the band of CO_2 and CO. No modification of the OH group has been observed in this condition.

- With gold electrodes:

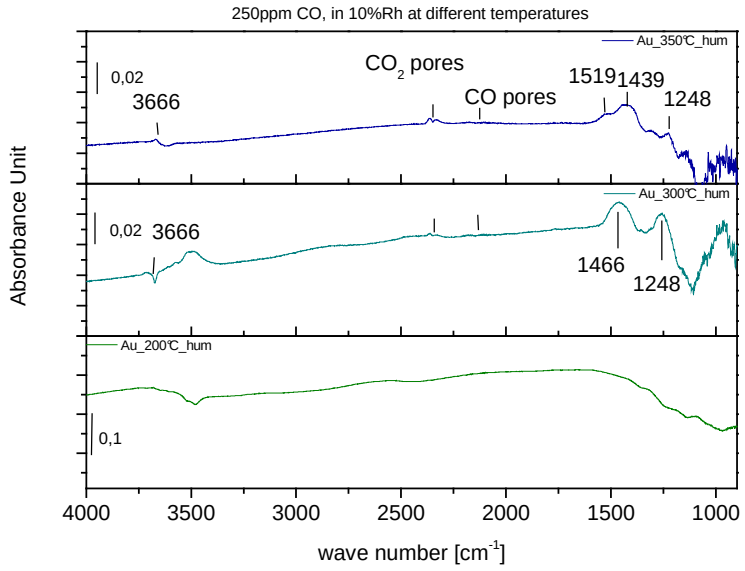

Figure 3-25 : Spectra in absorbance for Au electrodes sensor exposed of CO at different temperatures in 10% RH. As a reference spectrum in air directly before CO exposure is used.

Figure 3-25 shows the spectra for different temperatures of the Au electrodes sensors exposed to 250 ppm CO in 10% RH.

- The intermediate bands are present at elevated temperature but not at 200°C
- The OH groups are modified during the CO exposure.
- No bands can be assigned at 200°C but when the temperature becomes superior the bands can clearly be identified. At 300°C, the band at 1466 cm^{-1} has been observed which proves the formation of monodentate carbonate. The band at 1248 cm^{-1} could be related to the water bending vibration well-pronounced in this particular experiment. At 350°C the band at 1466cm^{-1} (broader than normally) is still present.

Not enough experiments have been complete, in humidity, to conclude on the influence of the humidity. Nevertheless, these experiments confirm the difference of the surface reactions on Pt sensors and Au sensors. Like in dry air, the sensor with gold electrodes shows more bands, in humidity, than the platinum one.

3.2.5.2.2 Summary of results with Conventional sensors

CO sensing investigated by DRIFT and DC measurements for sensors provided with two types of electrodes: Au or Pt.

The higher sensitivity of the sensor provided with Pt electrodes is explained by the different manner in which the conversion of CO to CO_2 takes place. The differences are illustrated by the different role of the reaction intermediates that indicates. In the case of Au electrodes, the intermediate species block the charge, previously trapped on the O^-, on the ionic CO_2^- and CO_3^-. On the opposite, for Pt electrodes one cannot observe an increase of the ionic intermediates, which suggest a very fast conversion from CO to desorbed CO_2 with the freeing of the charge

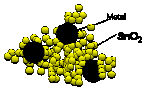

3.2.5.2.3 Powders

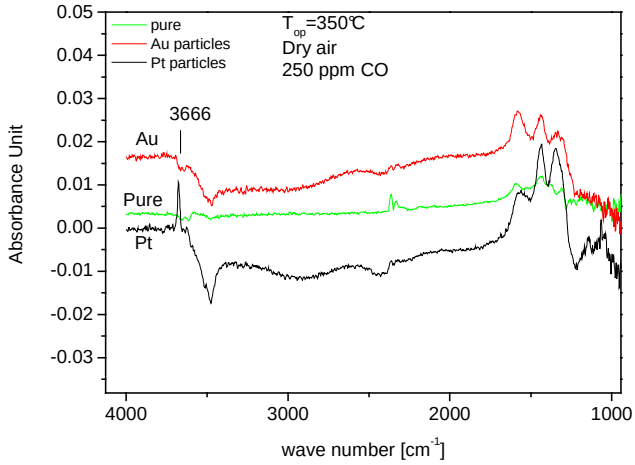

Figure 3-26 : The whole DRIFT spectra of mixed powder of SnO_2+metal particles exposed at 350°C to 250 ppm CO in dry air (- Au particles,-Pt particles, -pure).The spectrum recorded before CO exposure was used as a reference for each type of sensors.

As we are not using a conventional method in DRIFT, it was important for us to complete the studies of DRIFT on sensors by some experiments performed directly on powders. Three types of powders were used as described in the chapter 2 § 2.1.1: Pure SnO_2 and mixed SnO_2 either with gold and platinum particles. For an easiest understanding, and due to fact that the effect is manifest, only the results at 350°C under 250ppm CO are shown in Figure 3-26:

- The three type of powders exhibit the CO_2 formation. This formation is favoured on pure SnO_2 powder.

- In OH region, different results can be pointed out. On pure powder, this region is still “insensitive” to the presence of CO. For the mixed Pt an increase of the peak at 3666cm^{-1} has been observed, whereas a decrease of OH group has been observed for the mixed Au powders. Results for this region are quite similar the ones observed with sensors.

- Some difference on carboxylate carbonate is present:

Carbonate and carboxylate species analysis.

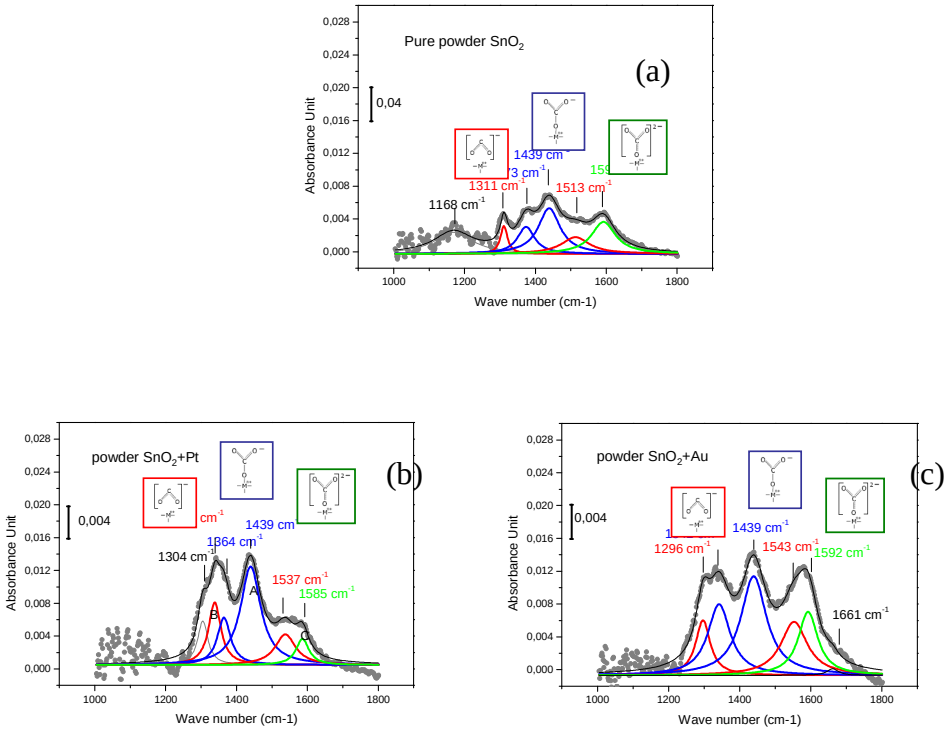

Figure 3-27 : Low wave number analysis DRIFT spectra of SnO_2 sensors recorded at 350°C under 250 ppm of CO. on top: (a) pure powder, at the bottom (b) sensor with platinum particles and (c) gold particles. The spectrum recorded before CO exposure was used as a reference.

Figure 3-27 shows the spectra analysis obtained for powders at 350°C. The amount of intermediate species for all powders is in the same range in term of intensity. Numerous species are present at the surface. The band of the monodentate carbonate (1439 cm^{-1}) is the most intensive for all powders. The presence of metal (Au or Pt) enhances the formation of the monodentate carbonate. In addition to the monodentate, the formation of free carbonate and carboxylate (ionic species) are present for all samples. Free carbonate was not present on sensors. Here, the morphology could explain the formation of new species at the surface of powders. Gold particles inside SnO_2 powder enhance the formations of intermediate species. With the presence of Pt particles, carboxylate and free carbonate species are formed but they are not stable, prove is the weak peaks at 1537, 1337 cm^{-1} (CO_2^-) 1585 cm^{-1}(CO_3^{2-}). In comparison with the conventional sensors, only the sensor provided with gold electrodes exhibits strong bands for the carboxylate and the others only trace was observed for the

others. The platinum reduces the presence at the surface of the more ionic species (carboxylate and free carbonate) which are not satble.

3.2.5.2.4 Summary of powder

It is important to note that on powders, besides the intermediates species identified on sensors, new ones are present like free carbonate. This may indicate the fact that the mixtures between the tin oxide and the metal powders are not perfectly mimicking the situation of the electrode/metal oxide contacts. This fact can be related to the different morphology (grain size, agglomeration, etc) of the metal powders when compared to the thick film electrodes. One should also note that the concentrations of common (sensor/powders) intermediates are higher because of the larger samples.

The most important finding, however, is that, similarly to the sensor situation; the presence of Pt reduces the amount of intermediate species especially for the ionic ones.

3.2.5.2.5 Mixed Sensor

The perturbation of the surrounding atmosphere of the DRIFT unit.

Due to a technical problem the mixed sample were studied with a new spectrometer where it was not possible to have the vacuum around the DRIFT unit (see section 3.2.2.1). So, the atmosphere around the cell is composed of a flow of pure Nitrogen. Due to this atmosphere, small amounts of water are present around the cell. Thus, Bands of the surface water stretching mode and bending are present on the recorded single channel spectra. These bands hide the variation in the OH region. Figure 3-28 illustrate typical DRIFT spectra in single channel in this condition.

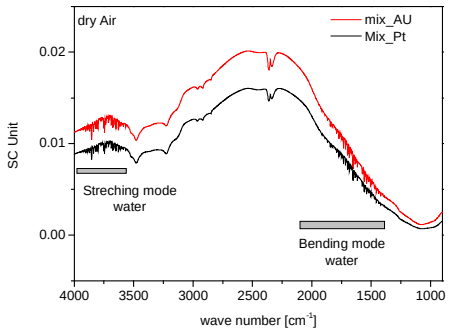

Figure 3-28: Single channel spectra of mixed gold (red) SnO_2 sensor and mixed platinum (black) SnO_2 sensor where water around the vibration of the surrounding water are present.

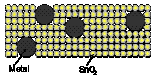

3.2.5.2.5.1 Without electrodes

Results under 250ppm CO at 350°C.

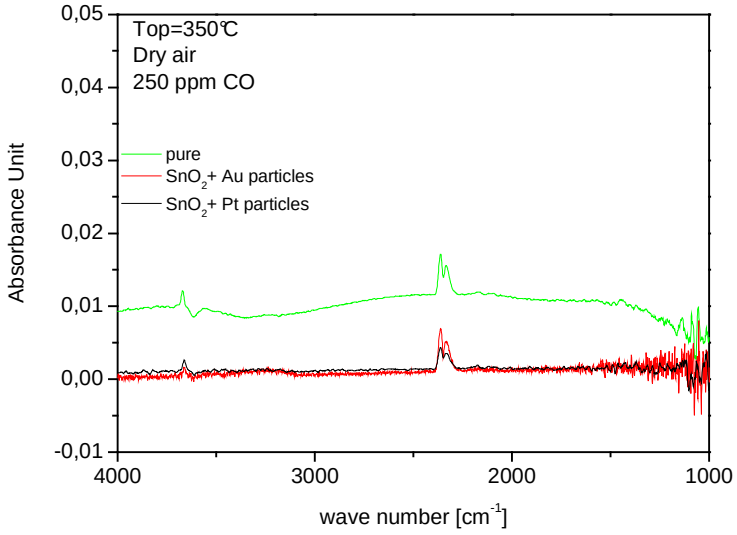

Figure 3-29 : The whole DRIFT spectra of mixed powder of SnO_2+metal particles deposited on Alumina substrate exposed at 350°C to 250 ppm CO in dry air (-Au particles,-Pt particles, -pure). The spectrum recorded before CO exposure was used as a reference for each type of sensors

The results for the mixed sensors without electrodes but with heater are shown in Figure 3-29. No bands can be assigned at low wave number. Only the bands of CO_2 and CO are assigned for all sensors. The CO conversion takes place but without any intermediate. For all, modification in the OH regions has been observed. The increase of the band at 3666, 3640cm^{-1} and the decrease at 3611cm^{-1} compared to the reference without CO are visible.

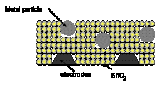

3.2.5.2.5.2 With platinum electrodes

DC measurements

Figure 3-30 shows the resistance and the sensor signal for the both types of sensor, SnO_2 mixed either gold or with platinum. The mixed powder was screen printing on the top of alumina substrate provide with platinum electrodes and heater in the backside.

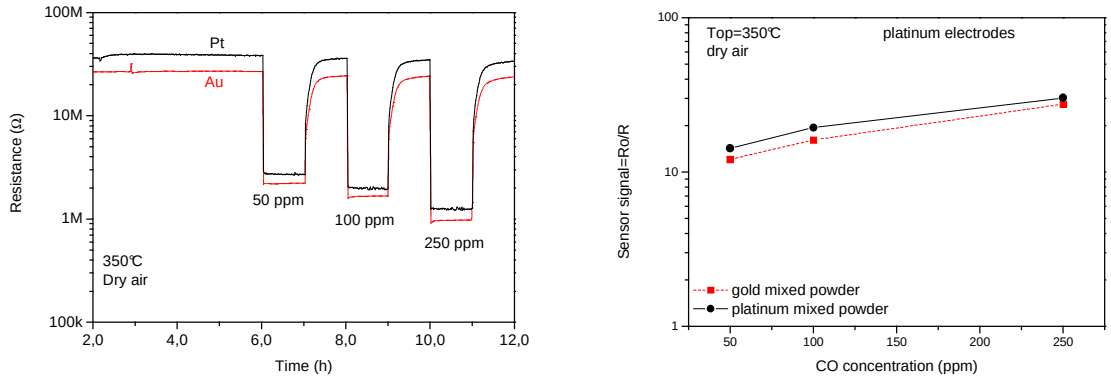

Figure 3-30 : Resistance and sensor signal dependence on the CO concentration in dry air at 350°C sensors working temperature. Sensor provided with platinum (Pt) electrodes and gold electrodes (Au)

As follow, the characteristic are:

- Identical performance is observed for both types of mixed SnO_2 based sensors.
- The baseline resistance for sensor contain Platinum mixed sensitive layer is little higher than mixed Gold sensor.
- The sensor signal (R0/R) is nearly the same. Platinum device is slightly higher than gold.

Figure 3-31 shows the spectra of the mixed gold and mixed platinum in absorbance representation recorded in the same time of the electrical measurement.

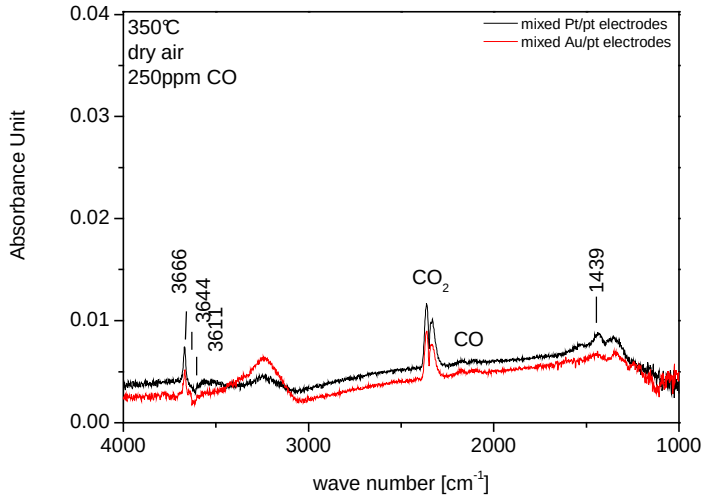

Figure 3-31 : **The whole DRIFT spectra of mixed powder of SnO_2+metal particles deposited on Alumina substrate provided with Pt electrodes exposed at 350°C to 250 ppm CO in dry air (-Au particles,-Pt particles, -pure). The spectrum recorded before CO exposure was used as a reference for each type of sensors**

- The band of CO_2 is present for each sensor. In Figure 3-32, the peak area of the CO_2 bands is plotted as a function of CO concentration. At low CO concentration, the amount of CO in the pores of the layer is the same for both types of sensors. At higher CO concentration, a higher CO_2 concentration is observed for mixed Pt sensor.

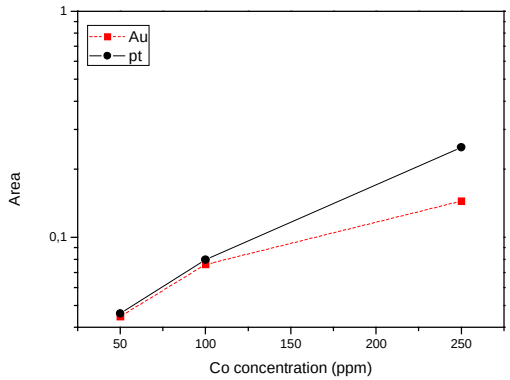

Figure 3-32: CO_2 bands area analysis.

- At low wave number, the same shape of the curve is observed for the both type of sensors; only the band corresponding to the carbonate species can be easily assigned. The spectra of metal mixed sensors provided with platinum electrodes is quite similar to the spectra obtained with pure SnO_2 sensor provided with Pt electrodes. The effect of the nature of the electrode is dominant in regard to the influence of metal inside sensitive layer.
- In the OH group region, the increase of the band at 3666cm^{-1} and 3641cm^{-1} is observed.

3.2.5.2.6 Summary of the mixed powder on alumina substrate

With the mixed powders layer on alumina substrate with the heater and without electrodes, the idea was to increase the electrodes/sensitive layer contact and enhance the phenomena.

The experiments reveal that the behaviour of each type of sensor (Pure, mixed gold and mixed platinum) is the same (Figure 3-29.) without electrodes. At low wave number, no bands appeared but CO_2 band was present and proved that reaction took place on the surface. The non-existence of intermediate bands prove that the morphology or/and the specific area of the sensitive layer are important for the “stability of the intermediate species” on the surface of the sensor. The catalytic role played by the metal is perhaps more active.

The same sensitive layer (mixed gold and mixed platinum) was used and deposited on alumina substrate provide with platinum electrodes to recorded the resistance. In this configuration, intermediate species appears at the surface of sensors. In fact, at low wave number, the band of the monodentate carbonate appears. The result proves that the electrodes are important for the presence of intermediate species. DRIFT spectra of mixed powders deposited on platinum electrodes is close to the DRIFT spectra of pure SnO_2 deposited on platinum electrodes. It is interesting to point out that electrodes manage the surface species. The influence of the electrodes is predominant to the role of metal dispersed in SnO_2. When platinum electrodes are present, similar resistance has been observed by DC measurement for both mixed sensors. The species at the surface are also the same, which explain why the resistance is equivalent.

3.2.6 DRIFT summary

The experimental spectroscopic studies of the influence of the electrodes on the CO sensing provide many useful outcomes that allow for a better understanding of the electrical findings.

By using DC measurements, it was found that the baseline, the sensor signal and its kinetic are affected by the nature of the electrodes.

In the DRIFT studies, 4 types of samples (conventional, powders, mixed without electrodes, mixed with electrodes) have been studied and most of our experiments were performed at 350°C; the reason is this temperature the difference were the most pronounced. The results from the DRIFT spectroscopy confirm the importance of the nature of the electrodes in gas detection. It was demonstrated that the chemistry of the CO pathways to form CO_2 is modified by the nature of the electrodes/metal used. In dry air or humid, the selection of the nature of the metal was shown to modified the surface species. The electrodes share to the gas detection is manifest.

CO reacts with ionosorbed oxygen (literature and following TPD experiments) and forms mainly two kind of intermediate species carboxylate and free carbonate (**more ionic and non stable**) and carbonate (**less ionic and more stable**) on its way to conversion to CO_2. The higher sensitivity of sensor provided by platinum electrodes can be explained by an increase of the CO to CO_2 conversion rate. This is demonstrated by the lower amount of intermediate species visible on absorbance spectra for all samples in which platinum was present as electrodes, due to the capability of platinum to speed up the reaction. The low sensitivity of the gold electrode sample is due to the fact that during the conversion to CO_2, the intermediates are playing a more important role, this means that especially the ionic species like carboxylate and non-coordinated carbonates-previously localised on the oxygen ion- will be allowed to block the charge longer. The charge will still be blocked at the surface, no more as O^- but as e.g. CO_3^-. Consequently, the sensor effect-change or resistance – is blocked even if the reaction between CO and O^- already took place.

The contrast between gold and platinum is also observed in the reaction kinetics. For gold, carboxylate are formed first and, after some time, the peak of the carbonates appears. On the opposite, for platinum the bands of carbonate and carboxylate are simultaneously appearing. In fact platinum presence helps to eliminate the carboxylate, so free sites are becoming available and can be easily occupied by the carbonates. This effect was even clearer for powders where the platinum helps to eliminate carboxylate and non-coordinated

carbonates which are more ionic but preserve a band for carbonate which is not ionic. Gold enhances the formation of the carboxylate and the non-coordinated carbonates. The consequence on the performance of the sensor is evident. The stability of ionic intermediate species at the surface demonstrated by their higher concentration on sensors with gold electrodes keeps the charge at the surface. With platinum the system converts quickly CO into CO_2 and desorbs it. So, the charge is released into the conduction bands.

Every time platinum is employed, the amount of surface species is quite low and the response is high. The background absorption level of the spectrum increases due to the increase of the free carrier density. This effect is more also important in the case of platinum.

To understand the complete story of the effect of the electrode another technique has to be used in order to get more information. The next part is devoted to the thermodesorption experiments

3.3 Thermodesorption (TPD)

3.3.1 Generalities

There are a range of techniques for studying surface reactions and molecular adsorption on surfaces which utilise temperature-programming to discriminate between processes with different activation parameters. Among these ones, the most useful for powders studies is Temperature Programmed Desorption (TPD).

When the technique is applied to a system in which the adsorption process is, at least in part, irreversible, and when *T*-programming leads to surface reactions, then this technique is often known as Temperature Programmed Reaction Spectroscopy (TPRS)

However, there is no substantive difference between TPRS and TPD. TPD is a powerful method to study the species absorption on solid. These species are characterised by their chemical nature and the binding energy with the adsorbent material. Ed is the energy required to break the bond between the species and the surface. By heating the sample, the energy Ed is supplied. The species are removed from the surface and analysed by a mass spectrometer.

3.3.1.1 The Desorption Process

An adsorbed species present on a surface at low temperatures may stay almost indefinitely in that state. As the temperature of the substrate (or adsorbent) is increased, however, there will come a point at which the thermal energy of the adsorbed species is such that one of several things may occur:

1. A molecular species may decompose to yield either gaseous products or other surface species.
2. An atomic adsorbate may react with the substrate to yield a specific surface compound, or diffuse into the bulk of the underlying solid.
3. The species may desorb from the surface and return into the gas phase.

The last of these options is the desorption process. In the absence of decomposition, the desorbing species will generally be the same as the ones originally adsorbed , but this is not necessarily always the case.

(An example is found in the adsorption of some alkali metals on metallic substrates exhibiting a high work function where, at low coverages, the desorbing species is the alkali metal ion as opposed to the neutral atom. Other examples would include certain isomerisation reactions.)

3.3.1.2 Desorption Kinetics

The rate of desorption, R_{des}, of an adsorbate from a surface can be expressed in the general form :

$\boldsymbol{R_{des} = k\, N^{x}}$ where x - kinetic order of desorption

k - rate constant for the desorption process

N - surface concentration of adsorbed species

The order of desorption can usually be predicted because it concerns an elementary step of a "reaction". Here are few examples

I. *Atomic or Simple Molecular Desorption*:

$$A_{(ads)} \rightarrow A_{(g)}$$
$$M_{(ads)} \rightarrow M_{(g)}$$

- Usually is a first order process (i.e. $x = 1$).

Examples

$W / Cu_{(ads)} \rightarrow W_{(s)} + Cu_{(g)}$ (desorption of Cu atoms from a W surface)

$Cu / CO_{(ads)} \rightarrow Cu_{(s)} + CO_{(g)}$ (desorption of CO molecules from a Cu surface)

II. *Recombinative Molecular Desorption*

$$2\, A_{(ads)} \rightarrow A_{2\,(g)}$$

- Will usually be a second order process (i.e. $x = 2$).

Examples

$Pt / O_{(ads)} \rightarrow Pt_{(s)} + O_{2\,(g)}$; desorption of O atoms as O_2 from a Pt surface

$Ni / H_{(ads)} \rightarrow Ni_{(s)} + H_{2\,(g)}$; desorption of H atoms as H_2 from a Ni surface

The rate constant for the desorption process may be expressed in an ArRHenius form,

$$\boldsymbol{k_{des} = A \exp\left(-E_a^{des} / RT \right)}$$

Where E_a^{des} is the activation energy for desorption ,

A is the pre-exponential factor; this can also be considered to be the "attempt frequency", ν , to overcome the barrier to desorption.

Then, the following general expression for the rate of desorption is obtained:

$$R_{des} = -dN/dt = \nu . N^{x} . \exp\left(-E_a^{des}/RT\right)$$

In the particular case of simple molecular adsorption, the pre-exponential/frequency factor (ν) may also be equated with the frequency of vibration of the bond between the molecule and substrate; this is because every time this bond is stretched during the course of a vibrational cycle can be considered as an attempt to break the bond and hence an attempt of desorption.

The rate of desorption of a surface species will in general be given by an expression of the form:

$$R_{des} = \nu . N^{X} \exp(\frac{-E_{des}}{RT}) \qquad (1)$$

Where

R_{des} - desorption rate (= -dN/dt)

x - Kinetic order of desorption (typically 0, 1 or 2)

E_a^{des} - activation energy for desorption

In a temperature programmed desorption experiment in which the temperature is increased linearly with time from some initial temperature T_o, then:

$$\boldsymbol{T = T_o + \beta . t} \quad \text{and} \quad \boldsymbol{dT = \beta . dt} \qquad (2)$$

The intensity of the desorption signal, I (T), is proportional to the rate at which the surface concentration of adsorbed species is decreasing. This is obtained by combining (1) and (2) to give

$$I(T) \infty -\frac{dN}{dT} = \frac{\nu N^{x}}{\beta} \exp\left(\frac{-E_a^{des}}{RT}\right) \qquad (3)$$

This problem may also be considered in a rather simplistic graphical way -the key to this is to recognise that the expression for the desorption signal given in the above equation is basically a product of a coverage term (N^x - where N depends on T) and an exponential term (involving both E_a and T).

Initially, at low temperatures $E_a >> RT$ and the exponential term is vanishingly small. However, as the temperature is increased this term begins to increase very rapidly when the value of RT approaches that of the activation energy, E_a .

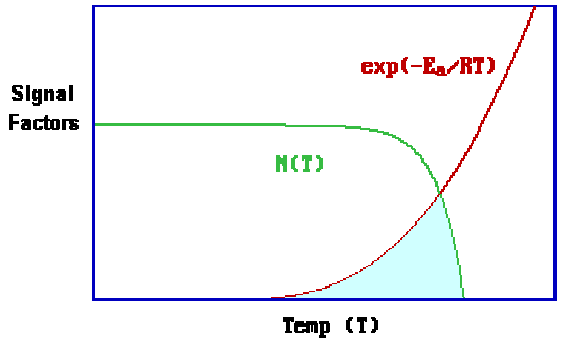

Figure 3-33: Illustration of the evolution desorption signal

By contrast, the pre-exponential term is dependent upon the coverage, $N(T)$, at the concerned temperature - this term will remain at the initial value until the desorption rate becomes of significance, as a result of the increasing exponential term. Thereafter, it will decrease ever more rapidly until the coverage is reduced to zero. The shaded area is an approximate representation of the product of these two functions, and hence also an approximate representation for the desorption signal itself - whilst this illustration may be overly simplistic, it does clearly show why the desorption process gives rise to a well-defined desorption peak.

3.3.1.3 Case of Molecular adsorption

In this case the desorption kinetics will usually be first order (i.e. $x = 1$)

The maximum desorption signal in the I(T) trace will occur when (dI / dT) = 0, i.e. when

$$\frac{d}{dT}\left[\frac{\nu N}{\beta}\exp\left(\frac{-E_a^{des}}{RT}\right)\right] = 0\,, \qquad (4)$$

Hence, remembering that the surface coverage changes with temperature i.e. $N = N(T)$,

$$\frac{E_a}{RT^2}\cdot\frac{\nu N}{\beta}\cdot\exp\left(\frac{-E_a^{des}}{RT}\right) + \frac{\nu}{\beta}\exp\left(\frac{-E_a}{RT_p}\right)\cdot\frac{dN}{dT} = 0\,, \qquad (5)$$

We have substituted E_a for E_a^{des} purely for clarity of presentation and defined the temperature at which the desorption maximum occurs to be $T = T_p$ (the *peak temperature*).

Substituting for dN/dT from eqn. (5) then gives

$$\frac{\nu N}{\beta}.\left[\frac{E_a}{RT^2}-\frac{\nu}{\beta}\exp\left(\frac{-E_a}{RT_p}\right)\right]\exp\left(\frac{-E_a}{RT_p}\right)=0, \qquad (6)$$

The solution is given by setting the expression in square brackets to be equal to zero, i.e.

$$\frac{-E_a}{RT_p^2}=\frac{\nu}{\beta}\exp\left(\frac{-E_a}{RT_p}\right)=0, \qquad (7)$$

Unfortunately, this equation cannot be re-arranged to give a simple expression of T_p but we can note that:

- As E_a^{des} (the activation energy for desorption) increases, then so T_p (the peak temperature) increases.
- The peak temperature is not dependent upon, and consequently does not change with, the initial coverage, $N_{t=0}$.
- The shape of the peak desorption will tend to be asymmetric, with the signal decreasing rapidly after the desorption maximum.

3.3.1.4 Experimental method to calculate Ea and υ

For the first order desorption kinetics (most of the case), it is possible to determine υ and Ea from the shift of the temperature ΔT from T_1 and T_2 when the temperature rate β change from β_2 and β_1.

$$\frac{-E_a}{RT_1^2}=\frac{\nu}{\beta_1}\exp\left(\frac{-E_a}{RT_1}\right) \qquad (8)$$

$$\frac{-E_a}{RT_2^2}=\frac{\nu}{\beta_2}\exp\left(\frac{-E_a}{RT_2}\right) \qquad (9)$$

$$\frac{T_2^2}{T_1^2} = \frac{\beta_2}{\beta_1} \exp\left(\frac{-E_a}{R} \left(\frac{T_2 - T_1}{T_2 T_1} \right) \right) \qquad (8)/\ (9) = (10)$$

$T_2 = T_1 + \Delta T$, one obtains expression (11)

$$\frac{T_1^2 \left(1 + \frac{2\Delta T}{T_1} + \frac{\Delta T^2}{T_1^2} \right)}{T_1^2} = \frac{\beta_2}{\beta_1} \exp\left(\frac{-E_a}{R} \left(\frac{\Delta T}{T_1^2 \left(1 + \frac{\Delta T}{T_1} \right)_1} \right) \right) \qquad (11)$$

If we consider that $T_1 >> \Delta T$, we have the expression of Ea

$$E_a = \frac{R T_1^2}{\Delta T} \log \frac{\beta_2}{\beta_1} \qquad (12)$$

Then the value of υ is derived from equation (8)

$$\upsilon = \frac{\beta_1 E_a}{R T_1^2} \exp\left(\frac{-E_a}{R T_1} \right) \qquad (13)$$

Hence, by performing two experiments with different heating rate β_2 and β_1 and measuring the maximum desorption temperature T_1 and T_2, it is possible to calculate Ea and υ

3.3.2 Experimental set up of TPD

For TPD measurements, both pure SnO_2 and SnO_2 mixed with Au and Pt particles were used in the form of powder. They were prepared like a paste for a sensor and annealed at 700°C. Tin dioxide powder used in the experiments was the same commercial powder used for sensors. Adsorption gases, oxygen (99,99%) and CO, were supplied by Air Liquide (France). For the TPD measurements, 30mg of SnO_2 powder was packed in a quartz chamber.

Figure 3-34 shows the set up of the TPD experiment. Each TPD run consisted in the following process (called “regular process”):

-Sample pre-treatment at 900°C under vacuum to clean up the surface of the powder.

-gas adsorption is done at the required temperature T_x during a certain time t.

Example: O_2 adsorbed at 500°C during 30 min

-The vacuum is done at the temperature T_x and immediately the sample is quenched to the room temperature (RT).

-Finally TPD run is launched at a heating rate of 20°C/min from room temperature (RT) to 900°C and the desorption is monitored by a BALZERS QMG 112 quadrupole mass spectrometer (Figure 3-34)

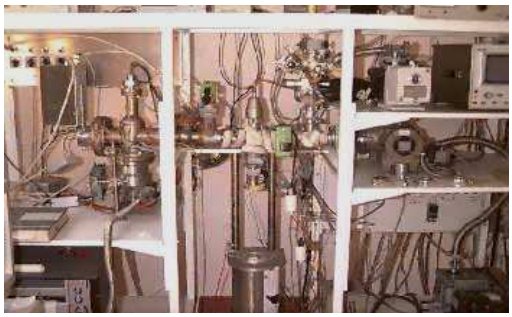

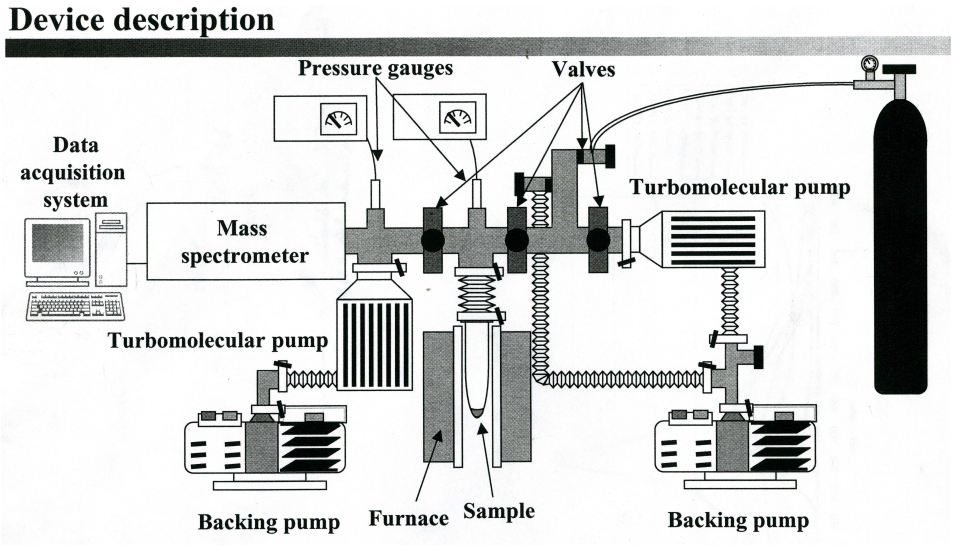

Figure 3-34: set up of *Temperature Programmed Desorption*

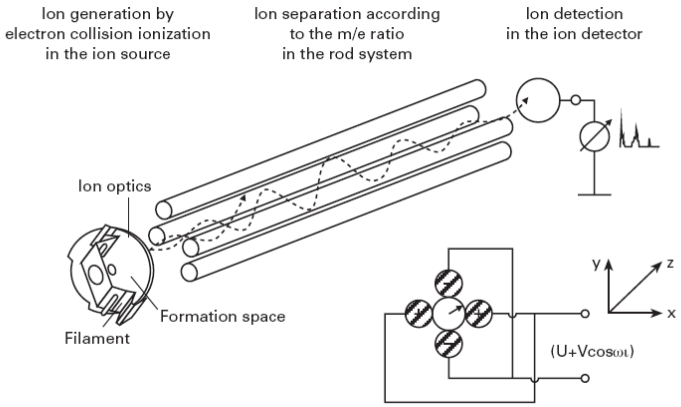

Figure 3-35 : A schematic of a quadrupole analyser of the mass spectrometer

3.3.3 Results and discussion

3.3.3.1 Adsorption of oxygen

3.3.3.1.1 On pure SnO_2

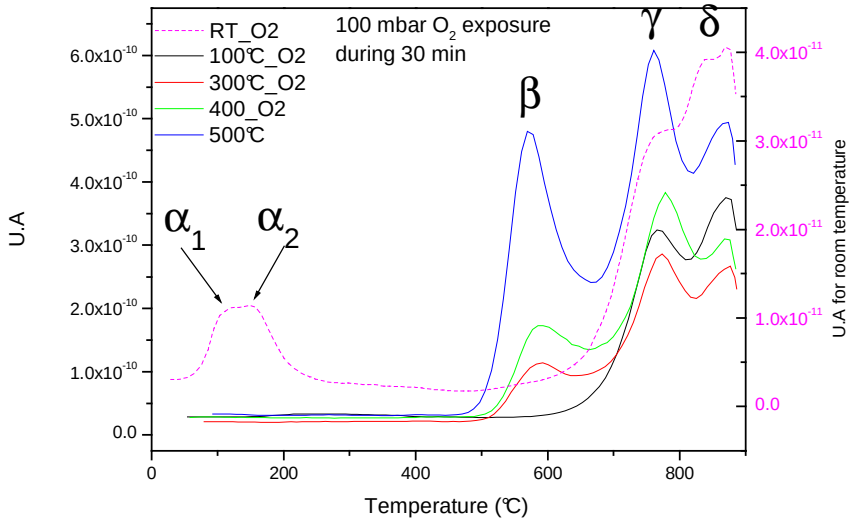

Figure 3-36 : TPD thermogram(mass 32) after 100 mbar O_2 exposure at different temperature. The scale for the dash curve (at RT) is in the right side.

For most application, the aim of sensor is to detect some traces of pollution in ambient atmosphere or at least in the presence of oxygen. It is convenient to describe first the thermal desorption of oxygen from pure SnO_2 powder. In Figure 3-36, the TPD thermogram after oxygen exposure is reported. SnO_2 powder was exposed to 100mBar of O_2 at different temperature from RT to 500°C during 30min. Depending on the exposure temperature, 5 kinds of adsorbed oxygen species can be characterized from TPD experiments. Each oxygen species have a specific behaviour. Oxygen from the bulk Lattice (O_L) is always present and independent on the temperature exposure. Its desorpion start around 880°C. We note it δ in our notation. The α_1 and α_2 species which desorbs in the range 80-200°C are only present for exposure at room temperature. β and γ species are formed if the exposure temperature is above 100°Cduring a long period. Time exposure and temperature control the intensity of the peaks. For species, β and γ, an exposure at 500°C, peak intensity is maximal. According to the literature (in chapter 1) on TPD [149], EPR, DRIFT and to the relation between the temperature and the Activation energy of desorption (Eq 12), the bond between the oxygen

species and the SnO_2 should be weak at low temperature. It is possible to assign the different peak to a specific oxygen species as follow: α_1 (80°C, O_2) and α_2 (150°C, O_2^-) β (450-600°C, often centred at 550°C, O^-), γ (around 730°C, $O_L$surface) and δ (above 800°C, O_{Lbulk}), where the temperature and species noted in parentheses indicate the approximate maximum desorption temperature (T_m) and the corresponding adsorbed oxygen species. The following table summarized the oxygen species at the surface of pure SnO_2.

Table 3-2 : Oxygen species at the surface of SnO_2

Name	Oxygen form	Temperature range (℃)	Tm(℃)
α	σ-O_2	80	
α	σ-O_2-	120-200	150
β	σ-O-	450-600	550
γ	$O_0^x(O_L)$+ σ		730
δ	$O_{L(bulk)}$		880

A simply mechanism can explained the formation of the oxygen species. Our starting point is the oxygen in the gas phase the process can be as follow:

	O_2 (gas) + σ	physisorption ⇌	σ-O_2	α_1
	σ-O_2 + e^-	⇌	σ-O_2^-	α_2
	O_2 + $2e^-$+ 2σ	⇌	2σ-O^-	β
Or	σ-O_2^- +e^- + σ	⇌	2σ-O	
	σ-O^- + e^-+$V_o^{\cdot\cdot}$	⇌	O_0^x+ σ	γ

Where σ is an adsorption site.

$V_o^{\cdot\cdot}$ and O_0^x represents respectively an oxygen vacancy and a lattice oxygen using Kroger Vink notation (O_0^x=O_L)

More the adsorption temperature increase, more oxygen species become ionic and thus strongly bond. Depending on the working temperature, each species can be also more or less present at the surface of SnO_2. For example, closer the temperature is to 200°C and more the O_2^- is dominant but O^- is also present

At elevated temperature, i.e. at temperature superior to 100°C but inferior to 600°C, only β and γ desorption peak are observable. Figure 3-37 (a) and (b) shows the dependencies of the

O_β peak and $O\gamma$ as a function of the temperature exposure and the pressure. For an exposure over 600°C the O_β desorption peak does not appear which confirms that O^- is not stable over this temperature whereas γ is stable. Secondly, at fixed temperature (500°C), in the Figure 3-38(b), by increasing the adsorption pressure (P) from 1mbar to 500mbar the intensity of the O_β peak increases. Figure 3-38(c) shows that the increase of O_β species versus pressure follows a logarithmic law. For the $O\gamma$ peak, the intensity is constant with the rise of pressure.

These results prove that the $O\gamma$ come from the oxygen lattice of the surface because the level is independent to pressure but the quantity of $O\gamma$ is definite. It is why a maximum can be observed. For O_β, The influence of oxygen pressure proves that we have a chemisorption of oxygen at the surface. This chemisorption, in this condition, form the O_β

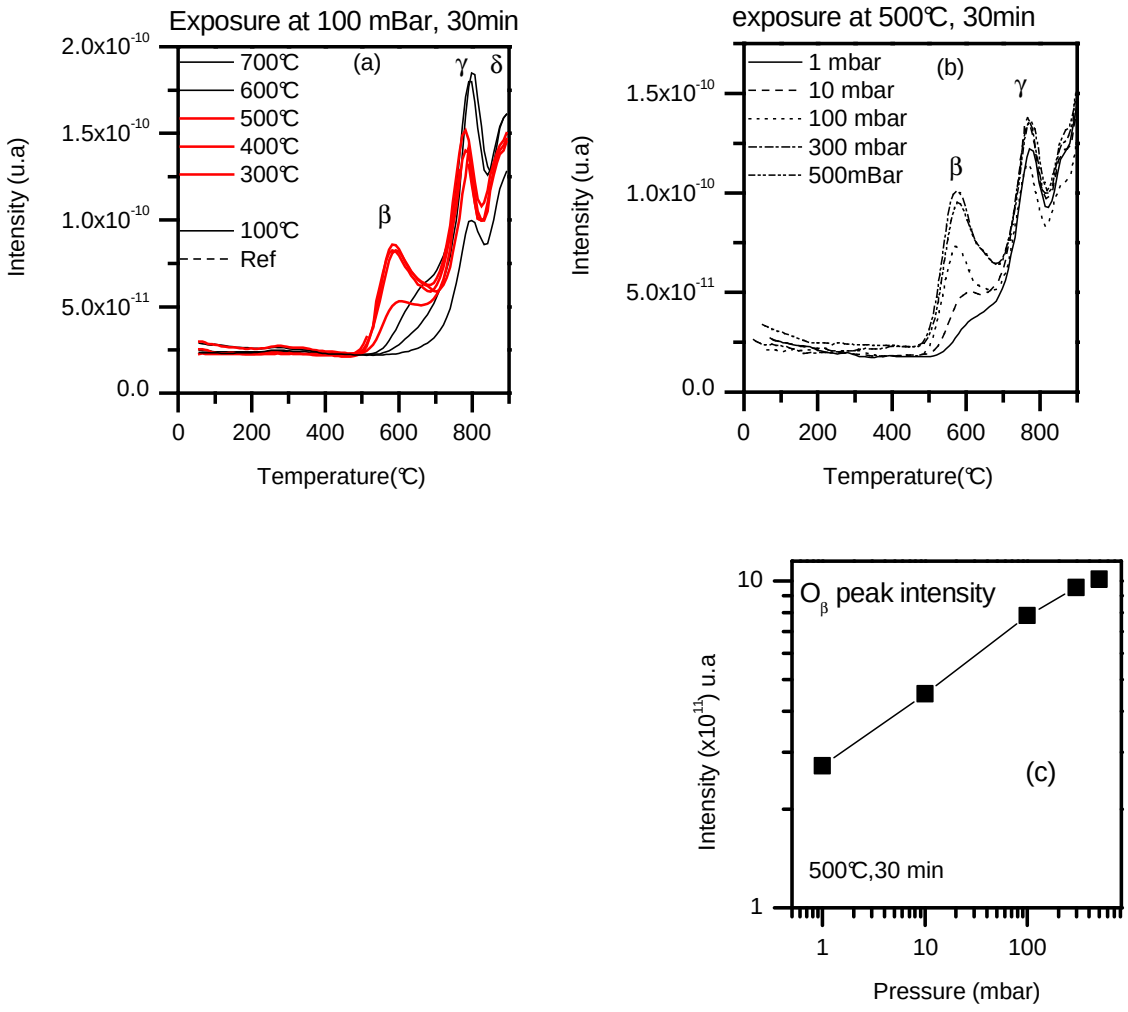

Figure 3-37: TPD thermogram (m/z= 32) after exposure at different temperature (a), at different pressure (b), and the relation between the height of the O_β peak and the pressure (c).

Comment about the ionisation fragment of O_2:

In the experiments, O_2 masses 32 and 16 were followed. Mass 16 is the main fragment of mass 32. The prove is shown in the Figure 3-38, for 100 mbar exposure at 500°C the shape between the mass 32 and the mass 16 is the same but intensity is less for the mass 16. It is why we prefer to show the mass 32

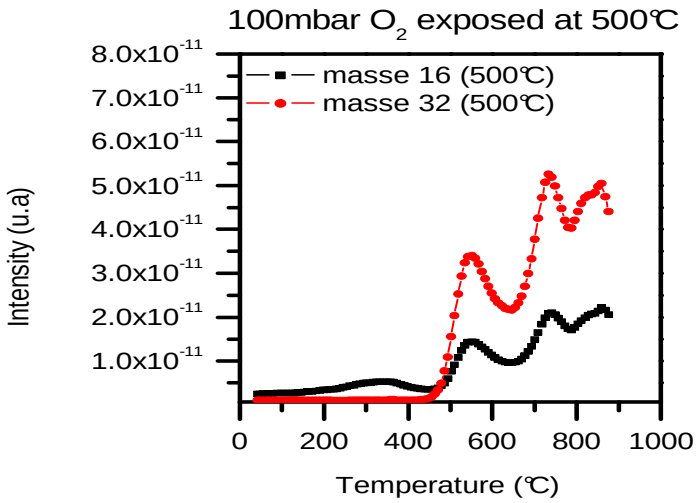

Figure 3-38 : TPD thermogramfor the mass 16 and 32, after 100mbar O_2 exposure at 500°C.

3.3.3.1.1.1 Energy of desorption and frequency factor

A way to confirm the nature of oxygen species is to calculate the desorption energy $E_a^{(des)}$. According to the experimental method (detailed in 3.3.1.4) and considering that desorption process is a first order, we can estimate $E_a^{(des)}$ and υ. Figure 3-39 shows the results obtain with three different heating rate 10, 20,30 °C/min. It can be seen that according to the desorption theory almost all peaks are shifted towards high temperature if the heating rate increase (table 3-1)

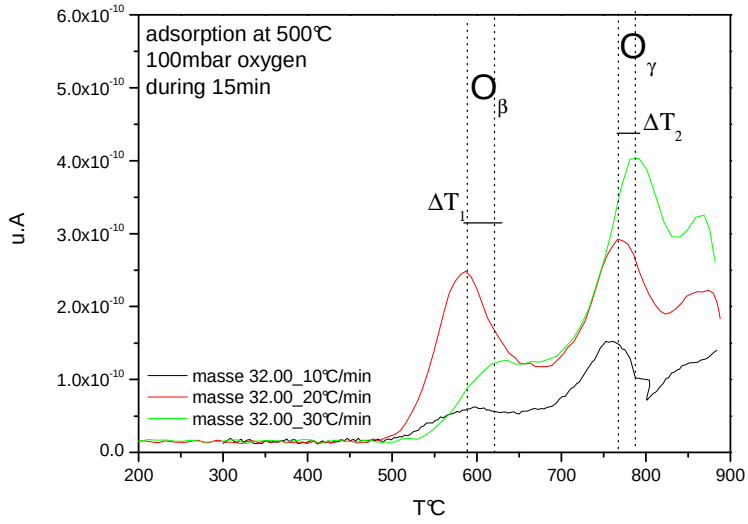

Figure 3-39 : TPD thermogram (mass 32) after 100mbar O_2 exposure at 500°C during 15min,for different heating rate.

One problem is observed for the peak corresponding to O_β at 10°C/min. the temperature of this peak is higher than expected. So the calculation are made with experiments at 20 and 30°C/min. measured value are reported in the Table 3-3

Table 3-3 : Temperature of the maximum desorption for each type of oxygen species O_β and $O\gamma$

β (heating rate)	$T_{O\beta}$(℃)	Toγ(℃)
β_1 10℃/min	598	759
β_2 20℃/min	587	771
β_3 30℃/min	625	792
$\Delta T=T_2-T_1$	38	21

The value of Ea and υ calculated thanks to expression (12) and (13) reported hereafter are indicate in the Table 3-4.

$$E_a^{des} \approx \frac{RT_2^2}{\Delta T}\ln\frac{\beta_3}{\beta_2} \quad \text{And} \quad \upsilon \approx \frac{\beta E_a^{des}}{RT_2^2}\exp\left(\frac{Ed}{RT_2}\right)$$

- The values 25kJ/mol for O_β species and 75kJ/mol for O_γ species are in the range of chemisorption energies which means that there are strongly bonded to the surface.

- The weaker value of E_a^{des} (O_β) indicates the relative facility of these species to react with other compounds.

Table 3-4 : value of Ea and υ for O_β and $O\gamma$ oxygen species

	T_2(℃)	E_a^{des}(j/mol)	υ(s^{-1})
$T_{O\beta}$	860	28495	54
Toγ	1044	75985	41243

3.3.3.1.1.2 Relation between water, hydroxyl and oxygen on pure SnO_2

With the aim of going deeper in the relation of oxygen with SnO_2, using the TPD technique, the influence of the oxygen with water and/or the hydroxyl groups was followed. Most metal oxides are covered with hydroxyl groups under normal condition which means in ambiant atmosphere. Since surface hydroxyl groups seems to have a great influence on the physical and chemical properties of metal oxide surface, it is important to have informations on the adsorbed state of water on the surface. In the previous section, the formation of the oxygen species at the surface of the SnO_2 has been described. It was found that the creation of oxygen species depends on temperature. In this section, no water vapour has been introduced but there is a certain amount of water and hydroxyl group at the surface of SnO_2 coming from time where the sample was in atmosphere. It is very difficult to remove water because a small amount is introduced during the oxygen exposure coming from the bottle and pipes. We have found a strong relation between the oxygen species O_β and the formation of a new OH group. Figure 3-40 shows the TPD thermogramfor the mass 17, 18 and 32 assigned to OH, H_2O and O_2 after adsorption of 100mBar oxygen at 500°C and 600°C.

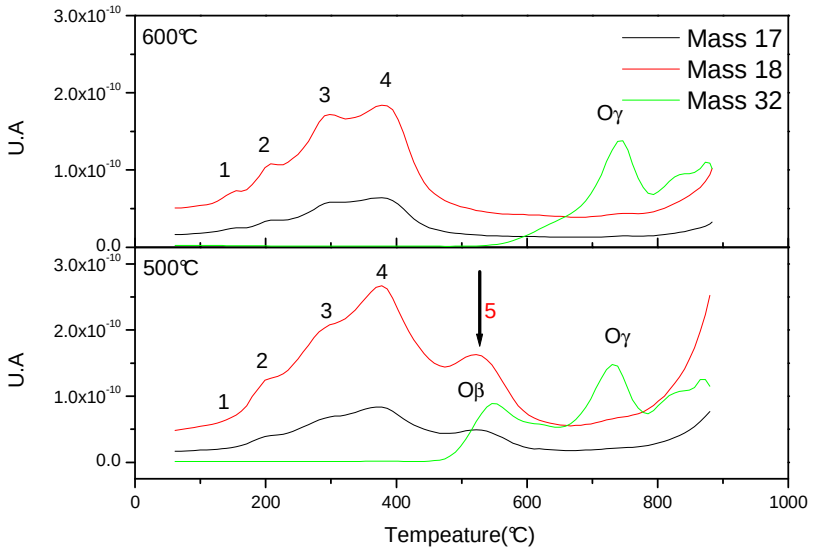

Figure 3-40 : TPD thermogram of water (mass 18), hydroxyl (mass 17) and oxygen (mass 32) after adsorption of oxygen at 500°C and 600°C

After adsorption of oxygen at 600°C, four water desorption peak appeared: (1) 150°C-175°C; (2) 200°C, (3) 286-305°C, (4) 375-385°C. Many authors [Y, Hand T, Eg,] studied the adsorption of water vapour and found two broad peaks: the first one centred at 150°C, and the second one centred at 400°C. They attributed the first peak to the water molecular desorption

and the second to hydroxyl groups. In our case, it was already mentioned that the amount of water is quite low. Based on the results of these authors, the four desorption peak in the present case can be also divided in two groups: the first group contains only the peak 1 corresponding to water molecule which is entirely desorbed at 175°C and the others peaks 2, 3, 4 which correspond to three different sites of hydroxyl group adsorbed. Usually these peaks cannot be identified when water vapour is exposed because of the highest level of water; in such condition, only the presence of broad peak is observed. One should remind that water observed here results only from water pre-adsorbed in atmosphere before using our sample. It puts in light that molecular water (weak peak n°1) can be considered as almost completely removed after the cleaning process whereas hydroxyl groups are still present and strongly bonded to the surface. The maximum temperature to remove the entire hydroxyl group is around 450°C-500°C. It is assumed that hydroxyl groups can affect the conductivity of SnO_2, but water molecule is considered to have a small influence on it. Temperatures of the maximum (T_m) desorption are given in a range roughly important due to the fact that T_m can shift in function of the molecule surrounding and the possibility to form hydrogen bond.

In the second experiment where oxygen has been pre-adsorbed to 500°C, a new band centred at 550°C appears. This new hydroxyl specie is correlated to the presence of oxygen O_β specie. Effectively, at 600°C, the peak O_β wasn't present as well as the OH peak at 550°C. A direct reaction between O^- (β) and H_2O can be suggested to explain this relation:

$$H_2O + \sigma\text{-}O^- + \sigma \leftrightarrow 2\ \sigma\text{-}OH + 1\ e^-$$

Thus, desorption of σ-OH species will lead to simultaneous emission pf water vapour (n/e=18) and O_β (σ-O^-)

By DRIFT, D. Koziej [150] have demonstrated the relation between oxygen concentration and the increase of a hydroxyl band, as shown in Figure 3-41. The band at 3640cm^{-1} suggests an increase of the hydroxyl group when the O_2 concentration is increased. TPD measurements complete this observation and also prove direct link between oxygen and hydroxyl group formation. The relation between the formations of OH group in the presence of O^- (O_β) is also important and should be taken in account to explain some detection mechanism of SnO_2 with a reducing gas. If a reducing gas (CO) is present, a possible competition can take place between the reaction of the formation of Hydroxyl group and the reaction with the reducing gas.

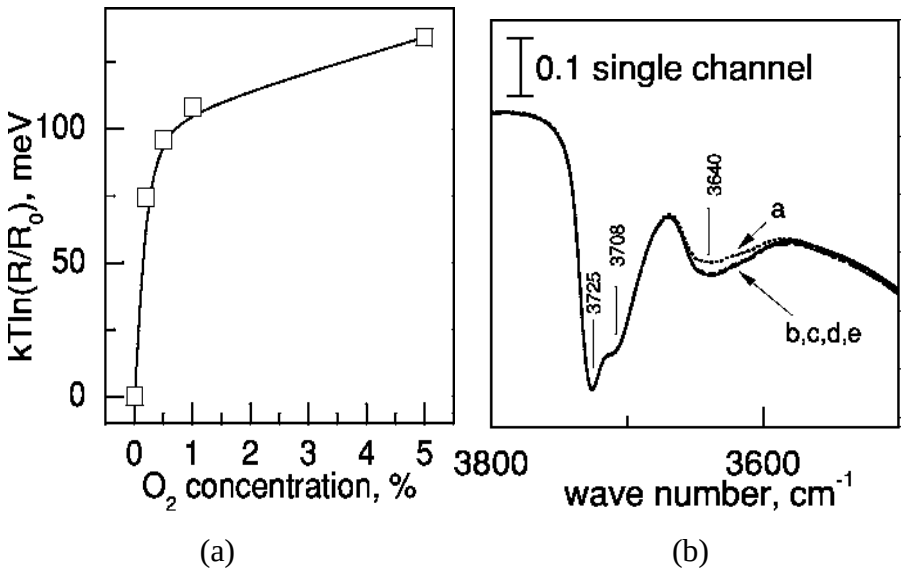

(a) (b)

Figure 3-41 :Changes of the band bending (a) and the respective single channel DRIFT spectra (b) of the tin dioxide sensor (U500Y) exposed to oxygen: a - 70 ppm, b - 2000 ppm, c - 5000 ppm, d - 10000 ppm, e - 50000 ppm at 400°*C* and at constant humidity level (3 ppm)[150].

3.3.3.1.1.3 Isotope exchange investigation

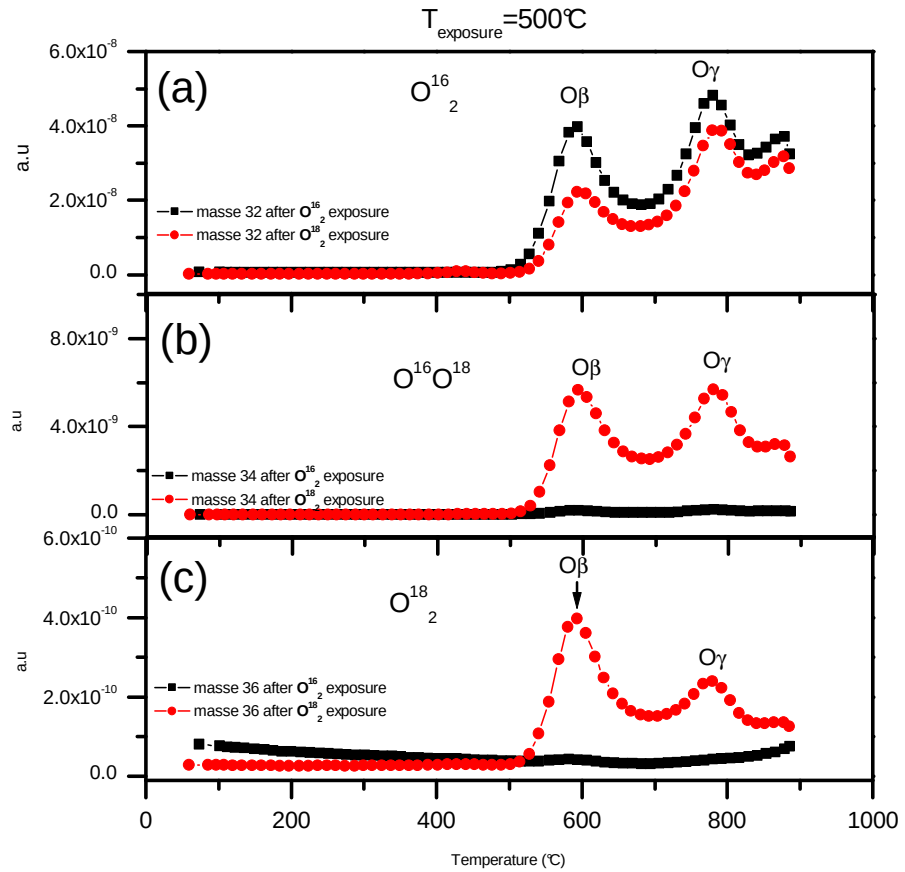

Figure 3-42 : TPD thermogram after exposure To O^{18}_2 at 500°C. TPD thermogram with O^{16}_2 exposure is used as reference. a) m/e=32 b) m/e=34 c) m/e=36

O_2^{18} exchange isotope was conducted in order to validate the ionosorption of the O_β specie. During the isotope exchange the signals m/z= 34 ($O^{16}O^{18}$), m/z= 36 ($O^{18}{}_2$) was followed in addition to m/z= 32 ($O^{16}{}_2$). Figure 3-42 illustrated the results obtained for an $O^{18}{}_2$ exposure at 500°C. In the same figure the O_2^{16}, exposure at 500°C is plotted to compare both effects. As already mentioned, when $O^{16}{}_2$ is adsorbed at elevated temperature and especially at 500°C, two main bands appear: O_β (550°C) and O_γ (760°C). No bands appears for m/z=34 and m/z=36 which is logic as no O_2^{18} was present.

When, the sample is exposed to O_2^{18}, the O_β and O_γ peaks are observed for all signals m/z=32, 34, 36. For m/z=32 (Figure 3-42 (a)), the comparison of signals measured after exposure to O_2^{18} and $O^{16}{}_2$ shows that the intensity of O_β (O-) peak is strongly decreased in the case of O_2^{18} exposure, whereas O_γ (O_L) peaks, intensity is only slightly decreased.

For m/z=34 (Figure 3-42 (b)) and (Figure 3-42 (c), it can be seen that the relative intensity of O_β (O-) peak increases comparably to the one of O_γ (O_L) peaks.

These results indicate that:

- $O^{16}{}_2$ is still present in our experiment, even in the case of O_2^{18} exposure because m/z=32 signal remains significant in this condition.
- O_β (O-) species mainly issued from previous absorption from gas surrounding the sample during exposure treatment according to reaction previously written:

$$O_2^{18} + 2e^- + 2\sigma \rightarrow 2\sigma\text{-}O^{18-} \quad \text{(formation } O_\beta\text{)}$$

- On the contrary, O_γ (O_L) species which are desorbed are mainly constituted from the oxygen of SnO_2 lattice, thus of isotope O^{16}

$$2O_O^x \rightarrow 2V_O^{\cdot\cdot} + O_2 + 2e^- \quad \text{(formation } O_\gamma\text{)}$$

- But, O_2^{18} can be incorporated in the lattice O_γ as peak m/z=34 and m/z=36 are significant. This incorporation during exposure step can occur from reaction previously reported, but from O_β

$$\sigma\text{-}O^{18-} + V_O^{\cdot\cdot} + e^- \rightarrow O_O^{X18} + \sigma$$

3.3.3.1.2 Adsorption of oxygen on SnO_2 With metal addition

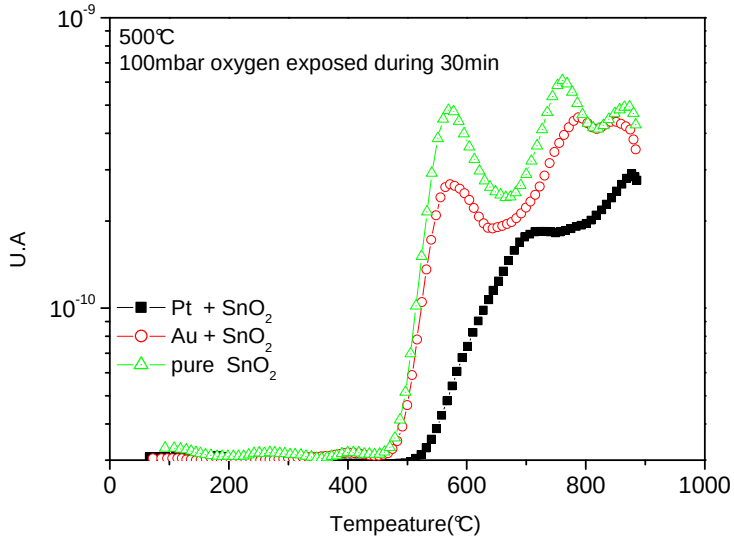

Figure 3-43 : TPD thermograms of oxygen for Pure SnO_2 powder, Au+ SnO_2 powder and Pt+ SnO_2 powder after the adsorption of 100mbar oxygen at 500°C.

The TPD thermograms of Oxygen desorption with the SnO_2 mixed with noble metal are shown in Figure 3-43. In comparison with pure SnO_2, the desorption of oxygen with Au mixed SnO_2 exhibits almost the same peak at 550°C (O_β), 760°C (O_γ), and a gradual desorption of oxygen after 800°C. The interaction of oxygen with the powder Pt mixed SnO_2 is quite different from pure and gold mixed powders. In fact, desorption of the first oxygen species (O_β) for gold mixed or pure SnO_2 starts at 460°C while starts at 510°C for the Pt mixed powder. Two peaks are present for both Au mixed and pure SnO_2 powders whereas only one peak in the neighbourhood of 705 °C is present for Pt mixed SnO_2 powder. a gradual desorption is observed in all cases corresponding of the O_δ desorption.

From the point of view of the adsorption and desorption processes of oxygen, in regards to the nature of the metal, it is obvious that platinum affects the process. The desorption temperature and the shape of the peak suggest a stronger bonds between platinum and oxygen species.

The catalytic role of the platinum is known for a long time even if the mechanism is not obvious. Two mechanisms are known: “the spill over effect” and “the “electronic effect”. The absence of visible desorption suggest that the oxygen prefers adsorbed directly on the platinum.

3.3.3.1.2.1 Effect of the adsorption temperature

To have a clear overview of the effect of the metal dispersed in SnO2 on the oxygen desorption, TPD measurements were done from different temperatures of gas exposure from room temperature (RT) to 600°C. The process was the same as the one used with pure SnO_2. After cleaning the surface, 100mBar of pure oxygen was exposed to the sample (mixed gold or mixed platinum) at the required temperature during 30min. Then, the sample is quenched to RT and the TPD program is running. The results are shown in Figure 3-44

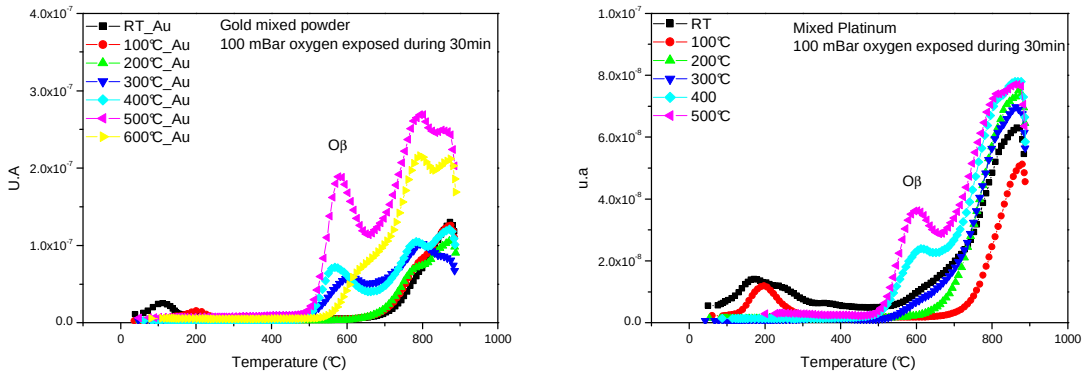

Figure 3-44 : Thermogram of the desorption of O_2 (m/z=32) after 100mBar exposure at different temperature for gold and platinum

- .O_β and O γ species.

With gold particles inside the SnO_2, the result is quite comparable to pure tin dioxide. At 300°C, the peak corresponding to O_β and O_γ desorption appear. With the increase of the temperature the intensity of the peaks increases. At 600°C the formation of the O_β is not possible, as already discovered with pure SnO_2. In case of platinum particles added to the SnO_2, the behaviour is not the same. The formation of O_β started at 400°C and the maximum desorption temperature (Tm) is shifted. The presence of the peak of Oγ is not real clear. It seems that only one species is present.

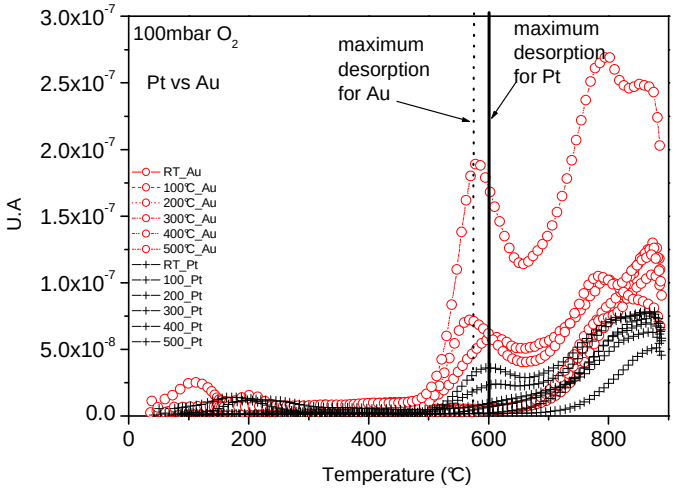

Figure 3-45 : Thermogramm of the desorption of O_2 after 100mBar exposure at different temperature for gold and platinum

Put in together the thermogram from gold and platinum samples reveals that the intensity is quite different. For platinum, on one hand the signal intensities are weaker and other hand the temperature of the maximum desorption is 40°C higher than that of gold sample. The difference of the maximum desorption temperature means simply that oxygen is better bond in the case of platinum than gold.

- α species

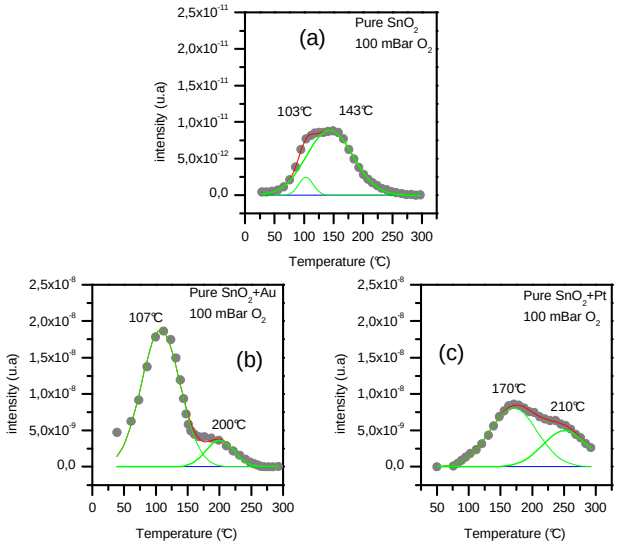

Figure 3-46 : Fit of the oxygen thermogram for an adsorption at RT for (a) pure, (b) SnO_2+Au and (c) SnO_2+Pt

The presence of the metal has an important effect on the adsorption of the oxygen species at room temperature (RT). On Figure 3-46, the thermograms are focused on the range from RT

to 300°C, when 100mBar of oxygen is adsorbed at RT during 30min, for the three types of powders. If the pure SnO_2 is considered as the reference the presence of the metal modified the adsorption of the oxygen. In presence of gold, the weak bond species α_1 is favoured whereas the platinum favours high bond species α_2. As a function of the nature of the metal, a predominance of oxygen species exist.

3.3.3.1.2.2 Influence of adsorption oxygen partial pressure

At an exposure temperature of 500°C, the influence of the adsorption oxygen partial pressure of oxygen exposed to the sample was checked. Figure 3-47 shows the result. Gold samples seem to be less affected by the pressure and desorbed usually the same quantity whereas for the platinum ones the intensity of the O_β species s increases with pressure.

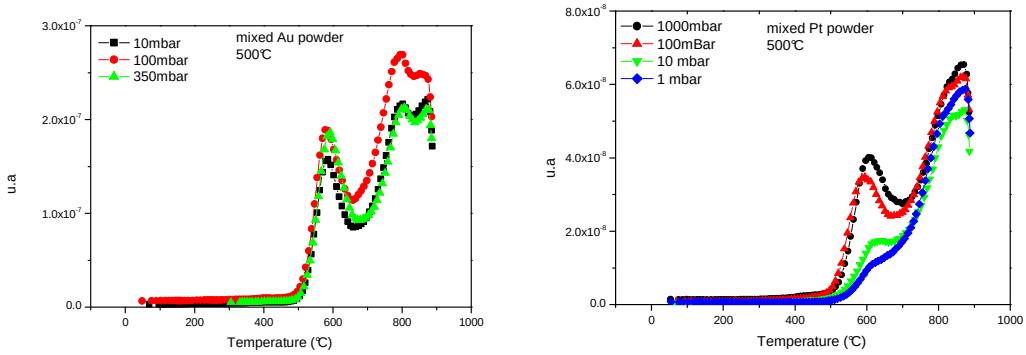

Figure 3-47 : Thermogram of the desorption of O_2 after oxygen exposure at 500°C at different pressure for gold and platinum

3.3.3.1.3 Summary of oxygen adsorption results

TPD thermograms of oxygen desorption from pure SnO_2 consist of 5 peaks: $O\alpha_1$ (80°C, O_2) and $O\alpha_2$ (150°C, O_2^-) Oβ (450-600°C, often centred at 550°C, O^-), Oγ (around 730°C, O_L and δ (above 800°C, O_{Lbulk}).. With platinum, the O_β (O^-) species is less significant its maximum desorption temperature is at a higher temperature. With Au, the situation is unchanged compared to pure SnO_2

3.3.3.2 Variation of oxygen desorption with coadsorption of reducing gas.

3.3.3.2.1 With pure SnO_2

Direct reaction.

Indeed, what happen for our system if a reducing gas is introduced? To observe the relation between oxygen and a reducing gas the following process was done. The sample was kept under 100mbar oxygen atmosphere at 400°C during 30min and a reducing gas, carbon monoxide or methane, has been introduced during short period. Then, the "regular process" has been used. As reference the TPD thermogram without any reducing gas adsorption has been taken, which exhibit a peak at 550°C (O_β). If a reducing gas is adsorbed, the O_β peak disappears totally, see Figure 3-48. With CO (300ppm) the effect is faster than CH_4 (1000ppm), after 5 min the peak (which means the species) disappears. Most people [151] have suggested a direct reaction with reducing gas and chemisorbed oxygen but it was never really proved until now, using TPD measurements. To avoid any other effect (desorption of these species due to the temperature in vacuum for example) a neutral gas (Argon) has been also introduced after the oxygen. The result with Argon is also shown in figure 6. The O_β peak is still present after the argon exposure. This last result proves a real reaction between reducing gas (CO or CH_4) and ionosorbed oxygen. The reaction can be written :

$$CO + \sigma\text{-}O^- \rightarrow CO_2 + \sigma + e^-$$

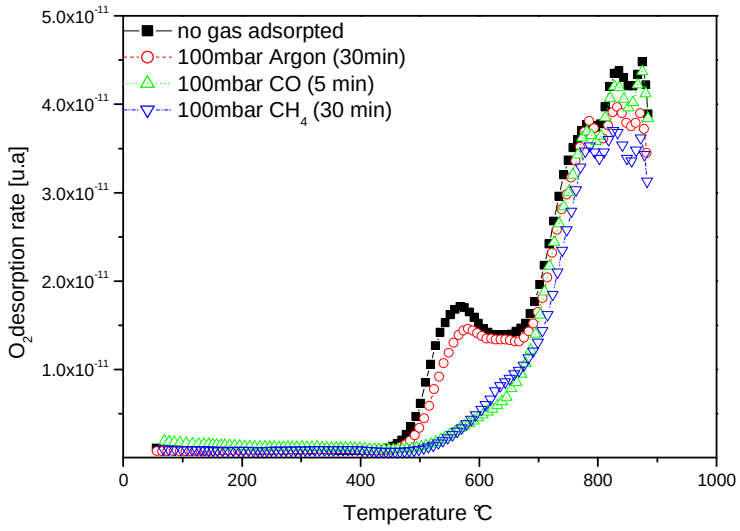

Figure 3-48 : TPD chromatograms of oxygen desorption (m/ z=32) in function of the gas co-adsorbed at 500°C after 100mbar oxygen adsorption On pure SnO_2.

Consequences and product.

In the previous section, a relation between O_β species and the formation of new hydroxyl species has been proved. It is interesting to inquire the consequence of the reaction of a reducing gas with O_β specie on the water desorption thermogram. Moreover, it is known that the product of the reaction of CO with the oxygen of the surface is CO_2. Figure 3-49 shows the thermogram of CO_2 (mass 44) and oxygen and Figure 3-50 shows the thermogram of water and oxygen. These two graphs illustrate the consequence the disappearance of the O_β on the hydroxyl group and CO_2. Only the case of CO is shown here. Two consequences of the reducing gas co-adsorbed after the oxygen pre-treatment are visible:

- Figure 3-49 reveals an increasing of the CO_2 peak desorption after CO adsorption. It confirms that the product of the reaction is mainly CO_2.

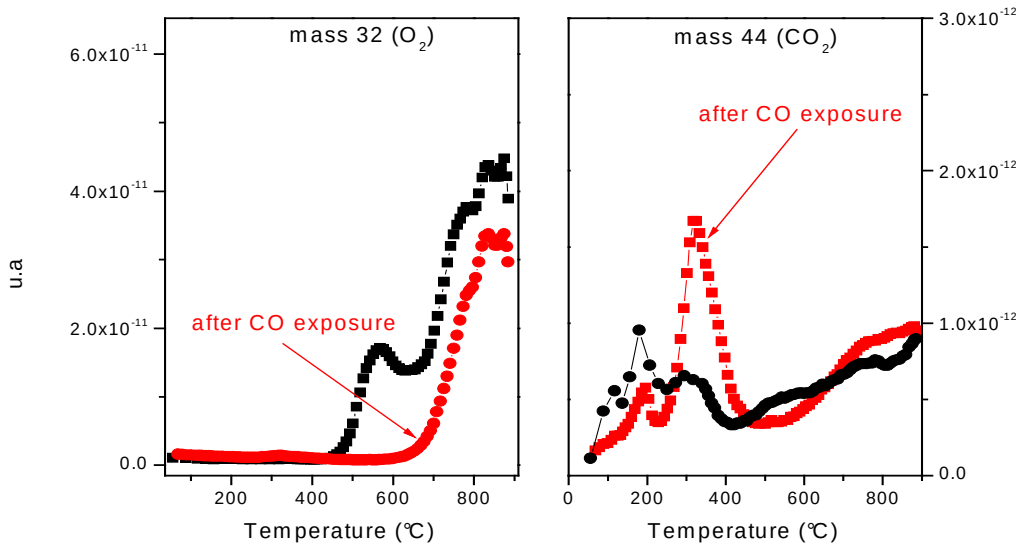

Figure 3-49 : TPD thermogram of oxygen desorption (m/z=32) and CO_2 (m/z=44) with or without CO co-adsorption.

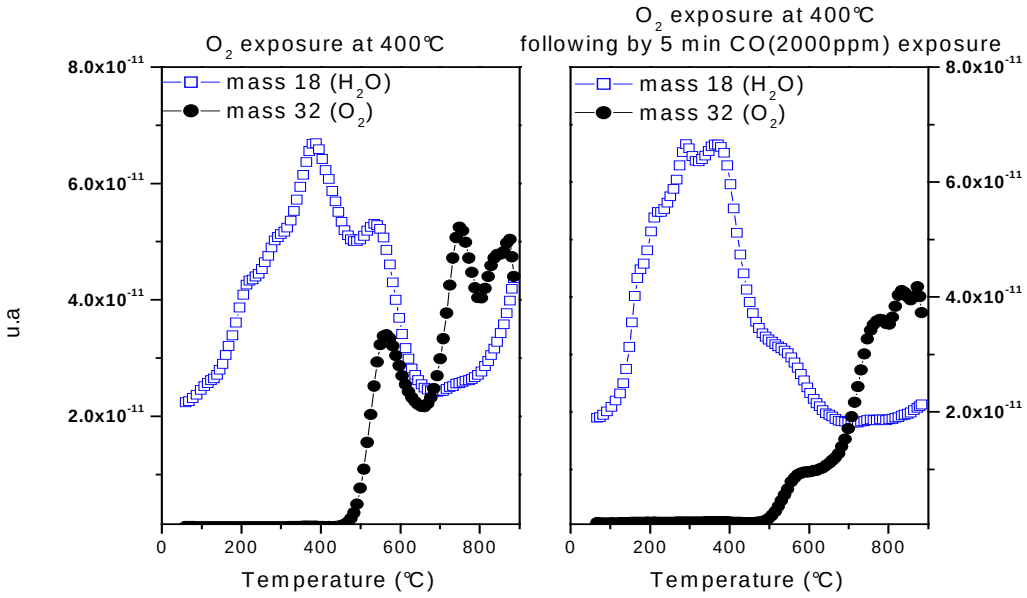

Figure 3-50 : TPD thermogram of oxygen desorption (m/z=32) and water (m/z=18) with or without CO co-adsorption.

- The OH_{550} peak is linked to the O_β peak decrease. These means that the reaction between CO and "O-"is dominant in comparison with the formation of the OH group.

A simple sketch explains this dominance in the Figure 3-51 The Starting point is the dissociation of water at the surface of the SnO_2 which as already known to be as follow.

$$H_2O+\sigma+O_o^x \rightarrow (OH— \sigma) + (OH)_o^* + e^-$$

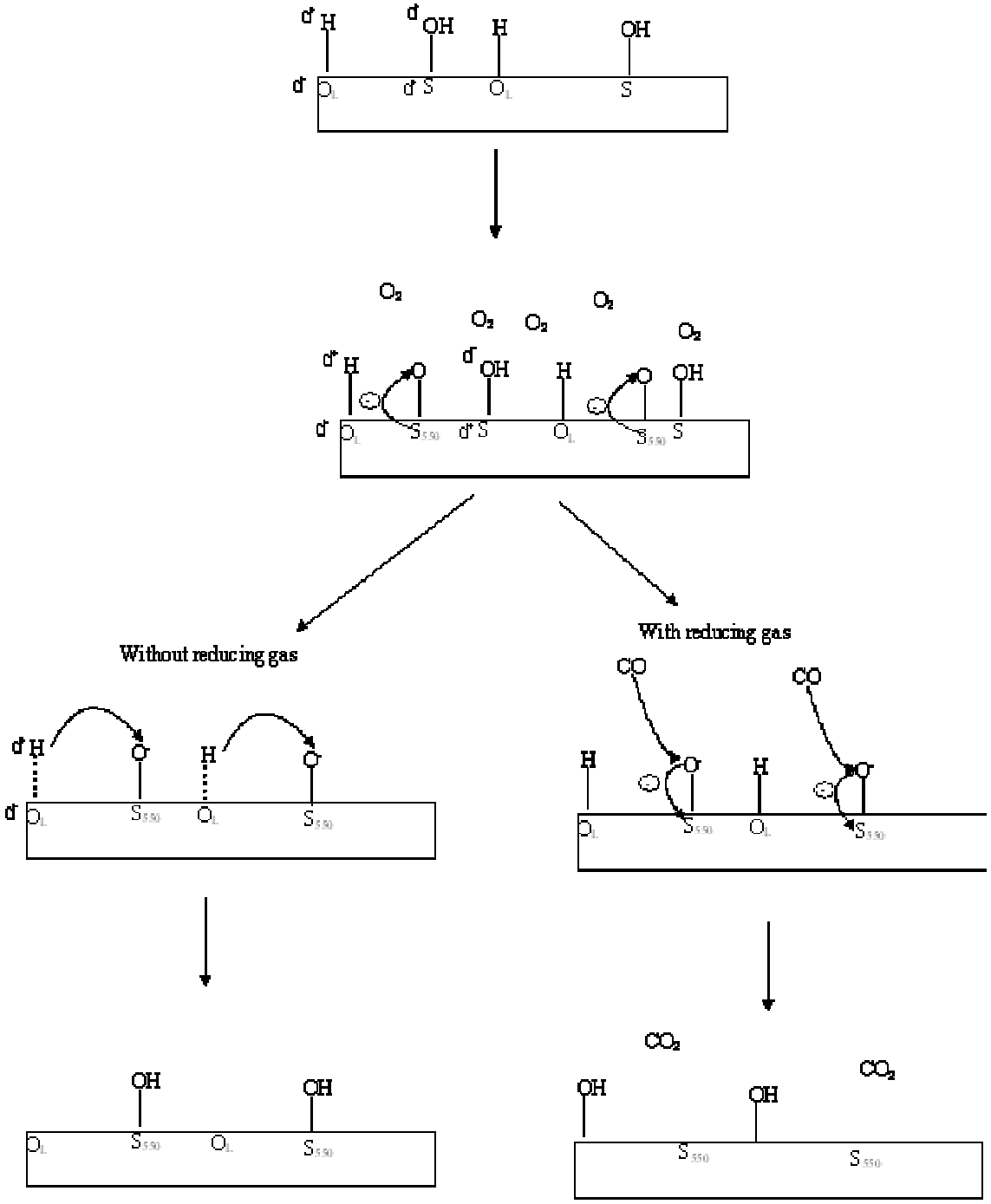

Figure 3-51: **Sketch of the relation between O_β (O^-) and the formation of OH group and the influence of the presence of a reducing gas CO**

3.3.3.2.2 With the presence of the metal

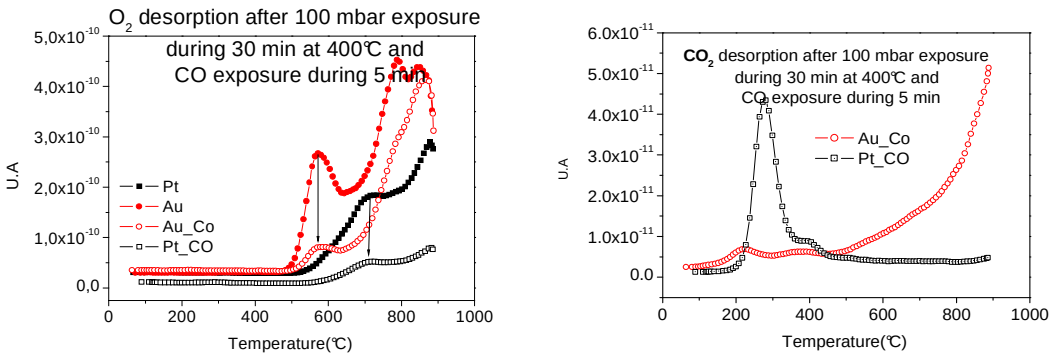

(a) **(b)**

Figure 3-52 : TPD thermogramfor mixed SnO_2 powder: (a) Oxygen (m/e= 32) and (b) CO_2 (m/e=44)

Similar test were performed with samples mixed with gold or platinum particles. The consequence of CO adsorption on the oxygen thermogram when the O_β is present is illustrated in Figure 3-52(a). The CO_2 desorption is measured at the same time, Figure 3-52(b). After the adsorption of oxygen at 400°C, two desorption peaks appear for gold and only one for the platinum sample as described previously. The adsorption of CO after the oxygen exposure reduce the peak of oxygen desorption for both mixed powder. In the case of gold, mainly the O_β peak is reduced which is the same behaviour as observed on pure powder. With platinum, the oxygen desorption declines strongly but keep the same shape. In Figure 3-52 (b), the CO_2 desorption is quite different for each type of metal. For gold, a gradual desorption of CO_2 is observed started at 400°C whereas a well pronounced CO_2 peak desorption is observed centred at 250°C in the case of Pt.

With platinum, The CO_2 peak desorption at 250°C where no oxygen site is present. This result suggests an easiest formation of CO_2 in the case of platinum and confirms the catalytic role played. Secondly, with gold, a gradual desorption suggest possible intermediate like CO_3, $CO_3^{2-}$and CO_2^- which can desorbed as CO_2 at different temperatures.

3.3.3.3 Summary of the interaction with a reducing gas

When a reducing gas (CO or CH_4) is exposed to SnO_2 powder after the oxygen exposure, the desorption of the O_β species is no more visible in the TPD oxygen thermogram and in the same time, the CO_2 desorption increases, which proves a direct reaction between O^- and the reducing gas.

$$CO + \sigma\text{-}O^- \rightarrow CO_2 + \sigma + e^-$$

When metal is present, the effect of Au and Pt are, as in the case of oxygen, quite different. For the Au sample the same results, as for the case of metal absence, are recorded. For the Pt sample, the CO_2 desorption is quite different, very sharp and at lower temperature (250°C).

3.3.3.4 Discussion on TPD

Observations of the oxygen state at the surface of a material are a big challenge. It was not possible to use DRIFT due to the set up of our experiment. Thermodesorption (TPD) was a good choice to follow oxygen species. In the DRIFT experiments, some questions remained unsolved. The main one was: how the platinum can activate the CO conversion to CO_2? Are the speeds up of the reaction at the surface and the low amount of intermediate species at the surface sufficient to explain the sensibility to CO?

Pure SnO_2 was studied before to study the influence of metal. We found 5 different oxygen species which can desorbed. The O_β species was found to be the most reactive to the reducing gas. The presence of gold doesn't change the mechanism. In other hand, 5 oxygen species desorbed were also found. With platinum, the behaviour of the oxygen desorption is different. In fact, only one species from the material (usually: O_γ surface and O_δ bulk) was found to desorb. Another result is the higher temperature of the O_β species desorption.

With the results found, it is obvious that the nature of the metal can modify the oxygen species at the surface. For gold, we can affirm that the surface is not modified. The effects of platinum on the oxygen species are related to the oxygen desorption. The higher temperature indicates a better bond between oxygen and the surface of the SnO_2.The fact that the oxygen bulk desorption is also modified can indicate that the surface sites are modified. The presence of platinum modifies the surrounding of the oxygen.

In addition to this result, the formation of CO_2 in the presence of metal was found to be favour by platinum. The oxygen is better bound at the surface of the SnO_2 + Pt, which means that the electron are delocalized to form this bond is a higher state. It means that in presence of CO, the reaction with O^- and the release of the electron will be more significant. This result correlates with the high sensitivity of sensor with platinum electrodes.

3.3.4 TPD Conclusion

Temperature-programmed desorption experiments for different as were performed in order to helps the understanding of the electrode material induced effects. For oxygen, based on the literature data, it was possible to assign the different peaks to specific oxygen species, as follow: α_1 (80°C) belongs to the molecular physisorbed oxygen O_2 and α_2 (around 150°C) to singly ionised molecular oxygen O_2^- . The β peak is currently attributed to the singly ionised atomic oxygen (450-600°C, often centred at 550°C, O^-). The 2 last ones can be assigned to oxygen form the lattice: first the γ (around 730°C) to surface O_L and δ (above 800°C), the lattice oxygen from the bulk $O_{L\ (bulk)}$. It is important to observe that, depending on the electrodes material, the maximum of the peak corresponding to O^- appears at different temperatures. Due to the fact that for Pt the maximum desorption is higher, one can consider that the bonding of O^- at the SnO_2 is stronger.

A little bit surprising is the funding that in the case of Pt, where the O^- is probably strongly bond to the surface, the CO_2 desorption after the simultaneous exposure of the powders to O_2 and CO, takes place much stronger and at lower temperatures if compared to the gold case. In the same experiment we can see that for all cases- SnO_2 and SnO_2 mixed with Pt and Au- the reaction between O^- and CO takes place. The adsorption of O_2 is practically eliminated. However, for SnO_2 and SnO_2 mixed with Au the elimination of the final reaction product (CO_2) is taking place with difficulty. These results are confirming the finding provided by DRIFT analysis about the blocking of CO/O/electrons at the surface in the form of ionic intermediates in absence of Pt.

Chapter 4

4 Conclusion

The reason for starting this work was the fact that there was a lack of knowledge about the influence of the electrodes into the sensing process of gas sensor. Previous study of O. Montmeat in MICC department proposed a macroscopic approach of the electrodes considering mainly electrical phenomena. So, the aim at the present work was to investigate deeper the implication of electrodes, at the microscopic scale.. To achieve that, the followed strategy was to have, in addition to the usual DC resistance measurement, phenomenological and spectroscopic (DRIFT and TPD) studies in order to investigate the influence of the electrodes.

- Electrical measurement

The first part of this work was devoted to the study of the influence of the geometry and of the nature of the electrode. It was proved that the nature of electrodes has an effect on the overall resistance on the gas sensor and on its performance. Different approaches were used to understand this problem with more or less success:

- Using SnO_2 mixed with big metal particles as sensitive layer for gas sensor in order to increase the metal-semiconductor interface. We discovered that the overall resistance is more influenced by the nature of electrodes rather than metal particles inside the layer.
- It was supposed that the one can increase the electrical effect by narrowing the gap. This effect was, in our case, just a geometrical one. By reducing the space between the electrodes, we just changed the resistance of the sensitive material placed between the two electrodes. No real qualitative effect of the electrode was identified.

- Spectroscopic information

Another method to investigate the role of the electrodes is to observe surface reactions during CO sensing with gas sensors. DRIFT was used simultaneously to the DC measurement of electrical resistance. One observes that, depending of the nature of the electrodes, the reaction pathway from CO to CO_2 is modified. On the basis of such studies a first finding is the identification of the commonly observed intermediate surface species being monodentate carbonates and carboxylates. Besides that, it was shown that platinum electrodes decrease the concentration of intermediate species and favour the formation of CO_2.The decrease is not uniform for all intermediate species: the monodentate carbonate decrease less because it is the

most stable species. On the opposite, with gold electrodes, many intermediates are present at the surface. The intermediates concentration can be correlated with the electrical performance of the sensor. Namely their presence indicates the fact that the charge transfer from the surface species to the conduction band is blocked. The system can “get rid of” the intermediates faster and simultaneous response is increased:
The formation of carboxylates and monodentates is a consequence of the direct reaction of CO with oxygen species. Unfortunately, up to date there is no adequate technique for a direct monitoring of oxygen ions in operando conditions.. To get more insights, TPD measurements were performed, mainly focused on observing the oxygen desorption from the powder. It was found that the pure and mixed gold SnO_2 powders show the same trend for oxygen desorption. With mixed platinum powders, it was found that oxygen is stronger bonded to the surface. Thus, the weak concentration of intermediate species observed by DRIFT is a consequence of the quantity of oxygen present at the surface, but the important sensitivity is mainly due to the quality of the bond of oxygen species when platinum is present.

Outlook

This thesis was a step ahead to understand the effect of the electrodes on sensors performances. The success was due to the approach of using different techniques to investigate a selected problem Many improvements can be done and especially on the electrical part: our main problem was the size of our system and by using micro technologies for building a new device on silicon substrate this withdraw could be eliminated. With this new device, impedance spectroscopy measurement technique could be done to complete the understanding. They could clarify the contribution of electrodes to the electrical transduction. The influence of the geometry (size of the electrode and gap between them) could also be clarified. Concerning the spectroscopic technique, one could improve the quality of the spectra recorded at higher sensor operating temperatures by using an optical filter. Thus, the saturation of the MCT detector should diminish.

In future research, Flash TPD, directly on sensor could be use to mach with the powder results.

Bibliography

[1] www.euro.who.int

[2] N. JAFFREZIC-RENAULT, *"Les microcapteurs chimiques"*, Spectra Analyse, **195**, mars-avril, (1997)

[3] N. Bârsan and U. Weimar, "Understanding the fundamental principles of metal oxide based sensors; the example of CO sensing with SnO_2 sensors in the presence of humidity", in. *J. Phys.: Condens. Matter* 15 (2003), R813-839

[4] R.Lalauze, N.Bui and C.Pijolat, "interpretation of the electrical properties of a SnO_2 gas sensors after treatment with sulfur dioxide", *Sensors and Actuators* 6 (1984) pp 119-125

[5]S. Saukko, V. Lantto," Influence of electrode properties of SnO_2-based gas sensor" *Thin Solid Films* 436 (2003) pp137-140

[6] Thesis of Pierre Montmeat, : "Rôle d'éléments métalliques sur les mécanismes de détection d'un capteur de gaz à base de dioxyde d'étain. Application à l'amélioration de la sélectivité à l'aide d'une membrane de platine",2003

7 N. Barsan, D. Koziej, U. Weimar **"**Metal oxide-based gas sensor research: How to?" *Sensors and Actuators B: Chemical, Volume 121, Issue 1, 30 January 2007, Pages 18-35*

[8] N. TAGUSHI, Japan Patent 45-38200, (1962)

[9] J.J. Robillard, Electrocatalytic photographic process, patent (GB) 1063029 (1967)

[10] Z.M. Jarzebski and J.P. Marton, Physical properties of SnO_2 materials: III. Optical properties, J. *Electrochem. Soc.*123 (10) (1976) 333C

[11] P. Barbarat, S.F. Matar, G. Le Blevennec, First-principles investigations of the electronic, optical and chemical bonding properties of SnO_2, Journal of Material Chemistry, 7 (12) (1997) p. 2547-2550.

[12] J.M. Themlin, M. Chtaïb, L. Henrard, Ph. Lambin, J. Darville, and J.M. Gilles, Characterization of tin oxides by x-ray-photoemission spectroscopy, *Phys. Rev. B* **46** (4) (1992) 2460.

[13] P. De Padova, M. Fanfoni, R. Larciprete, M. Mangiantini, S. Priori, and P. Perfetti, A synchroton radiation photoemission study of the oxidation of tin, Surface Science, 313 (1994) p. 379-391

[14] L. Kövér, G. Moretti, Zs. Kovács, R. Sanjinés, I. Cserny, G. Margaritondo, J. Pálinkás, and H. Adachi, High resolution photoemission and Auger parameter studies of electronic structure of tin oxides, Journal of Vacuum Science Technology A 13(3) (1995) p. 1382-1388.

[15] J.P. Joly, L. Gonszalez-Cruz, Y. Arnaud, Bulletin de la Société Chimique de France (1986) p. 11-17.

[16] W.M.H. Sachtler and P. van der Plank, The role of individual surface atoms in chemisorption and catalysis by nickel-copper alloys *Surf. Sci.*, 18 (1969) 62

[17] Z. Knor, Chemisorption Complexes and Their Role in Catalytic Reactions on Transition Metals, Advances in Catalysis, 22 (1972) 51****

[18] F.F. Volkenshtein, The electronic theory of catalysis on semiconductors, MacMillan, New York (1963)

[19] S.G. Davidson and J.P. Levine, in vol. 25 of *Solid State Physics,* ed. F. Seitz and D. Turnbull, Academic Press, New York (1970)

[20] S.R. Morrison, *The chemical physics of surfaces,* 2nd ed., Plenum press, New York (1990)

[21] S.R Morrrison, Semiconductor gas sensors, Sensors and Actuators, 2 (1982) 329-341.

[22] N. Yamazoe and T. Seiyama, Sensing mechanism of oxide semiconductor gas sensors, Proc. 3rd Int. Conf. Solid-State Sensor and Actuators (Tranducers 1985), Philadelphia, P.A, USA, June 7-11, 1985,pp 376-379.

[23] Yamazoe

[24] C.G. Fonstad, R.H. Rediker, Electrical properties of high-quality stannic oxide crystals, Journal of Applied Physics, 42 (1971) p. 2911-2918.

[25] S. Samson, C.G. Fonstad, Defects structures and electronic donor levels in stannic oxide crystals, Journal of Applied Physics, 44 (1973) p. 4618-4621

[26] M. Henzler and W. Göpel in: *Oberflächenphysik des Festkörpers,* Teubner, Stuttgart (1994)

[27] A. Hierlemann, Fundamental principles and thermodynamics of chemical sensing, *1st NOSE I short course,* Bressanone, Italy (2002) 11

[28] N. Yamazoe, J. Fuchigami, M. Kishikawa, and T. Seiyama. Interactions of tin oxide surface with O2, H2O and H2. *Surface Science,* 86:335–344, 1978

[29] S. Saukko, U. Lassi, V. Lantto, M. Kroneld, S. Novikov, P. Kuivalainen, T. T. Rantala, and J. Mizsei. Experimental studies of O2-SnO2 surface interaction using powder, thick films and monocrystalline thin films. *Thin Solid Films,* 490(1):48–53, 2005.

[30] S.C. Chang. Oxygen chemisorption on tin oxide: Correlation between electrical conductivity and EPR measurements. *J. Vac. Sci. Technol.,* 17:366, 1980

31 S. Emiroglu, N. Barsan, U. Weimar, V. Hoffmann, Thin Solid Films 391 (2001) 176.

[32]S. Lenaerts, J. Roggen, G. Macs, FTIR characterization of tin dioxide gas sensors materials under working conditions, Spectorchimica Acta Part A, 51 (1995) p. 883-894

[33] J. P. Joly, L. Gonszales-Cruz, Y. Arnaud, Bulletin de la Societe Chimique de France, 11, 1986

[34] B. Gillot, C. Fey, D. Delafosse, Journal de Chimie Physique et de Physico-Chimie Biologique, 73, 1976, p 19

[35] N. Yamazoe, J. Fuchigami, M. Kishigawa, T. Seiyama, Surface Science,86, 1979, p. 366

[36] A. M. Volodin, A. E. Cherkasin, Reaction Kinetics and Catalysis Letter, 17, 1981, p. 329

[37] S. C. Chang, Journal of Vacuum Science & Technology, 17, 1980,p. 366

[38] M.A. Barteau, Site requirements of reactions on oxide surfaces, Journal of Vacuum Science Technology A 11 (1993) p. 2162

[39] G. Heiland and, D. Kohl in T Seiyama (ed.), Chemical Sensor Technology, Vol. 1 Kodansha, Tokyo, p. 1-35.

[40] D. Kohl, Oxidic semiconductor gas sensors, G. Sberveglieri (ed.), Gas sensors, p. 43-88

[41] M. Egashira, M. Nakashima, S. Kawasumi, Change of thermal desorption behaviour of adsorbed oxigen with water coadsoption on Ag+-doped tin(IV) oxide, Journal Chemical Society Chemical Communications (1981) p. 1047-1049.

[42] K. Morishige, S. Kittaka, T. Morimoto, The thermal desorption of surface hydroxide on tin (IV) oxide, *Bull. Chem. Soc. Japan*, 53 **(1980)** 2128

[43] N. Yamazoe, J. Fuchigami, M. Kishikawa, T. Seiyama, Interactions of tin oxide surface with O_2, H_2O and H_2, Surface Science, 86 (1979) p. 335-344

[44] E.W. Thornton, P.G. Harrison, Tin oxide surfaces Part I: Surface hydroxyl groups and the chemisorption of carbon dioxide and carbon monoxide on tin(IV)oxide, Journal of the Chemical Society, Faraday Transaction I, 71 (1975) p. 461-472

[45] A. Guest, PhD Thesis, University of Nottingham, (1985).

[46] S. Lenaerts, J. Roggen, G. Macs, FTIR characterization of tin dioxide gas sensors materials under working conditions, Spectorchimica Acta Part A, 51 (1995) p. 883-894

[47] F. Berger, E. Beche, R. Berjoan, D. Klein, A. Chambaudet, An XPS and FTIR study of SO_2 adsorption on SnO_2 surfaces, Applied Surface Science, 93 (1996) p. 9.

[48] P.K. Clifford, D.T. Tuma, Characteristics of semiconductor gas sensors I: Steady state gas response, Sensors and Actuators, 3 (1982/83) p. 233-254.

[49] B. Gillot, C. Fey, D. Dalafosse, Study of the oxidation kinetics of finely-divided magnetites. II. Influence of chromium substitution, Material Research Bulletin, 11 (7) (1976), p. 843-849.

[50] Y. Matsuura, K. Takahata, K. Ihokura, Mechanism of gas sensitivity change with time of SnO_2 gas sensors, Sensors and Actuators, 14 (1988) p. 223-232

[51] K.D. Schierbaum, U. Weimar, W. Göpel, Conductance, work function and catalytic activity of SnO_2 based gas sensors, Sensors and Actuators B, 3 (1991) p. 205-214.

[52] S.R. Morrison: The chemical physics of surfaces, 2nd (edn.), Plenum Press, New York (1990).

[53] V.A. Henrich and P.A. Cox, The Surface Science of Metal Oxides, University Press, Cambridge (1994), p. 312-316.

[54] M. Caldararu, D. Sprinceana, V.T. Popa, N. I.. Ionescu, Surface dynamics in tin dioxide containing catalysts II, Sensors and Actuators B, 30 (1996) p. 35-41

[55] D.S. Vlachos, P.D. Skafidas, J. N. Avaritsiotis, Transient effects of tin oxide CO sensors in the presence of water vapour, Applied Physics Letters, 63 (1999) p. 39-42.

[56] R. Ionescu, A. Vancu, C. Moise, A. Tomescu, Role of water vapour in the Interaction of SnO_2 Gas Sensors with CO and CH_4, Sensors and Actuators B, 61 (1999) p. 39-42.

[57] M. Egashira, M. Nakashima, S. Kawasumi, T. Selyama, Temperature programmed desorption study of water adsorbed on metal oxides, Journal of Physical Chemistry 85 Iss. 26 (1981) p. 4125-30.

[58] L. Morris, D.E. Williams, Pt(II) as an electronically active surface site in the room temperature CO response of Pt modified gas sensitive resistors, Journal of Physical Chemistry B, 105 (2001), p. 7272-7279.

[59] P.K. Clifford, D.T. Tuma, Characteristics of semiconductor gas sensors I: Steady state gas response, Sensors and Actuators, 3 (1982/83) p. 233-254.

[60] V.A. Henrich and P.A. Cox, The Surface Science of Metal Oxides, University Press, Cambridge (1994), p. 312-316.

[61] J.F. Boyle, K.A. Jones, The effects of carbon monoxide, water vapor and surface temperature on the conductivity of a tin(IV) oxide gas sensor, Journal of Electronic Materials, 6 (6) (1977) p. 717-33.

[62] S.J. Gentry, T. A. Jones, The role of catalysis in solid-state gas sensors, Sensors and Actuators 10(1-2) (1986) p. 141-163.

[63] H. Windischmann, P. Mar, A model for operation of thin-film SnO_x conductance modulation carbon monoxide sensor, Journal of electrochemical Society: Solid-State Science Technology, 126 (1979) p. 627-633

[64] E.W. Thornton, P.G. Harrison, Tin oxide surfaces Part I: Surface hydroxyl groups and the chemisorption of carbon dioxide and carbon monoxide on tin(IV)oxide, Journal of the Chemical Society, Faraday Transaction I, 71 (1975) p. 461-472

[65] S. Lenaerts, J. Roggen, G. Macs, FTIR characterization of tin dioxide gas sensors materials under working conditions, Spectorchimica Acta Part A, 51 (1995) p. 883-894

[66] M.J. Willett, Spectroscopy of surface reactions, in P.T. Moseley, J. Norris, D.E. Williamjs, Techniques and mechanisms in gas sensing, vol. 3, Adam Hilger, Bristol (1991) p. 61

[67] S.R. Morrison, Mechanism of semiconductor gas sensor operation, Sensors and Actuators, 11 (1987) p. 283-287

[68] N. Bârsan and U. Weimar, Conduction model of metal oxide gas sensors, Journal of Electroceramics, 7 (2001) p. 143-167

[69] Figaro Engineering Inc.: Figaro gas sensor, Products Catalogue (1995).

[70]N. Bârsan, Conduction models in gas-sensing SnO_2 layers: Grain-size effects and ambient atmosphere influence, Sensors and Actuators B, 17 (1994) p. 241

[71] H. Windischmann, P. Mar, A model for operation of thin-film SnO_x conductance modulation carbon monoxide sensor, Journal of electrochemical Society,Solid, 126 (1979) p. 627-633.

[72] H. Pink, L. Treitinger, L. Vite, Preparation of fast detecting SnO_2 gas sensors, Japanese Journal of Applied Physics, 19 (1980) p. 513-517.

[73]N. Bârsan, R. Grigorovici, R. Ionesc, M. Motronea, A. Vancu, Mechanism of gas detection in polycrystalline thick film SnO_2 sensors, Thin solid films, 171 (1989) p. 53-63.

[74] M. Ippomatsu, H. Sazaki, H. Yanagida, Sensing mechanism of tin dioxide gas sensors, Journal of Material Science, 25 (1990) p. 259-262

[75] K.D. Schierbaum, U. Weimar, W. Göpel, Conductance, work function and catalytic activity of SnO_2 based gas sensors, Sensors and Actuators B, 3 (1991) p. 205-214.

[76] P.K. Clifford, D.T. Tuma, Characteristics of semiconductor gas sensors I: Steady state gas response, Sensors and Actuators, 3 (1982/83) p. 233-254

[77] M. Egashira, M. Nakashima, S. Kawasumi, Change of thermal desorption behaviour of adsorbed oxigen with water coadsoption on Ag+-doped tin(IV) oxide, Journal Chemical Society Chemical Communications (1981) p. 1047-1049

[78] R. Ionescu, A. Vancu, Time-dependence on the conductance of SnO_2:Pt:Sb in atmospheres containing oxygen, carbon monoxide and water vapour I, Applied Surface Science, 74 (1994) p. 297-212.

[79] K.D. Schierbaum, U. Weimar, W. Göpel, Conductance, work function and catalytic activity of SnO_2 based gas sensors, Sensors and Actuators B, 3 (1991) p. 205-214.

[80] J. Kappler, N. Bârsan, U. Weimar and W. Göpel, Influence of water vapour on nanocrystalline SnO_2 to monitor CO and CH_4, Conf. Proc. EUROSENSORS XI, Warschau (P) (1999), ISBN 83-908335-0-6, 9/1997, p. 1177-1180

[81] N. Yamazoe, J. Fuchigami, M. Kishikawa, T. Seiyama, Interactions of tin oxide surface with O_2, H_2O and H_2, Surface Science, 86 (1979) p. 335-344.

[82] D.E. Cox, T.B. Fryberger, S. Semancik, Oxygen vacancies and defect electronic states on the SnO_2 (110) 1x1 surface, Physical Reviews B, 38 (1998) p. 335-344

[83] J.F. McAleer, P.T. Moseley, J.O.W. Norris and D.E. Wiliams, tin oxide gas sensors Part 1, Journal of the Chemical Society, Faraday Transaction Part 1, 83 (1987) p. 1323-1346.

[84] Y. Matsuura, K. Takahata, K. Ihokura, Mechanism of gas sensitivity change with time of SnO_2 gas sensors, Sensors and Actuators, 14 (1988) p. 223-232

[85] P.K. Clifford, D.T. Tuma, Characteristics of semiconductor gas sensors I: Steady state gas response, Sensors and Actuators, 3 (1982/83) p. 233-254.

[86] S. Strässler, A. Reis, Simple models for n-type metal oxide gas sensors, Sensors and Actuators, 4 (1983) p. 465-472.

[87] N. Bârsan, R. Ionescu, The mechanism of the interaction between CO and a SnO_2 surface: the role of water vapour, Sensors and Actuators B, 61 (1993) p. 71.

[88] K.D. Schierbaum, U. Weimar, W. Göpel, Conductance, work function and catalytic activity of SnO_2 based gas sensors, Sensors and Actuators B, 3 (1991) p. 205-214.

[89] O. Safonova, I. Bezverkhy, P. Fabrichnyi, M. Rumyantseva and A. Gaskov, Mechanism of sensing CO in nitrogen by nanocrystalline SnO_2 and SnO_2 (Pd) studied by Mössbauer spectroscopy and conductance measurements, Journal of Materials Chemistry, 12 (2002) p. 1174-1178.

[90] A.G. Maddock, Mössbauer spectroscopy, principles and applications, Horwood chemical science series, Chister 1997, ISBN 1-898563-16-0.

[91] C. Canevali, N. Chiodini, P. Di Nola, F. Morazzoni, R. Scotti, C.L. Bianchi, Surface reactivity of SnO_2 obtained by sol–gel type condensation: interaction with inert, combustible gases, vapour-phase H_2O and air, as revealed by electron paramagnetic resonance spectroscopy, Journal of Material Chemistry, 7 (1997) p. 997-1002.

[92] G. Sberveglieri, S. Groppelli, P. Nelli, C. Perego, G. Valdre, A. Camanzi, Detection of sub-ppm H_2S concentrations by means of SnO_2 (Pt) thin films, grown by the RGTO technique, Sensors and Actuators B, 15-16 (1993) p. 86-9.

[93] N. Bârsan and U. Weimar, Conduction model of metal oxide gas sensors, Journal of Electroceramics, 7 (2001) p. 143-167.

[94] N. Bârsan, Conduction models in gas-sensing SnO_2 layers: Grain-size effects and ambient atmosphere influence, Sensors and Actuators B, 17 (1994) p. 241.

[95] M. Bauer, N. Bârsan, K. Ingrisch, A. Zeppenfeld, I. Denk, B. Schuman, U. Weimar, W. Göpel, Influence of measuring voltage, geometry and electrodes on the characteristics of thick film SnO_2 gas sensors, Proc. of the 11th European Microelectronic Conference, Venice, Italy, May 14-16 (1997).

[96] M. Schweizer-Berberich, Gas sensors based on stannic oxide, PhD Thesis, University of Tübingen (1998), Shaker Verlag (D), ISBN 3-8265-4182-0.

[97] U. Hoefer, K. Steiner, and E. Wagner, Contact and sheet resistances of SnO_2 thin films from transmission-line model measurements, Sensors and Actuators B 26-27 (1995) p. 59-63.

[98] H.L. Pang, X.H. Zhang, X.X. Zhong, B. Liu, X.G. Wei, Y.F. Kuang, J.H. Chen Preparation of Ru-doped SnO_2-supported Pt catalysts and their electrocatalytic properties for methanol oxidation, Journal of Colloid and Interface Science, Volume 319, Issue 1, 1 March 2008, Pages 193-198

[99] G. Korotcenkov. Gas response control through structural and chemical modificationsof metal oxide films: state of the art and approaches. Sensors and Actuators, pages 209–232, 2005.

[100] B. Mirkelamoglu and G. Karakas. CO oxidation over palladium- and sodium-promoted tin dioxide: catalyst characterization and temperatureprogrammed studies. Applied Catalysis a-General, 281(1-2):275–284, 2005.

[101] S.C. Tsang, C.D.A. Bulpitt, P.C.H. Mitchell, and A.J. Ramirez-Cuesta. Some new insights into the sensing mechanism of palladium promoted tin (IV) oxide sensor. Journal of Physical Chemistry B, 105(24):5737–5742, 2001.

[102] S. Morrison , « Selectivity in semi conductor gas sensors », Sensors and Actuators 12 (1987) 425-440

[103] N.D. Gangal, N.M. Gupta, and R.M. Iyer. Microcalometric study of the interaction of CO, O2 and CO + O2 with Pt/SnO2 and SnO2 catalysts. Journal of Catalysis, 126:13–25, 1990.

[104] N. Yamazoe. New approaches for improving semiconductor gas sensors. Sensor and Actuators B: Chemical, 5:7–19, 1991.

[105] C. Pijolat , « Etudes des propriétés physico-chimiques et des propriétés électriques du dioxyde d'étain en fonction de l'atmosphère gazeuse environnante. Application à la détection sélective des gaz », thèse d'état INPG 1986

[106] *Electrode Effects on Gas Sensing Properties of Nanocrystalline SnO_2 Gas Sensors*, M. Schweizer-Berberich, N. Bârsan, U. Weimar, J.R. Morante and W. Göpel, Conf.Proc.Eurosensors XI, **1997**, 1377-1380, Warschau (P), 83-908335-0-6.

[107] S.M.A. Durrani, The influence of electrode metals and its configuration on the response of tin oxide thin film CO sensor, *Talanta, Volume 68, Issue 5, 28 February 2006, Pages 1732-1735*

[108] A. Ylinampa, V. Lantto and S. Leppävuori, Some differences between Au and Pt electrodes in SnO_2 thick-film gas sensors, *Sensors and Actuators B: Chemical, Volume 14, Issues 1-3, June 1993, Pages 602-604*

[109] S. Saukko and V. Lantto, Influence of electrode material on properties of SnO_2-based gas sensor, *Thin Solid Films, Volume 436, Issue 1, 22 July 2003, Pages 137-140.*

[110] S.M.A. Durrani, The influence of electrode metals and its configuration on the response of tin oxide thin film CO sensor, *Talanta, Volume 68, Issue 5, 28 February 2006, Pages 1732-1735*

[111] X. Vilanova, E. Llobet, J. Brezmes, J. Calderer and X. Correig, Numerical simulation of the electrode geometry and position effects on semiconductor gas sensor response, *Sensors and Actuators B: Chemical, Volume 48, Issues 1-3, 30 May 1998, Pages 425-431*

[112] Uma Jain, A. H. Harker, A. M. Stoneham and D. E. Williams, Effect of electrode geometry on sensor response, *Sensors and Actuators B: Chemical, Volume 2, Issue 2, May 1990, Pages 111-114*

[113] S. Capone, P. Siciliano, F. Quaranta, R. Rella, M. Epifani and L. Vasanelli, Moisture influence and geometry effect of Au and Pt electrodes on CO sensing response of SnO_2 microsensors based on sol–gel thin film, *Sensors and Actuators B: Chemical, Volume 77, Issues 1-2, 15 June 2001, Pages 503-511*

[114] Simonetta Capone, Mauro Epifani, Luca Francioso, Saulius Kaciulis, Alessio Mezzi, Pietro Siciliano and Antonella M. Taurino, Influence of electrodes ageing on the properties of the gas sensors based on SnO_2, *Sensors and Actuators B: Chemical, Volume 115, Issue 1, 23 May 2006, Pages 396-402.*

[115] U. Hoefer, K. Steiner and E. Wagner, « Contact and sheet resistance of SnO_2 thin films from transmission-line model measurements », Sensors and Actuators B 26-27 (1995), 59-63

[116] U. Weimar, W. Göpel : « A.C. measurements on tin oxide sensors to improve selectivity and sensitivities », Sensors and Actuators B 26-27 (1995) 13-18

[117] O.K. Varghese, L. Malhotra , « Electrode sample capacitance effect on ethanol sensitivity of nano-grained SnO_2 thin films », Sensors and Actuators B 53 (1998) 19-23

[118] Pierre Montmeat, Jean-Claude Marchand, René Lalauze, Jean-Paul Viricelle, Guy Tournier and Christophe Pijolat , Physico-chemical contribution of gold metallic particles to the action of oxygen on tin dioxide sensors,*Sensors and Actuators B: Chemical, Volume 95, Issues 1-3, 15 October 2003, Pages 83-89*

[119] J.-P. Viricelle, B. Riviere and C. Pijolat ,Optimization of SnO_2 screen-printing inks for gas sensor applications,*Journal of the European Ceramic Society, Volume 25, Issue 12, 2005, Pages 2137-2140*

[120] J. J. Benitez, M. A. Centeno, O. M. Merdrignac, J. Guyader, Y. Laurent, and J.A. Odriozola. DRIFTS chamber for in situ and simultaneous study of infrared and electrical response of sensors. Applied Spectroscopy, 49:1094–1096,1995.

[121] J.J. Benitez, M.A. Centeno, C Louis Dit Picard, O Merdrignac, Y. Laurent, and J.A. Odriozola. In situ diffuse reflectance infrared spectroscopy (DRIFTS) study of the reversibility of CdGeON sensors towards oxygen. Sensors and Actuators, B: Chemical, 31(3):197–202, 1996.

[122] R. Pohle, Fleischer M., and H. Meixner. In situ infrared emission spectroscopic study of the adsorption of H_2O and hydrogen containing gases on Ga_2O_3 gas sensors. Sensor and Actuators B, 68:151–156, 2000.

[123] R. Pohle, M. Fleischer, and H. Meixner. Infrared emission spectroscopic study of the adsorption study of the adsorption of the oxygen on gas sensors based on polycrystalline metal oxide films. Sensor and Actuators B, 78:133–137, 2001.

[124] N. Yamazoe, J. Fuchigami, M. Kishikawa, T. Seiyama, Interactions of tin oxide surface with O_2, H_2O and H_2, Surface Science, 86 (1979) p. 335-344

[125] J.P. Joly, L. Gonzales-Cruz and Y. Arnaud, *Bull. Soc. Chim. Fr.* **1** (1986), p. 11 (in French).

[126] J. Tamaki, M. Nagaishi, Y. Teraoka, N. Miura and N. Yamazoe, *Surf. Sci.* **221** (1989), p. 183

[127] F. Gaillard, M. Abdat, J.P. Joly and A. Perrard, *Appl. Surf. Sci.* **238** (2004), p. 91.

128 Dorota Koziej, Phenomenological and Spectroscopic Studies on Gas Detection Mechanism of Selected Gases with Tin Dioxide Based Sensors, PhD Thesis, 2006

[129] J.H. Lambert. Photometria sive de mensura et grodibus luminis colorum et umbrae. page Augustatae Vindelicorum, 1760.

[130] G. Kortüm. Reflectance Spectroscopy. Springer-Verlag, New York, 1969.

131 T. Armarolli, T. Becue, and S. Gautier. Diffuse reflection infrared spectroscopy (DRIFTS): Application to the in situ analysis of catalysts. Oil & Gas Science and Technology-Revue De L Institut Francais Du Petrole, 59(2):215–237, 2004

[132] R. Griffiths, Peter and M. Olinger, Jill. Continuum theories of diffuse reflection. In P. R. Chalmers, J. M.; Griffiths, editor, Handbook of vibrational spectroscopy. John Wiley & Sons Ltd, 2002.

[133] A. Schuster. Radiation through a foggy atmosphere. Astrophysical Journal, 21: 1, 1905.

[134] P. Kubelka and F. Munk. Ein Beitrag zur Optik der Farbanstriche. Zeitschrift

für technische Physik, 12:593–601, 1931.

[135] J. Dahm, Donald and D. Dahm, Kevin. Discontinuum theory of diffuse reflection. In P. R. Chalmers, J. M.; Griffiths, editor, Handbook of vibrational.spectroscopy. John Wiley & Sons Ltd, 2002.

[136] K. Seeger. Semiconductor Physics: an introduction. Springer, 1999.

[137] F.J. Blatt. Physics of Electronic Conduction in Solids. McGraw- Hill Series in Materials Science and Engineering. 1968.

[138] M. I. Baraton and L. MeRHari. Nanoparticles-based chemical gas sensors for outdoor air quality monitoring microstations. Materials Science and Engineering B-Solid State Materials for Advanced Technology, 112(2-3):206–213, 2004.

[139] M. I. Baraton and L. MeRHari. Determination of the gas sensing potentiality of nanosized powders by FTIR spectrometry. Scripta Materialia, 44(8-9):1643– 1648, 2001.

[140] P. A. Cox, R. G. Egdell, W. R. Flavell, J. P. Kemp, F. H. Potter, and C. S. Rastomjee.Influence of carrier-free surface-layers on infrared reflectance spectra of n-type metallic oxides. Journal of Electron Spectroscopy and Related Phenomena, 54:1173–1182, 1990.

[141] Z. Crnjak Orel, B. Orel, M. Hodoscek, and V. Kaucic. Conductive SnO2/Sb powder: preparation and optical properties. Journal of Materials Science, 27: 313–318, 1992.

[142] P. A. Cox, R. G. Egdell, W. R. Flavell, J. P. Kemp, F. H. Potter, and C. S. Rastomjee.Influence of carrier-free surface-layers on infrared reflectance spectra of n-type metallic oxides. Journal of Electron Spectroscopy and Related Phenomena, 54:1173–1182, 1990.

[143] P.J. Brimmer and P. R. Griffiths. Effect of absorbing matrices on diffuse reflectance infrared spectra. Analytical Chemistry, 58:2179–2186, 1986.

[144] M. A. Barteau, Journal of Vacuum Science & Technology, 11, 1993,p. 2162

[145Anatoli Davydov, Molecular spectroscopy of oxide catalyst surface, Edited by N. T. Sheppard, Wiley, 20003

[146] Serpil Harbeck, Phd Thesis

[147] *Electrode Effects on Gas Sensing Properties of Nanocrystalline SnO_2 Gas Sensors*, M. Schweizer-Berberich, N. Bârsan, U. Weimar, J.R. Morante and W. Göpel, Conf.Proc.Eurosensors XI, **1997**, 1377-1380, Warschau (P), 83-908335-0-6.

[148]Anatoli Davydov, Molecular spectroscopy of oxide catalyst surface, Edited by N. T. Sheppard, Wiley, 20003

[149] S. Saukko, Ulla Lassi, V. Lantto, M. Kroneld, S. Novikov, P. Kuivalainen, T.T. Rantala and J. Mizsei Experimental studies of O_2–SnO_2 surface interaction using powder, thick films and monocrystalline thin films, *Thin Solid Films*, *Volume 490, Issue 1, 21 October 2005, Pages 48-53*

[150] Dorota Koziej, Nicolae Bârsan, Udo Weimar, Jacek Szuber, Kengo Shimanoe and Noboru Yamazoe, Water–oxygen interplay on tin dioxide surface: Implication on gas sensing, *Chemical Physics Letters, Volume 410, Issues 4-6, 20 July 2005, Pages 321-323*

[151] *CO sensing with SnO_2 thick film sensors: role of oxygen and water vapour*, S. Hahn, N. Barsan, U. Weimar, S.G. Ejakov, H.J. Visser, R.E. Soltis,, Thin Solid Films, 436, **2003**, 17-24.

Acknowledgements

First of all I would like to thank Prof. C. Pijolat and PD. Dr. U. Weimar for giving me the opportunity to carry on my PhD studies under their joined supervision inside the network of excellence GOSPEL.

I would like to thanks Dr U Weimar for giving me the opportunity to work inside his laboratory and also to participate to GOSPEL event. Even he is extremely busy, he was nice to have to discuss with him.

Je souhaite remercier C. Pijolat pour m'avoir proposé ce sujet difficile mais au combien passionnant.

I am particularly thankful to Dr. N. Barsan with whom I had a great pleasure to work. I appreciate our scientific discussion. He has been teaching me a lot and not only from the scientific point of view. I hope, I will put into practice some of advices he give to me. In Rugby, we say that I should transform the try.

Je voudrais remercier J. P Viricelle pour son soutien, son implication, sa patience. Je le remercie particulièrement pour les corrections qu'il a apporté à mon rapport final.

I am very grateful to Dr Dorota KOZIEJ for his guidance in IR spectroscopy. She has introduced me all the technical and theoretical aspects of DRIFT. She suffers a lot from my lack of rigour but we have some fun moment around a cup of coffee.

Ce travail n'aurait pas pu s'accomplir sans la solide participation de P. Breuil, G. Tournier, J.C Marchand et A. Boyer (le dernier arrivé) qui forment l'ossature du département MICC. Je tiens à remercier P. Breuil pour ses conseils dans le domaine de l'instrumentation et de la modélisation électrique. Je transmets ma sincère reconnaissance que G. Tournier m'a apportée en TPD et pour nos discussions sur les capteurs de gaz. Merci à J-C. Marchand pour sa grande disponibilité.

I thank Ute Harbusch for her help for the accommodation, administrative part and her good spirits.I would like to thank Alexandru Oprea for his technical support and for speaking French with me for time to time.

Je tiens à remercier l'ensemble du personnel de l'Ecole des Mines pour sa disponibilité, en particulier les secrétaires du département SPIN.

I would like to thanks all the IPC members: Niko papamichail for his help concerning GOPSEL and for his wonderful sofa! Melanie Sahm specially for the time during the gospel school, Frank Rock the don Juan of Tübingen, Cristi thanks for our scientific discussion around a bottle of wine (keep the wave), Suman: go for the goal!!, Thomas Heine the geek, Alexender Haensch for the work in DRIFT, Michael Wandel for his advice in computer and in barbecue science and also wolfram Simmendinger, Michael.

J'ai également une pensée pour tous les doctorants de l'Ecole des Mines qui m'ont entouré pendant ces années. Spécialement ceux de l'équipe MICC : Maryline Roumanie qui fut ma

première collègue de bureau et pour son enthousiasme caché; Guillaume Bes toujours débordé mais qui m'a rendu bien des services, Willy Porcher pour nos soirées et nos sorties sportives. Merci à Geoffroy Gadcsz et Sorina-Nicoletta Udroiu pour nos brillantes discussion et surtout pour la pause café (message personnel : arrêtez de vous engueuler), Malick Camara pour nos partie de foot après le labo, Jing pour qui tout va toujours bien, Arthur (tu verras SnO_2 c'est de la m…..) et aussi Jean-philippe Guillemin, David Rotureau, Marc Kamionka, Nicolas Guillet et Pierre Montmeat.

Merci à mes amis du Master Recherche, à mes collègues d'Angers et mes copains de Lycée qui sont présents dans toutes les situations.

Je finirais par remercier ma famille pour m'avoir soutenu tout au long de ces années. A Agnès et Lucie mes deux sœurs qui m'ont posé mille fois la question "quand finis tu ?, à mon Oncle et ma grand-mère Alice qui m'ont toujours encouragés. Je tiens à remercier tous ceux qui se sont intéressé de loin ou de prêt à mes travaux de thèse. J'ai une pensé pour les membres de la famille de Cécile qui m'ont encouragés. A la famille de l'Ile de la Réunion que j'aimerais voir plus souvent.

A ma mère, Marie-Ange, à qui je dédie cette thèse.

A Cécile, mon épouse qui m'a toujours secondé dans cette période et ce malgré les exigences d'éloignement que ces travaux exigeaient : je t'en suis reconnaissant. Et maintenant d'autres challenges nous attendent notamment avec Alwena.

Curriculum Vitae

Johan Bertrand

Date of Birth: 15/01/1980
Place of Birth: Saint Brieuc (cotes d'Armor, France)
Marital Status: married
Nationality: French

Education:

2004 –2008	**PhD** studies in the frame of Joint Doctoral Degree Project of the GOSPEL Network of Excellence between ecole des mines de St Etienne (France) and University of Tübingen (Germany). "Spectroscopic and electrical studies of the influence of electrodes on SnO_2 based sensors"
2004	**Master research** defence "Synthesis and characterization of new oxynitride materials for chemical gas sensors application"
2004 - 2003	Master research Study of inorganic and molecular chemistry at University of Rennes1, Glass and ceramics, Rennes, France
2003-1998	**Study of chemistry**, University of Rennes1, France
1998- 1995	**A level**, Lycée JEAN XX III, Quintin, Bretagne, France
1995- 1991	Collège JEAN XX III, Quintin, Bretagne, France

Ecole Nationale Supérieure des Mines
de Saint-Etienne

N° d'ordre : 487 GP

Prénom Nom JOHAN BERTRAND

Titre de la thèse Spectroscopic and electrical studies of the influence of electrodes on SnO_2 based sensors

Spécialité Chemical and process engineering

Mots clefs SnO_2, electrodes, DRIFT, Temperature Programmed Desorption,

Résumé The influence of the electrode nature on the performance of semiconducting metal oxide based gas sensors is recognized and experimentally proven. Here, for the first time we are providing clear spectroscopic evidence (DRIFTS) for the influence of the electrodes nature (Pt and Au) on the surface chemistry associated to CO detection with SnO_2 thick film sensors. Our results show that the nature and concentration of the CO reaction intermediates (carbonates and carboxylates) depend on the presence and nature of the electrodes. Moreover, Thermodesorption measurements prove that the influence of the electrodes nature plays a key role on oxygen adsorption at the SnO_2 surface. The result will be discuss in order to be useful for basic understanding of gas sensors.

Ecole Nationale Supérieure des Mines
de Saint-Etienne

N° d'ordre : 487 GP

Prénom Nom Johan BERTRAND

Titre de la thèse : Etude électrique et spectroscopique de l'influence de l'électrode sur les capteurs de gaz à base de SnO2

Spécialité Génie des procédés

Mots clefs : SnO_2, électrodes, DRIFT, thermodesorption, propriétés électrique.

Résumé : L'influence de la nature des électrodes sur les performances des capteur de gaz à base d'oxyde métallique semiconducteur sont reconnu et prouvé expérimentalement. Ici, pour la première fois nous fournissons une mise en evidence par spectroscopie infrarouge (DRIFTS) de l'influence de la nature d'électrodes (Pt et Au) sur la chimie de surface lors de la détection de CO aux sur couche épaisse de SnO_2. Nos résultats montrent que la nature et la concentration des intermédiaires de réaction de CO (les carbonates et carboxylates) dépendent de la présence et de la nature des électrodes. De plus, les mesures en Thermodesorption prouvent que l'influence de la nature d'électrodes joue un rôle clé sur l'adsorption d'oxygène à la surface SnO2. Ces résultats sont discutés au sein d'un modèle empirique.